REFINING NEUROIMAGING METHODOLOGY TO BETTER UNDERSTAND BRAIN RESTING-STATE NETWORK FUNCTIONAL CONNECTIVITY IN OLDER ADULTS

By

Zachary Fernandez

A DISSERTATION

Submitted to
Michigan State University
in partial fulfillment of the requirements
for the degree of

Neuroscience – Doctor of Philosophy

2024

ABSTRACT

The brain requires a consistent supply of oxygenated blood to meet its high metabolic energy demands. Through a process termed neurovascular coupling, neural activity increases local cerebral blood flow to meet regional metabolic energy demands. Functional magnetic resonance imaging (fMRI) is a non-invasive tool capable of indirectly quantifying brain activity through the blood oxygenation level dependent (BOLD) response. Interestingly, spatially distinct brain regions that are functionally connected while performing a task maintain their synchronized BOLD response time courses at baseline in the absence of a task. Regions that exhibit these highly correlated BOLD responses at rest are grouped together and referred to as a resting state network (RSN). Studies that focus on resting-state fMRI (rs-fMRI), a task-free adaptation of fMRI, have found RSNs to hold predictive power in a wide range of neurodevelopmental and neurodegenerative disorders. However, there are no set standards for conducting rs-fMRI research. Further investigation into optimizing rs-fMRI methodology is beneficial to ensure reproducibility of results, particularly those of clinical significance. To assist with this, this dissertation will examine the effects of various rest conditions used during rs-fMRI data acquisition on RSN functional connectivity and introduce a novel age-appropriate functional atlas for older adults.

Rest conditions can vary between studies. This often includes entirely different sets of instructions to the subjects which can impact the data. Aim 1 of this dissertation investigates the effects of rest conditions with differing levels of cognitive load on a complete set of predefined RSNs. Rs-fMRI datasets were obtained from twenty-two healthy college students (22 ± 4 years old, 12 females) on a 3T MRI scanner. Each subject was scanned under four different conditions: (1) eyes open in dim light (Eyes-Open), (2) eyes closed and awake (Eyes-Closed), (3) eyes closed while remembering four numbers through the scan session (Eyes-Closed-Number) and (4) asked to watch a movie (Movie). Overall, we found conditions with more

external stimulation led to more global changes in functional connectivity during rs-fMRI. However, when considering each RSN of an existing functional atlas individually, there were differential changes between conditions. The results of this study can aid in future study interpretation and design.

Next, we address the disproportion of functional atlases available for older adults. A functional atlas is a predefined set of recognizable RSNs that can be used to define regions in studies with subjects of a similar demographic. Most functional atlases that are currently available were derived from young and healthy populations. While often used to study RSNs in older adults, these atlases do not account for age-related brain atrophy and changes in RSN connectivity. Here, our goal was to use the baseline anatomical and rs-fMRI scans from the recently completed Risk Reduction for Alzheimer's Disease (rrAD) clinical trial to create a robust functional atlas that is better-matched to study older populations. The rrAD sample is comprised of 420 hypertensive older adults (60 to 84 years, 68.8±5.9) scanned across five different 3T MRI scanners. Using a combination of seed-based and data-driven approaches, we created a functional atlas of recognizable RSNs that more adequately describes RSN functional connectivity of the rrAD cohort. We expect the rrAD420 rs-fMRI atlas to be directly applicable to study outcomes related to the functional connectivity of the rrAD population. However, we also believe the rrAD420 functional atlas would also be a suitable option for older populations in general. As such, our functional atlas can assist in the identification of RSN deviations with potential to serve as age-related biomarkers of disease in the future.

To Manda Fernandez, Robert (Bobbo) Fernandez,
Jarad Fernandez, Nichole Fernandez-Mulligan, and Mary Ann Shepherd

ACKNOWLEDGEMENTS

My project required a unique and diverse skillset, almost all of which I had to acquire while in graduate school (and during a pandemic - thank you COVID). This would have been impossible without a team that was dedicated to helping me develop into the scientist I hoped I could be. I'm so thankful to say that's exactly the team I found. I would like to express my sincere gratitude to my mentor, Dr. David Zhu, for believing in me and allowing me to branch out of my comfort zone. Thank you for letting me be a part of something bigger than myself, and for challenging me to think in new ways. Also, a huge thank you to Dr. Norman Scheel for your infectious curiosity, willingness to help, and words of wisdom in and out of the lab. You set an excellent example for us to follow. Josh Hubert, thank you for asking the tough questions and for bringing a sense of playfulness to the lab. Dr. Josh Baker (and Dr. Sarah Tilden!), you made this quite the adventure and it would never have been the same without you, we did it buddy.

Thank you to my dissertation committee, who contributed excellent ideas, time, and support and this accomplishment is largely attributed to their guidance. Thank you, Dr. Andrew Bender, for always advocating for me and staying after lab meeting to talk one on one. Thank you, Dr. Scott Counts, for your desire to try new things and work with others. You've taught me the importance of interdisciplinary collaboration and the value in combining multiple approaches to get the most out of a study.

During my first year, I got excited about the idea of adding a translational element to my research project. I owe an enormous thank you to Dr. Anne Dorrance for hearing my ideas out and making my dream come true. Thank you to the Dorrance Lab, and Dr. Bill Jackson, for adopting a complete novice and showing me the ropes of animal work. I truly felt welcomed from the beginning as you allowed me to crash your lab meetings, included me in discussions, and gave me a chance to present the occasional neuroimaging paper at journal club. A special

thank you to Dr. Teri Lansdell and Dr. Laura Chambers for your patience and encouragement every step of the way. I really appreciate all the time and effort you put in.

I am immensely grateful to Dr. Chunqi Qian, whose positivity and generosity really helped me to get across the finish line. I look forward to my continued work with Dr. Qian as a postdoc in his lab. In addition, thank you to Dr. Yi Chen who seemed to show up at the perfect time to take me under her wing. Her expertise and passion transformed the long nights in the scanner room into a fun learning experience. It was such an absolute privilege to work with all of you.

Also, thank you to my program cohort Dr. Luis Martinetti Dr. Christine Kwiatkowski, and Hannah Rudolph for your instant friendship and being awesome people in general. Finally, thank you to my family who never doubted me. I wouldn't be where I am today without you.

TABLE OF CONTENTS

CHAPTER 1: INTRODUCTION

1.1 – Brain power

Although the brain only accounts for 2% of total body weight, it is the most metabolically active organ in the body as it utilizes roughly 20% of our total energy at rest (1). The relationship between the brain and cerebral vasculature is highly important because the brain, unlike other organs, does not possess a reserve that allows for the storage of nutrients for later use (2). Instead, it relies on an intricate cerebrovascular network for the constant delivery of oxygen-rich blood and nutrients in real-time, in which each individual neuron is positioned within 15 micrometers of its own capillary (3). Oxygenated blood is preferentially directed to regions of the brain that show relatively higher levels of neural activation through functional hyperemia (4). Specifically, functional hyperemia, also described as neurovascular coupling, is the process by which neural activity increases local cerebral blood flow to meet regional metabolic energy demands. This hemodynamic response is achieved through specific coordinated vascular changes that induce arterial relaxation and direct cerebral blood flow to active regions, which can be noninvasively quantified through state-of-the-art neuroimaging techniques (4,5).

1.2 – Introduction to functional magnetic resonance imaging

Functional Magnetic Resonance Imaging (fMRI) leverages neurovascular coupling induced hyperoxia in active brain regions, together with the differential magnetic properties of oxygenated and deoxygenated hemoglobin, to measure the blood oxygenation level dependent (BOLD) response (6,7). The BOLD response is used to indirectly assess localized neural activation and functional connectivity of spatially distinct brain regions. Typically, fMRI is thought to include a task that assesses a particular cognitive domain while subjects are in the scanner. In this setting, brain regions that show synchronized increases in BOLD activity during active task periods are thought to be functionally connected to each other and work together to allow for the completion of the task at hand. To this end, traditional task-based fMRI has been crucial

to understanding the regional localization and differentiation of brain function by identifying brain regions that actively contribute to subjects performing specific tasks (8).

Resting-state fMRI (rs-fMRI), a task-free adaptation of traditional fMRI, focuses on the low-frequency fluctuations (traditionally <0.1 Hz) of BOLD signal in the brain and is considered to represent the innate functional connectivity of the brain at rest (9). Biswal and colleagues identified task-evoked connections between brain regions in the motor cortex that were associated with subjects performing a bilateral finger-tapping task. When examining spontaneous BOLD fluctuations at lower signal frequencies during rest periods, he found these connections were also maintained in a strikingly similar manner relative to active task periods. Furthermore, Biswal's group related their findings to an animal electrophysiology study that presented correlations of electrical activity in the rat cerebral cortex with previously unrecognized spontaneous fluctuations in regional cerebral blood flow reported the year prior (10). Together, the results of these investigations highlight neurovascular coupling as an important feature to support baseline spontaneous neural activity, and that functionally connected brain regions show similar oscillations in their respective BOLD response time course even in a baseline resting state. Regions that show highly correlated BOLD response at rest throughout the time course are grouped together and referred to as a resting state network (RSN). Rs-fMRI studies have since made great strides in identifying distinct RSNs throughout the brain which have a consistent and reproducible organization (11–14). Collectively, all RSNs in a single parcellation can be considered as a functional atlas of the brain. Existing functional atlases are commonly used to perform node-based network modeling analyses and compare RSN functional connectivity between distinct subject groups or conditions.

1.3 – Lots of ways to do nothing - methodological choices of rest conditions in rs-fMRI

There are pragmatic benefits to a task-free approach because there is relatively little set-up involved for the experimenter. Furthermore, rs-fMRI can be performed with any subject population, including children or individuals afflicted by neurodegenerative disorders that may inhibit their ability to perform complex tasks in the more conventional task-based fMRI setting. However, currently there is no set standard regarding the optimal conditions that should be adhered to when acquiring rs-fMRI data. For instance, some studies request subjects to keep their eyes open during the scan, while others ask that they close their eyes without falling asleep (13,15). Additionally, some studies ask subjects to focus on something specific, such as the sounds of the scanner to reach a somewhat meditative state, while others instruct subjects to let their minds wander or think of nothing in particular (16,17). Extant literature has already found the subtle differences in instructions between certain rest conditions to influence the functional connectivity of some RSNs (18,19) . For example, Patriat and colleagues compared RSN functional connectivity between three rest conditions, specifically eyes-closed, eyes-open, and eyes-open while focusing on a fixation cross (19). They observed changes in the auditory, default-mode, and attentional networks between rest conditions, and the most reliable reproducibility of these RSNs was captured when subjects were instructed to focus on a fixation cross. Likewise, Kawagoe and colleagues examined changes in RSN functional connectivity between two eyes-open rest conditions with different pre-scan instructions (18). One rest condition requested subjects to let their minds wander, while the other asked them to think of nothing. This slight difference in instruction subsequently led to significant differences in default-mode network (DMN) functional connectivity between conditions. Previous work on this topic tends to focus on selected primary RSNs of interest or only test a few rest conditions at a time. Thus, it remains unclear how exactly each individual RSN responds to conditional changes between numerous rest conditions in a single study. The first aim of this dissertation was

designed with the intent to elucidate the effects of multiple rest conditions on all RSNs presented in the existing functional atlas defined by Yeo and colleagues (14). Accomplishing this aim offers a more comprehensive understanding of RSN deviations between rest conditions in healthy subjects, which will assist in better study design and interpretation of results in future clinically relevant rs-fMRI studies, such as in the case of Alzheimer's Disease (AD).

1.4 – Alzheimer's Disease

Dementia is a broad classification of neurological symptoms that includes several subtypes of pathological age-related cognitive decline that severely reduces qualify of life. Aside from the clear detrimental impact of dementia on healthy aging in the elderly, there is also a large economic burden that has been estimated at $200 billion per year (20). Given the growing concern of dementia due to the rapidly increasing elderly population, there is an urgent need for further investigation into better prevention and treatment options (21). AD has long been recognized as the most prominent dementia subtype, affecting an estimated 5.4 million Americans, as well as a leading cause of death in adults 65 and older (22,23). Patients with AD present with impaired memory, judgement, reasoning skills, visuospatial abilities, language function, and changes in personality or behavior that interfere with activities of daily living (24). The leading hypothesis for underlying pathophysiological mechanisms of AD suggests that aggregation of amyloid beta and tau proteins contribute to subsequent neurodegeneration and cognitive decline (25). In fact, while symptoms and biomarkers are useful in determining probable AD cases, a definite AD diagnosis can only be confirmed after both amyloid beta plaques and neurofibrillary tangles composed of tau proteins are identified in post-mortem brain tissue analysis (26). However, technological advancements have allowed for the identification of these key features in vivo through positron emission tomography (PET), which has led to a conceptual understanding that AD progresses along a continuum (27). Specifically, these findings showed that amyloid beta and tau accumulation precede AD-associated cognitive

deficits. This is further supported when considering patients with mild cognitive impairment (MCI), an intermediate phase between normal cognition and AD, as they also exhibit presymptomatic amyloid beta and tau accumulation, albeit to a lesser extent (27,28). Subjective cognitive impairment (SCI) has also been identified as a state that precedes MCI along the AD continuum (29,30). SCI is described as a subjective perception of cognitive decline, without observable deficits in neuropsychological testing. Older individuals with SCI are estimated to be twice as likely to progress to MCI or AD, and some have considered SCI as the first symptomatic sign of AD as they share some biomarkers with patients with MCI and AD (29,31).

1.5 – Implications of RSN functional connectivity in Alzheimer's Disease

Clinical studies involving rs-fMRI have shown deviations in RSN connectivity to possess cognitive and clinical implications which have the potential to serve as viable biomarkers of disease states (32–34). In line with this, altered connectivity of RSNs such as the well-studied DMN has been associated with aging and aspects of cognitive decline (35,36). The DMN was discovered in task-based fMRI, presenting as negatively correlated activation (12,15,37). Specifically, the DMN includes brain regions such as the prefrontal cortex, precuneus, posterior cingulate cortex, hippocampus, inferior parietal lobule, and angular gyri (38,39). The DMN has since been associated with the internal processing of self-relevant information, inward thinking and preparation for future cognitive tasks (39,40). Prior work has shown the functional connectivity of the DMN is reduced in patients with AD and MCI which can occur years before the appearance of neuropsychological deficits (39,41–44). Interestingly, PET studies have revealed that hyperphosphorylated tau and amyloid beta, established hallmarks of AD, aggregate within primary DMN regions including the precuneus and posterior cingulate cortex (45,46). Recent work has also shown a similar pattern of amyloid beta deposition and diminished DMN connectivity in cases of MCI (47). Furthermore, rs-fMRI studies have shown early DMN connectivity disruptions in individuals with SCI (48). These findings suggest that

amyloid and tau deposition coincide with reduced DMN connectivity in AD patients, and these brain changes often occur before the manifestation of cognitive decline (27). In addition to DMN, other RSNs such as the frontoparietal network, salience network, dorsal attention network, and limbic network have also show deviations in functional connectivity that have been related to AD-associated pathology (49,50). Differences in RSN functional connectivity throughout AD progression can also be distinguished by machine learning algorithms, which have recently been used to automatically classify normal cognition, early MCI, late MCI, and AD patients based solely on rs-fMRI data (51,52). As such, measures of RSN functional connectivity can provide valuable insight for early AD detection and test the effectiveness of treatment strategies in preserving RSN integrity and cognition throughout the AD continuum (36,53,54).

1.6 – Interplay between Hypertension and Alzheimer's Disease

Current treatments focus on mitigating AD symptoms and do not preserve cognitive function (55). Thus, it is necessary to gain a better understanding of modifiable risk factors of cognitive decline and the progression of AD. A recent postmortem study demonstrated that most AD cases have significant underlying vascular contributions, indicating a role of the cardiovascular system in AD pathophysiology (56). Furthermore, studies have observed the cortical vascular network to be disrupted in AD that can exacerbate AD-associated degeneration (57,58). Indeed, longitudinal evidence has provided more insight suggesting many modifiable risk factors associated with cardiovascular disease, such as obesity, smoking, diabetes, physical inactivity, and hypertension, to also be associated with the progression of AD (59–61). Of these risk factors hypertension is of particular interest due to its high prevalence, affecting more than 60% of individuals over the age of 65 (62,63). Chronic hypertension compromises neurovascular coupling, causing stiffening of cerebral arteries and a restructuring of vascular organization which can result in subsequent small vessel disease, white matter lesions, oxidative stress, and decreased beta-amyloid clearance (64–67). The indirect inference of neuronal activity through

regional changes in BOLD signal makes fMRI an optimal technique to detect changes in brain functional connectivity following challenges to vascular integrity (59). Hypertension has been shown to lead to a reduction in resting cerebral blood flow, which can in turn impact RSN connectivity (68). This claim is further supported by a recent near-infrared spectroscopy study showing that hypertension alone can elicit altered coupling strength in brain functional connectivity and worsened cognitive performance (69). Moreover, as mentioned previously, it is known that RSNs, including the DMN, are susceptible to alterations in patients with AD (39,70). These alterations can be exaggerated in hypertensive AD patients, as they exhibit even weaker DMN connectivity compared to their normotensive counterparts (71). While the study of the relationship between hypertension and AD has gained interest, there are still large gaps in knowledge regarding the effects of hypertension and blood pressure reduction on brain health and function.

The potential cognitive benefits of lowering systolic blood pressure (SBP) through standard antihypertensive treatment (SBP target of $\leq$ 140 mmHg) are currently controversial and require further investigation (72–74). Recent trials involving a more intensive antihypertensive treatment option (SBP target of $\leq$ 125 mmHg) have shown the more aggressive option to be safe and yield a greater benefit in preventing cardiovascular disease over standard treatment (75,76). Subsequently, evidence from the Systolic Blood Pressure Intervention Trial (SPRINT) study served as the primary basis for the American Heart Association's decision to update their recommended treatment goal to be less than 130 mmHg (77). In addition, a follow-up study of the SPRINT cohort revealed a lower incidence of MCI and AD following intensive blood pressure reduction compared to standard treatment (78). However, since the SPRINT study was cut short after the primary aims of the study regarding cardiovascular disease were achieved, the effects of intensive hypertensive treatment on preserving cognitive faculties remain unclear. In addition, fMRI was not included in the SPRINT study as it was unnecessary

to achieve those aims, thus the effects of intensive hypertensive treatment on preserving brain connectivity also remains unclear.

To fill this gap, the Risk Reduction for AD (rrAD) clinical trial was designed to investigate the effects of intensive blood pressure lowering and aerobic exercise on neurocognitive function and brain connectivity in a sample entirely comprised of hypertensive individuals with a high familial risk of AD. The rrAD trial enrolled 640 cognitively normal older subjects aged 60 to 85 years old with hypertension and a family history of AD. Although these subjects showed no deficits in cognition, individuals with a family history of AD are more likely to experience neurodegenerative symptoms and cognitive decline at an earlier onset (79). However, apart from the family history and the hypertension diagnosis, all subjects enrolled in the trial were otherwise healthy. As stated in the recently published rationale and methods of the rrAD trial, subjects were randomly assigned to treatment groups: standard treatment, intensive reduction of vascular risk factors (ISVR), exercise training, and ISVR in combination with exercise training (80). Groups that were designated to receive ISVR had a blood pressure target of SBP $\leq$ 125 mmHg that was achieved through a stepwise approach (Figure 1.1) under the supervision of a clinician. Groups that were designated to receive exercise training performed a structured moderate to vigorous aerobic exercise training supervised by exercise professionals at local facilities. They were taught basic exercise techniques in weeks 1-4 three times a week by their trainers. Additionally, they each wore heart rate monitors and were taught how to stay within a specific target heartrate zone during exercise sessions. The exercise intensity was increased over the first three months, and those unable to exercise continuously performed intermittent bouts until the heart rate target zone was reached. After week 13 the subjects were allowed to exercise at home, however, to remain compliant with the study they were required to keep an exercise log. Physical exercise is highly recommended to reduce blood pressure in hypertensive individuals to prevent cardiovascular disease, especially in cases where hypertensive

medications are not enough to manage hypertension on their own (81,82). Exercise is also an important factor to consider with respect to preserving cognition and brain health because studies have associated physical inactivity with decreased Brain Derived Neurotrophic Factor (BDNF) expression, hippocampal atrophy, cognitive decline, and higher incidence of dementia (83–85). To provide a control for participation in a structured exercise program, the ISVR and standard treatment groups without the aerobic exercise component were enrolled into a stretching and balance program that focused on range of motion and flexibility (86). In order to assess the effectiveness of each treatment group in preserving RSN connectivity, rs-fMRI data collected from the rrAD will be used to compare RSN connectivity between groups from anatomical and rs-fMRI scans obtained at baseline and at 24 months following treatment. However, to accomplish this primary aim of the rrAD trial it is important to accurately define RSNs that are pertinent to the population demographics of the study.

1.7 – Age-appropriate functional atlas for older adults

A variety of methods have been used to define RSNs. This includes the hypothesis-driven seed-based correlation approach, which was the voxel-based approach originally used by Biswal and colleagues (9). The seed-based correlation strategy requires the experimenter to select a region of interest (ROI) to generate the RSN that will be used in the study. The BOLD time course is then extracted from the chosen ROI and compared to the BOLD time course of all other regions throughout the entire brain to obtain R-coefficients. Brain regions that follow a similar BOLD time course relative to the selected ROI are included in the RSN generated in the following analysis. The seed-based correlation approach is limited to defining one RSN at a time and requires an in-depth understanding of the RSN from existing literature to select the optimal ROI for each specific RSN of interest. This can present an issue when the goal of a study is to compare multiple RSNs or to examine RSN dynamics between groups.

Data-driven approaches such as group independent component analysis (GICA) and probabilistic functional mode decomposition (PROFUMO) can also be used to identify RSNs within a rs-fMRI dataset (87,88). GICA and PROFUMO are considered exploratory model-free methods of blind source separation that can summarize the entire dataset without the need for experimenter input. GICA is regarded as the current standard data-driven blind source separation technique to decompose raw rs-fMRI data into components that are maximally spatially independent from one another, such that each individual piece of the data belongs to a single component (87). Recently, PROFUMO has also emerged as a data-driven tool to extract RSNs in groups and individuals with some advantages over GICA without the requirement for spatial independence (88). This advantage allows PROFUMO to capture multimodal brain regions in multiple spatial maps, which results in combinatory RSNs and representative RSN subnetworks that GICA could otherwise miss.

Another common approach in rs-fMRI functional connectivity analysis is to use an already established functional atlas to perform node-based network modeling. In this technique, the experimenter identifies regions of each RSN from an existing functional atlas within their own sample and examines the connections between them. When using a network modeling approach, it is important to consider the population demographics in which the functional atlas was created and determine if it is well-matched to the demographics of the current study. The majority of current functional atlases were defined based on young and healthy populations and are aligned a standard space that is also based on younger adults, such as MNI152 (11,13,14,89). While often used to study RSNs in older adults, these atlases do not account for age-related brain atrophy and changes in RSN connectivity (90–93). The second aim of this dissertation sought to provide a more age-appropriate solution to investigate the primary outcomes of the rrAD by creating a functional atlas that adequately describes RSN functional connectivity of older adults. To accomplish this, we performed a combination of hypothesis-

driven and data-driven approaches on the baseline rs-fMRI scans from the rrAD study in order to define a comprehensive set of RSNs. The RSN spatial maps of our functional atlas were defined in rrAD420 standard space, an MNI152-adjacent template that captures features of an aging brain such as ventricular enlargement and atrophy patterns. The rrAD420 space was created through SPM12's segmentation and non-linear DARTEL registration and derived from 420 rrAD subjects with good quality neuroimaging data (94).

This dissertation expands on current rs-fMRI methodology and presents a solution to better enable the study of hypertension and AD interplay on RSN functional connectivity. First, in Chapter 2, we examine the effects of multiple rest conditions with varying levels of cognitive load on RSN functional connectivity using the 17-network parcellation solution presented by Yeo and colleagues (14). Chapter 3 introduces the novel rrAD420 functional atlas and offers a detailed description of the methods used in its creation as well as the RSNs that were identified. Finally, chapter 4 discusses the future directions and direct applications of our contributions.

REFERENCES

1. Attwell D, Laughlin SB. An Energy Budget for Signaling in the Grey Matter of the Brain. 2001.
2. Nation DA, Sweeney MD, Montagne A, Sagare AP, D'Orazio LM, Pachicano M, et al. Blood–brain barrier breakdown is an early biomarker of human cognitive dysfunction. Nat Med. 2019 Feb 1;25(2):270–6.
3. Zlokovic B V. Neurovascular mechanisms of Alzheimer's neurodegeneration. Vol. 28, Trends in Neurosciences. Elsevier Ltd; 2005. p. 202–8.
4. Nippert AR, Biesecker KR, Newman EA. Mechanisms Mediating Functional Hyperemia in the Brain. Vol. 24, Neuroscientist. SAGE Publications Inc.; 2018. p. 73–83.
5. Iadecola C. Neurovascular regulation in the normal brain and in Alzheimer's disease. Vol. 5, Nature Reviews Neuroscience. Nature Publishing Group; 2004. p. 347–60.
6. Heeger DJ, Ress D. What does fMRI tell us about neuronal activity? Vol. 3, Nature Reviews Neuroscience. 2002. p. 142–51.
7. Ogawa S, Lee TM, Kay AR, Tank DW. Brain magnetic resonance imaging with contrast dependent on blood oxygenation (cerebral blood flow/brain metabolism/oxygenation) [Internet]. Vol. 87. 1990. Available from: https://www.pnas.org
8. Linden D, Prvulovic D, Formisano E, Vollinger M, Friedhelm Z, Goebel R, et al. The Functional Neuroanatomy of Target Detection: An fMRI Study of Visual and Auditory Oddball Tasks. Cerebral Cortex. 1999;9(8):815–23.
9. Biswal B, Zerrin Yetkin F, Haughton VM, Hyde JS. Functional connectivity in the motor cortex of resting human brain using echo-planar mri. Magn Reson Med. 1995;34(4):537–41.
10. Golanov E V, Yamamoto S, Reis DJ. Spontaneous waves of cerebral blood flow associated with a pattern of electrocortical activity. Journal of American Physiology. 1994;266:204–14.
11. Shirer WR, Ryali S, Rykhlevskaia E, Menon V, Greicius MD. Decoding subject-driven cognitive states with whole-brain connectivity patterns. Cerebral Cortex. 2012 Jan;22(1):158–65.
12. Fox MD, Raichle ME. Spontaneous fluctuations in brain activity observed with functional magnetic resonance imaging. Nature Reviews Neuroscience. 2007.
13. Damoiseaux J, Rombouts S, Scheltens P, Stam CJ, Smith SM, Beckmann CF. Consistent resting-state networks across healthy subjects. Proc Natl Acad Sci U S A [Internet]. 2006 [cited 2012 May 7];(2). Available from: http://www.pnas.org/content/103/37/13848.short
14. Yeo BT, Krienen FM, Sepulcre J, Sabuncu MR, Lashkari D, Hollinshead M, et al. The organization of the human cerebral cortex estimated by intrinsic functional connectivity. J Neurophysiol. 2011 Sep;106(3):1125–65.

15. Fox MD, Snyder AZ, Vincent JL, Corbetta M, Essen DC Van, Raichle ME. The human brain is intrinsically organized into dynamic, anticorrelated functional networks. Proc Natl Acad Sci U S A [Internet]. 2005 Jul;102(27):9673–8. Available from: http://dx.doi.org/10.1073/pnas.0504136102

16. Mazoyer B, Zago L, Mellet E, Bricogne S, Etard O, Houde O, et al. Cortical networks for working memory and executive functions sustain the conscious resting state in man. Brain Res. 2001;54(3):287–98.

17. Kilpatrick LA, Suyenobu BY, Smith SR, Bueller JA, Goodman T, Creswell JD, et al. Impact of mindfulness-based stress reduction training on intrinsic brain connectivity. Neuroimage [Internet]. 2011;56(1):290–8. Available from: http://dx.doi.org/10.1016/j.neuroimage.2011.02.034

18. Kawagoe T, Onoda K, Yamaguchi S. Different pre-scanning instructions induce distinct psychological and resting brain states during functional magnetic resonance imaging. European Journal of Neuroscience. 2018 Jan 1;47(1):77–82.

19. Patriat R, Molloy EK, Meier TB, Kirk GR, Nair VA, Meyerand ME, et al. The effect of resting condition on resting-state fMRI reliability and consistency: A comparison between resting with eyes open, closed, and fixated. Neuroimage. 2013 Sep;78:463–73.

20. Hurd MD, Martorell P, Delavande A, Mullen KJ, Langa KM. Monetary Costs of Dementia in the United States. New England Journal of Medicine. 2013 Apr 4;368(14):1326–34.

21. Nichols E, Steinmetz JD, Vollset SE, Fukutaki K, Chalek J, Abd-Allah F, et al. Estimation of the global prevalence of dementia in 2019 and forecasted prevalence in 2050: an analysis for the Global Burden of Disease Study 2019. Lancet Public Health. 2022 Feb 1;7(2):e105–25.

22. Brookmeyer R, Evans DA, Hebert L, Langa KM, Heeringa SG, Plassman BL, et al. National estimates of the prevalence of Alzheimer's disease in the United States. Alzheimer's and Dementia. 2011 Jan;7(1):61–73.

23. Association A. Alzheimer ' s disease facts and figures. 2013;12:459–509.

24. McKhann GM, Knopman DS, Chertkow H, Hyman BT, Jack CR, Kawas CH, et al. The diagnosis of dementia due to Alzheimer's disease: Recommendations from the National Institute on Aging-Alzheimer's Association workgroups on diagnostic guidelines for Alzheimer's disease. Alzheimer's and Dementia. 2011;7(3):263–9.

25. Serrano-Pozo A, Frosch MP, Masliah E, Hyman BT. Neuropathological alterations in Alzheimer disease. Cold Spring Harb Perspect Med. 2011 Sep;1(1).

26. Deture MA, Dickson DW. The neuropathological diagnosis of Alzheimer's disease. Vol. 14, Molecular Neurodegeneration. BioMed Central Ltd.; 2019.

27. Aisen PS, Cummings J, Jack CR, Morris JC, Sperling R, Frölich L, et al. On the path to 2025: Understanding the Alzheimer's disease continuum. Vol. 9, Alzheimer's Research and Therapy. BioMed Central Ltd.; 2017.

28. Petersen RC, Lopez O, Armstrong MJ, Getchius TSD, Ganguli M, Gloss D, et al. Practice guideline update summary: Mild cognitive impairment report of theguideline development, dissemination, and implementation. Neurology. 2018 Jan 1;90(3):126–35.

29. Slot RER, Sikkes SAM, Berkhof J, Brodaty H, Buckley R, Cavedo E, et al. Subjective cognitive decline and rates of incident Alzheimer's disease and non–Alzheimer's disease dementia. Alzheimer's and Dementia. 2019 Mar 1;15(3):465–76.

30. Schmand B, Jonker C, Hooijer C, Lindenboom J. Subjective Memory Complaints May Announce Dementia. Neurology . 1996;46(1):121–5.

31. Mitchell AJ, Beaumont H, Ferguson D, Yadegarfar M, Stubbs B. Risk of dementia and mild cognitive impairment in older people with subjective memory complaints: Meta-analysis. Acta Psychiatr Scand. 2014 Dec 1;130(6):439–51.

32. Pfannmöller J, Lotze M. Review on biomarkers in the resting-state networks of chronic pain patients. Brain Cogn. 2019 Apr 1;131:4–9.

33. Zhu DC, Covassin T, Nogle S, Doyle S, Russell D, Pearson RL, et al. A potential biomarker in sports-related concussion: Brain functional connectivity alteration of the default-mode network measured with longitudinal resting-state fMRI over thirty days. J Neurotrauma. 2015;32(5):327–41.

34. Wolf RC, Sambataro F, Vasic N, Depping MS, Thomann PA, Landwehrmeyer GB, et al. Abnormal resting-state connectivity of motor and cognitive networks in early manifest Huntington's disease. Psychol Med. 2014 Nov 12;44(15):3341–56.

35. Varangis E, Habeck CG, Razlighi QR, Stern Y. The Effect of Aging on Resting State Connectivity of Predefined Networks in the Brain. Front Aging Neurosci. 2019 Sep 4;11.

36. Simic G, Babic M, Borovecki F, Hof PR. Early failure of the default-mode network and the pathogenesis of Alzheimer's disease. Vol. 20, CNS Neuroscience and Therapeutics. Blackwell Publishing Ltd; 2014. p. 692–8.

37. Shulman G, Fiez J, Corbetta M, Buckner R, Miezin F, Raichle M, et al. Common Blood Flow Changes across visual Tasks: II. Decreases in Cerebral Cortex. J Cogn Neurosci. 1997;9(5):648–63.

38. Binder JR, Frost JA, Hammeke TA, Bellgowan PSF, Rao SM, Cox RW. Conceptual Processing during the Conscious Resting State: A Functional MRI Study. J Cogn Neurosci [Internet]. 1999;11(1):1–14. Available from: papers2://publication/uuid/4EB1DEEA-D766-4D1B-A36D-072AE45D2B3C

39. Buckner RL, Andrews-Hanna JR, Schacter DL. The brain's default network: Anatomy, function, and relevance to disease. Ann N Y Acad Sci. 2008;1124:1–38.

40. Ekhtiari H, Nasseri P, Yavari F, Mokri A, Monterosso J. Neuroscience of drug craving for addiction medicine: From circuits to therapies. In: Progress in Brain Research. Elsevier B.V.; 2016. p. 115–41.

41. Desgranges B, Mevel K, Chételat G, Eustache F. The default mode network in healthy aging and Alzheimer's disease. International Journal of Alzheimer's Disease. 2011.

42. Greicius MD, Menon V. Default-mode activity during a passive sensory task: Uncoupled from deactivation but impacting activation. J Cogn Neurosci. 2004;16(9):1484–92.

43. Grothe MJ, Teipel SJ. Spatial patterns of atrophy, hypometabolism, and amyloid deposition in Alzheimer's disease correspond to dissociable functional brain networks. Hum Brain Mapp. 2016;37(1):35–53.

44. Hohenfeld C, Werner CJ, Reetz K. Resting-state connectivity in neurodegenerative disorders: Is there potential for an imaging biomarker? Neuroimage Clin [Internet]. 2018;18(March 2018):849–70. Available from: https://doi.org/10.1016/j.nicl.2018.03.013

45. Sperling RA, LaViolette PS, O'Keefe K, O'Brien J, Rentz DM, Pihlajamaki M, et al. Amyloid Deposition Is Associated with Impaired Default Network Function in Older Persons without Dementia. Neuron. 2009 Jul 30;63(2):178–88.

46. Han F, Liu X, Mailman RB, Huang X, Liu X. Resting-state global brain activity affects early β-amyloid accumulation in default mode network. Nat Commun [Internet]. 2023 Nov 27;14(1):7788. Available from: https://www.nature.com/articles/s41467-023-43627-y

47. Scheel N, Tarumi T, Tomoto T, Cullum CM, Zhang R, Zhu DC. Resting-state functional MRI signal fluctuation amplitudes are correlated with brain amyloid-β deposition in patients with mild cognitive impairment. Journal of Cerebral Blood Flow and Metabolism. 2022 May 1;42(5):876–90.

48. Sharma N, Murari G, Vandermorris S, Verhoeff NPLG, Herrmann N, Chen JJ, et al. Functional Connectivity between the Posterior Default Mode Network and Parahippocampal Gyrus Is Disrupted in Older Adults with Subjective Cognitive Decline and Correlates with Subjective Memory Ability. Journal of Alzheimer's Disease. 2021;82(1):435–45.

49. Badhwar AP, Tam A, Dansereau C, Orban P, Hoffstaedter F, Bellec P. Resting-state network dysfunction in Alzheimer's disease: A systematic review and meta-analysis. Alzheimer's and Dementia: Diagnosis, Assessment and Disease Monitoring. 2017;8:73–85.

50. Li R, Wu X, Fleisher AS, Reiman EM, Chen K, Yao L. Attention-related networks in Alzheimer's disease: A resting functional MRI study. Hum Brain Mapp. 2012 May;33(5):1076–88.

51. Noh JH, Kim JH, Yang HD. Classification of Alzheimer's Progression Using fMRI Data. Sensors. 2023 Jul 1;23(14).

52. Guo H, Zhang Y. Resting State fMRI and Improved Deep Learning Algorithm for Earlier Detection of Alzheimer's Disease. IEEE Access. 2020;8:115383–92.

53. Yamashita KI, Uehara T, Taniwaki Y, Tobimatsu S, Kira JI. Long-Term Effect of Acetylcholinesterase Inhibitors on the Dorsal Attention Network of Alzheimer's Disease Patients: A Pilot Study Using Resting-State Functional Magnetic Resonance Imaging. Front Aging Neurosci. 2022 Apr 5;14.

54. Koch W, Teipel S, Mueller S, Benninghoff J, Wagner M, Bokde ALW, et al. Diagnostic power of default mode network resting state fMRI in the detection of Alzheimer's disease. Neurobiol Aging. 2012 Mar;33(3):466–78.

55. Long JM, Holtzman DM. Alzheimer Disease: An Update on Pathobiology and Treatment Strategies. Cell [Internet]. 2019;179(2):312–39. Available from: https://doi.org/10.1016/j.cell.2019.09.001

56. Santisteban MM, Iadecola C. Hypertension, dietary salt and cognitive impairment. Journal of Cerebral Blood Flow and Metabolism. 2018;38(12):2112–28.

57. De la Torre JC. Hemodynamic consequences of deformed microvessels in the brain in Alzheimer's disease. In: Annals of the New York Academy of Sciences. Blackwell Publishing Inc.; 1997. p. 75–91.

58. Suter OC, Sunthorn T, Kraftsik R, Straubel J, Darekar P, Khalili K, et al. Cerebral hypoperfusion generates cortical watershed microinfarcts in Alzheimer disease. Stroke. 2002;33(8):1986–92.

59. de la Torre J. The Vascular Hypothesis of Alzheimer's Disease: A Key to Preclinical Prediction of Dementia Using Neuroimaging. Vol. 63, Journal of Alzheimer's disease : JAD. NLM (Medline); 2018. p. 35–52.

60. Tini G, Scagliola R, Monacelli F, La Malfa G, Porto I, Brunelli C, et al. Alzheimer's Disease and Cardiovascular Disease: A Particular Association. Vol. 2020, Cardiology Research and Practice. Hindawi Limited; 2020.

61. Farnsworth Von Cederwald B, Josefsson M, Wåhlin A, Nyberg L, Karalija N. Association of Cardiovascular Risk Trajectory With Cognitive Decline and Incident Dementia. Neurology. 2022 May 17;98(20):E2013–22.

62. Ungvari Z, Toth P, Tarantini S, Prodan CI, Sorond F, Merkely B, et al. Hypertension-induced cognitive impairment: from pathophysiology to public health. Vol. 17, Nature Reviews Nephrology. Nature Research; 2021. p. 639–54.

63. Shang X, Hill E, Zhu Z, Liu J, Ge BZ, Wang W, et al. The Association of Age at Diagnosis of Hypertension With Brain Structure and Incident Dementia in the UK Biobank. Hypertension. 2021 Nov 1;78(5):1463–74.

64. Iadecola C, Gottesman RF. Neurovascular and Cognitive Dysfunction in Hypertension: Epidemiology, Pathobiology, and Treatment. Circ Res. 2019;124(7):1025–44.

65. Toth P, Tarantini S, Csiszar A, Ungvari Z. Functional vascular contributions to cognitive impairment and dementia: Mechanisms and consequences of cerebral autoregulatory dysfunction, endothelial impairment, and neurovascular uncoupling in aging. Am J Physiol Heart Circ Physiol. 2017;312(1):H1–20.

66. Dai W, Lopez OL, Carmichael OT, Becker JT, Kuller LH, Gach HM. Abnormal regional cerebral blood flow in cognitively normal elderly subjects with hypertension. Stroke. 2008;39(2):349–54.

67. Sierra C. Hypertension and the Risk of Dementia. Front Cardiovasc Med. 2020;7(January):1–7.

68. Pires PW, Dams Ramos CM, Matin N, Dorrance AM. The effects of hypertension on the cerebral circulation. Am J Physiol Heart Circ Physiol [Internet]. 2013;304:1598–614. Available from: http://ajpheart.physiology.org/.

69. Bu L, Huo C, Xu G, Liu Y, Li Z, Fan Y, et al. Alteration in brain functional and effective connectivity in subjects with hypertension. Front Physiol. 2018;9(MAY):1–12.

70. Greicius MD, Srivastava G, Reiss AL, Menon V, Raichle ME. Default-mode network activity distinguishes Alzheimer's disease from healthy aging: Evidence from functional MRI [Internet]. 2004. Available from: www.fmridc.org

71. Son SJ, Kim J, Lee E, Park JY, Namkoong K, Hong CH, et al. Effect of hypertension on the resting-state functional connectivity in patients with Alzheimer's disease (AD). Arch Gerontol Geriatr [Internet]. 2015;60(1):210–6. Available from: http://dx.doi.org/10.1016/j.archger.2014.09.012

72. Forette F. The Prevention of Dementia With Antihypertensive Treatment<subtitle>New Evidence From the Systolic Hypertension in Europe (Syst-Eur) Study</subtitle>. Arch Intern Med [Internet]. 2002 Oct 14;162(18):2046. Available from: http://archinte.jamanetwork.com/article.aspx?doi=10.1001/archinte.162.18.2046

73. Hsu CY, Huang CC, Chan WL, Huang PH, Chiang CH, Chen TJ, et al. Angiotensin-receptor blockers and risk of alzheimer's disease in hypertension population - A nationwide cohort study. Circulation Journal. 2013;77(2):405–10.

74. Cunningham E, Todd S, Passmore P, Bullock R, Mcguinness B. Pharmacological treatment of hypertension in people without prior cerebrovascular disease for the prevention of cognitive impairment and dementia (Review). 2021;

75. The SPRINT Research Group, Wright JT, Williamson JD, Whelton PK, Snyder JK, SinkS KM, et al. A Randomized Trial of Intensive versus Standard Blood-Pressure Control. New England Journal of Medicine. 2015;373(22):2103–16.

76. O'Connor PJ, Venkat Narayan KM, Anderson R, Feeney P, Fine L, Ali MK, et al. Effect of intensive versus standard blood pressure control on depression and health-related quality of life in type 2 diabetes: The ACCORD trial. Diabetes Care. 2012;35(7):1479–81.

77. Supiano MA, Williamson JD. New Guidelines and SPRINT Results: Implications for Geriatric Hypertension. Vol. 140, Circulation. Lippincott Williams and Wilkins; 2019. p. 976–8.

78. Williamson JD, Pajewski NM, Auchus AP, Bryan RN, Chelune G, Cheung AK, et al. Effect of Intensive vs Standard Blood Pressure Control on Probable Dementia: A Randomized Clinical Trial. In: JAMA - Journal of the American Medical Association. American Medical Association; 2019. p. 553–61.

79. Fox N, Warrington EK, Seiffer AL, Agnew SK, Rossor MN. Presymptomatic cognitive deficits in individuals at risk of familial Alzheimer's disease. Brain. 1998;121:1631–9.

80. Szabo-Reed AN, Vidoni E, Binder EF, Burns J, Cullum CM, Gahan WP, et al. Rationale and methods for a multicenter clinical trial assessing exercise and intensive vascular risk reduction in preventing dementia (rrAD Study). Contemp Clin Trials [Internet]. 2019;79(March):44–54. Available from: https://doi.org/10.1016/j.cct.2019.02.007

81. Dassanayake S, Sole G, Wilkins G, Skinner M. Exercise: a therapeutic modality to treat blood pressure in resistant hypertension. Physical Therapy Reviews [Internet]. 2020;25(3):149–58. Available from: https://doi.org/10.1080/10833196.2020.1733781

82. Juraschek SP, Blaha MJ, Whelton SP, Blumenthal R, Jones SR, Keteyian SJ, et al. Physical fitness and hypertension in a population at risk for cardiovascular disease: The Henry Ford ExercIse Testing (FIT) Project. J Am Heart Assoc. 2014;3(6):1–10.

83. Kim JM, Stewart R, Bae KY, Kim SW, Yang SJ, Park KH, et al. Role of BDNF val66met polymorphism on the association between physical activity and incident dementia. Neurobiol Aging [Internet]. 2011;32(3):551.e5-551.e12. Available from: http://dx.doi.org/10.1016/j.neurobiolaging.2010.01.018

84. Hashimoto M, Araki Y, Takashima Y, Nogami K, Uchino A, Yuzuriha T, et al. Hippocampal atrophy and memory dysfunction associated with physical inactivity in community-dwelling elderly subjects: The Sefuri study. Brain Behav. 2017;7(2):1–8.

85. García-Mesa Y, Pareja-Galeano H, Bonet-Costa V, Revilla S, Gómez-Cabrera MC, Gambini J, et al. Physical exercise neuroprotects ovariectomized 3xTg-AD mice through BDNF mechanisms. Psychoneuroendocrinology. 2014;45:154–66.

86. McDaniel MA, Binder EF, Bugg JM, Waldum ER, Dufault C, Meyer A, et al. Effects of cognitive training with and without aerobic exercise on cognitively demanding everyday activities. Psychol Aging. 2014;29(3):717–30.

87. Beckmann CF, Smith SM. Probabilistic Independent Component Analysis for Functional Magnetic Resonance Imaging. IEEE Trans Med Imaging. 2004;23(2):137–52.

88. Harrison SJ, Woolrich MW, Robinson EC, Glasser MF, Beckmann CF, Jenkinson M, et al. Large-scale probabilistic functional modes from resting state fMRI. Neuroimage. 2015 Apr 1;109:217–31.

89. Mazziotta J, Toga A, Evans A, Fox P, Lancaster J. A probabilistic Atlas of the Human Brain: Theory and Rationale for Its Development. The International Consortium for Brain Mapping (ICBM). 1995;2(2):89–101.

90. Damoiseaux JS. Effects of aging on functional and structural brain connectivity. Neuroimage. 2017 Oct 15;160:32–40.

91. Raz N, Gunning F, Head D, Dupuis J, McQuain J, Briggs S, et al. Selective Aging of the Human Cerebral Cortex Observed in Vivo: Differential Vulnerability of the Prefrontal Gray Matter. Cerebral Cortex. 1997;7(3):268–82.

92. Doucet GE, Labache L, Thompson PM, Joliot M, Frangou S. Atlas55+: Brain Functional Atlas of Resting-State Networks for Late Adulthood. Cerebral Cortex. 2021 Mar 1;31(3):1719–31.

93. Deery HA, Di Paolo R, Moran C, Egan GF, Jamadar SD. The older adult brain is less modular, more integrated, and less efficient at rest: A systematic review of large-scale resting-state functional brain networks in aging. Vol. 60, Psychophysiology. John Wiley and Sons Inc; 2023.

94. Ashburner J. A fast diffeomorphic image registration algorithm. Neuroimage. 2007 Oct 15;38(1):95–113.

APPENDIX

FIGURES

Figure 1.1: Schematic outlining intensive treatment steps to achieve target blood pressure of SBP ≤ 125 mmHg (Adapted from funded HIPAC parent grant).

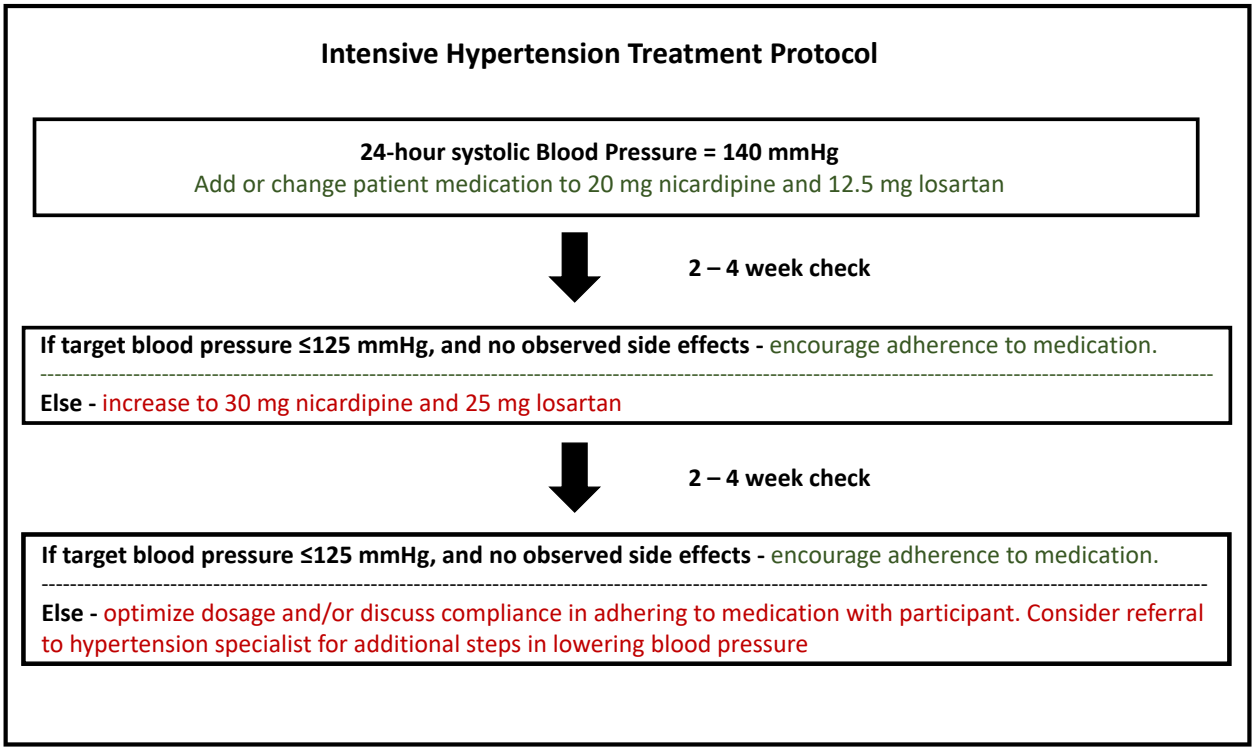

CHAPTER 2: FUNCTIONAL CONNECTIVITY OF CORTICAL RESTING-STATE NETWORKS IS DIFFERENTIALLY AFFECTED BY REST CONDITIONS

This chapter was adapted from: Fernandez, Z., Scheel, N., Baker, J. H., & Zhu, D. C. (2022). Functional connectivity of cortical resting-state networks is differentially affected by rest conditions. Brain Research, 1796, 148081. https://doi.org/10.1016/j.brainres.2022.148081

2.1 – Abstract

Optimal conditions for resting-state functional magnetic resonance imaging (rs-fMRI) are still highly debated. Here, we comprehensively assessed the effects of various rest conditions on all cortical resting-state networks (RSNs) defined by an established atlas. Twenty-two healthy college students (22 ± 4 years old, 12 females) were scanned on a GE 3T MRI scanner. Rs-fMRI datasets were collected under four different conditions for each subject: (1) eyes open in dim light (Eyes-Open), (2) eyes closed and awake (Eyes-Closed), (3) eyes closed while remembering four numbers through the scan session (Eyes-Closed-Number) and (4) asked to watch a movie (Movie). We completed a thorough examination of the 17 functional RSNs defined by Yeo and colleagues. Importantly, the movie led to changes in global connectivity and should be avoided as a rest condition. Conversely, there were no significant connectivity differences between conditions within the frontoparietal control and limbic networks and the following subnetworks as defined by Yeo et al.: default-*B*, dorsal-attention-*B* and salience/ventral-attention-*B*. These were not even significant when compared to the highly stimulative Movie condition. A significant difference was not found between Eyes-Closed and Eyes-Closed-Number conditions in whole-brain, within-network, and between-network comparisons. When considering other rest conditions, however, we observed connectivity changes in some subnetworks, including those of the default-mode-network. Overall, we found conditions with more external stimulation led to more changes in functional connectivity during rs-fMRI. In conclusion, the comprehensive results of our study can aid in choosing rest conditions for the study of overall and specific functional networks.

2.2 – Introduction

Resting-state functional MRI (rs-fMRI) measures low-frequency fluctuations (<0.1 Hz) of Blood-Oxygen-Level-Dependent (BOLD) signals in the brain in the absence of a task and is considered to capture the innate functional connectivity (functional connectivity) of the brain at rest (9). Rs-fMRI studies have revealed a consistent organization of distinct resting-state networks (RSNs) within the brain (12–14,94). Therefore, changes in RSN functional connectivity may be a measurable pathophysiologic change that could serve as a biomarker of various neurological disorders (33,95–99). Furthermore, rs-fMRI is instrumental for understanding brain functions in those who cannot perform specific tasks in task-based fMRI studies, such as pediatric populations or patients with Alzheimer's Disease (99,100).

While rs-fMRI is widely used, factors such as rest condition, scan length, and subject cardiovascular variability have been shown to impact the reliability of measures, including RSN connectivity (19,101,102). In this study, we specifically aim to address the effects of rest conditions on the functional connectivity of cortical RSNs. Examples of various conditions used in rs-fMRI studies include: (1) Ask subjects to keep their eyes open and look at a target (e.g., a fixation cross) (15,103). (2) Ask subjects to "close your eyes, think of nothing in particular, and do not fall asleep" or to simply close their eyes during scanning (13,16). (3) Request subjects to focus on the sounds of the scanner with their eyes closed to achieve a meditative state (17). (4) Watch a movie during scan acquisition for the benefit of minimizing subject motion, especially in children (104). With all the various approaches to rest conditions applied in prior studies, deciding on the most appropriate condition becomes challenging.

When choosing a rest condition, it is important to consider how condition-specific environmental stimulation, or the introduction of subtle tasks, could violate a true "resting state". For example, watching a movie may help to minimize subject motion, but it also introduces a continuously changing stimulus that can lead to dynamic alterations in RSN functional

connectivity (105–107). Similarly, requesting participants to intently focus on scanner noises with their eyes closed could affect the functional connectivity of the highly responsive auditory network (108).

Though variations in environmental stimulation between rest conditions are more subtle, compared to explicitly performing a task, previous work has shown that these differences may still invoke significant changes in observed RSN functional connectivity patterns (19,106,109). For example, Patriat and colleagues compared the rest conditions: eyes-closed, eyes-open, and eyes focused on a fixation cross. They demonstrated that the auditory, default-mode, and attentional networks were most reliably reproduced when subjects were instructed to focus on a fixation cross (19). Yan and colleagues also investigated changes between eyes-closed, eyes-open, and eyes-fixated rest conditions. They specifically assessed the functional connectivity of the default-mode network and found significant connectivity differences between rest conditions. Their results suggested that eyes-open rest conditions lead to more reproducible results of the default-mode network when compared to the eyes-closed rest condition (109). Kim and colleagues further expanded on these findings by comparing a movie-watching condition to an eyes-open rest condition. They found significant resting-state functional connectivity alterations at the global level as well as within the visual and attention networks of the Gordon-Lauman parcellation (106,110).

Prior studies, like those above, focused on only a few selected networks or conditions, leaving a need for a more comprehensive examination. Here, we investigated the effects of four rest conditions with varying levels of stimulation on functional connectivity of all cortical RSNs using the parcellation of Yeo and colleagues, in a demographically similar sample of young adults (14). Based on the rs-fMRI data from 1000 healthy young subjects, Yeo et al. divided the cerebral cortex into highly reproducible organizations of 7 “coarse” and 17 “fine-resolution” networks. Choosing the latter, Yeo’s 17 network parcellation, decreases the risk of averaging

time courses of large regions that may be significantly different, thereby reducing the risk of committing a Type II error (14,95). In this study, rs-fMRI datasets were acquired while subjects were asked to adhere to the following conditions:

(1) eyes open in a dim light (Eyes-Open condition),

(2) eyes closed and asked to stay awake (Eyes-Closed condition),

(3) eyes closed and asked to remember four numbers before the scan started (Eyes-Closed-Number condition); the subjects were also informed that they would be quizzed on the numbers after this sequence by responding on a keypad, and

(4) eyes open and asked to watch a movie clip from *Finding Nemo* (Movie condition).

We mainly evaluated the effects of different rest conditions on 1) the global average within-network functional connectivity, 2) each of Yeo's 17 distinct RSNs, and 3) the individual node-to-node connections within each RSN. We conducted the investigation following a top-down systematic approach. Specifically, we first analyzed if the different rest conditions could drive a significant global connectivity difference. After we found a difference at the global level, we investigated which networks drove the global differences. After a network was found to be affected by the rest conditions, we further elucidated the connection(s) that drove the connectivity differences within that network. To supplement this main evaluation, we also investigated the whole-brain and between-network functional connectivity. With these comprehensive evaluations, we aimed to gain a more complete understanding of the effect of different conditions on functional connectivity stability throughout the cortex. We hypothesize that the functional connectivity of all cortical RSNs is differentially susceptible to varying levels of environmental stimulation. The RSNs that will likely experience connectivity alterations are those that play a role in the attentional, auditory, or visual information processing (14,19,106). For the readers' reference the 17 RSNs from Yeo's work, as well as the regions of each RSN, are listed in Figure 2.1. Additionally, the reader will find a brief overview of these 17 networks and their function below.

2.2.1 – Frontoparietal Control Network (FPN)

Control-*A*, -*B,* and -*C* resemble subnetworks of the FPN. The FPN spans frontal, parietal, and cingulate regions of the brain that have been associated with executive functions (95,111). Prior work has shown that this network is most active while performing a wide range of novel tasks (112). In addition, Cole and colleagues show that FPN regions further accommodate ongoing tasks by adjusting global functional connectivity to better meet current cognitive demands.

2.2.2 – Default-Mode Network (DMN)

Default-*A*, -*B,* and -*C* resemble subnetworks of the DMN. Of these three subnetworks, Default-*A* contains the classically labeled DMN regions such as the prefrontal cortex, posterior cingulate cortex, and angular gyri (38,39). The DMN was discovered in task-based fMRI, presenting as negatively correlated activation (12,15). The DMN has since been associated with the internal processing of self-relevant information and preparation for future cognitive tasks (39).

2.2.3 – Dorsal Attention Network (DAN)

Dorsal-attention-*A* and -*B* describe subnetworks of the DAN. The DAN is comprised of frontal and parietal regions involved in goal-directed processing related to visual attention (113). Specifically, the DAN includes the frontal eye fields, superior parietal lobule, and intraparietal sulcus (14,113,114).

2.2.4 – Limbic Network

Limbic-orbitofrontal and limbic-temporal-pole resemble subnetworks of the limbic network. The limbic network is a key component in emotional processing (115–117). The limbic-orbitofrontal subnetwork is comprised of two contralateral orbitofrontal regions, while the limbic-

temporal-pole subnetwork is composed of two contralateral temporal pole regions. The orbitofrontal cortex is suggested as a crucial region for limbic valence by associating an emotional value with experiences and reinforcing beneficial behaviors (118–120). Neuroimaging studies have further supported this claim, revealing deactivation of the medial orbitofrontal cortex in subjects that experienced both a psychological stressor and a subsequent significant increase in the stress hormone cortisol (121). In contrast, a comprehensive examination of the temporal pole region by Olson et al. (2007) suggests that its role involves facilitating the pairing of emotional responses to visual and auditory sensory information that has already been thoroughly processed by the brain.

2.2.5 – Salience/Ventral Attention Network (VAN)

The subnetworks labeled as salience/ventral-attention-*A* and -*B* closely resemble the salience network and VAN respectively (122,123). Subcortical regions were not included in Yeo's network parcellation, explaining this grouping of subnetworks (14). Regions of the salience network and VAN that were included overlap, and thus were grouped in this parcellation.

The salience network, mostly represented by salience/ventral-attention-*A*, partially overlaps with the VAN but also includes multiple subcortical and limbic regions such as the amygdala, medial thalamus, hypothalamus, and ventral tegmental area (122). Seeley proposes that the salience network is involved in the integration of emotion with highly processed sensory data to assist in goal-oriented decision-making.

The VAN, resembled by salience/ventral-attention-*B,* is functionally complementary to the DAN and is comprised of the temporoparietal junction and regions of the ventral, frontal, and parietal cortex (123). These regions are collectively associated with directing attention to stimuli outside the scope of the task at hand (Corbetta and Shulman, 2002; Farrant and Uddin, 2015;

Shulman et al., 2002). Shulman's study demonstrates its activity is highly dependent on the specific nature of the task at hand. The importance of considering the VAN independently from the DAN has been highlighted in other previous works due to the suspected differences in resting-state functional connectivity of these two networks (124).

2.2.6 – Somatomotor Network

Somatomotor-*A* and -*B* are subnetworks of the somatomotor network (125). The somatomotor network includes the primary and secondary motor areas, as well as the insula. It functions in the planning and execution of body movements (125–127).

2.2.7 – Auditory Network

Within the 17 networks, the temporal-parietal network resembles a subnetwork of the auditory network, which includes cortical auditory regions that are crucial for processing language and other auditory information (128). The left and right temporal-parietal regions encompass the auditory cortices and the single bilateral connection between these two regions makes up the temporal-parietal network (14). Furthermore, this network has been implicated in directing auditory attention when selective listening is required (129). Hence, its connectivity could be influenced by acoustic scanner noises (130).

2.2.8 – Visual Network

Visual-central and visual-peripheral are subnetworks of the visual network. Task-based fMRI studies have shown the visual cortex to be functionally organized into the visual central network, associated with the visual processing of detailed objects (e.g., faces), and the visual-peripheral network, associated with processing less detailed images of larger objects (e.g., buildings) (131). As visual RSN connectivity fluctuations occur even in complete darkness, slight changes in environmental stimulation could also show an influence on the visual network functional connectivity (132).

2.3 – Results

In this study, Eyes-Open, Eyes-Closed, Eyes-Closed-Number, and Movie conditions were compared in 22 healthy college students. For all statistical analyses, the threshold of significance was set at $p \leq 0.05$. Unless indicated otherwise, the p values shown in the Results section are after Bonferroni correction for multiple comparison. Repeated-measures ANOVA (RM-ANOVA) revealed that the global average of the absolute between-node connectivity (representing whole-brain connectivity), the global average within-network connectivity, as well as the connectivity of 9 individual RSNs, were significantly affected by rest conditions (Table 2.1). Furthermore, RM-ANOVA confirmed that our findings were not driven by the differences in motion between conditions. The Movie condition invoked a significant decrease in average within-network connectivity when compared to all other conditions. The paired *t*-tests further revealed significant differences in connectivity between conditions in the 9 RSNs found significantly affected by the rest conditions based on RM-ANOVA. No significant differences were found between conditions that required the subjects to keep their eyes closed (Eyes-Closed vs Eyes-Closed-Number) in any pairwise comparison. Connections between regions of significant networks were visualized for each condition using the BrainNet Viewer software package, except for the somatomotor-*A* and temporal-parietal subnetworks which each only contains one connection (133) (Figures 2.2, 2.3, and 2.4). For detailed information on significant connections of each network refer to Table S2.1-S2.6 in the Supplementary Materials. RM-ANOVA and the paired t-tests also revealed significant effect of the rest conditions on the between-network connectivity. Interesting, no significant difference was found between Eyes-Closed and Eyes-Closed-Number conditions. Detailed information regarding the between-network analyzes can be referred to Figure S2.1 in the Supplementary Materials. Below the reader will find our results specific to each network.

2.3.1 – Frontoparietal Control Network (FPN)

Analyzing the FPN subnetworks, RM-ANOVA did not reveal significant functional connectivity differences, in control-*A, -B,* or *-C* subnetworks (Table 2.1). However, there was a trend level difference ($p = 0.008$ before Bonferroni correction) in control-*A* subnetwork functional connectivity (Table 2.1).

2.3.2 – Default-Mode Network (DMN)

A significant difference in functional connectivity was revealed for the default-*A* subnetwork shown in Table 2.1 ($p \leq 0.001$). Network-level pairwise comparisons revealed a significant decrease in functional connectivity when the Movie condition was compared to Eyes-Closed ($p = 0.013$), Eyes-Open ($p \leq 0.001$), and Eyes-Closed-Number conditions ($p \leq 0.001$). We also observed a significant decrease when the Eyes-Closed condition was compared to the Eyes-Open condition ($p = 0.012$). We further observed differences in eight connections when the Eyes-Open condition was compared to the Movie condition and identified differences in five connections when the Eyes-Closed-Number condition was compared to the Movie condition (Figure 2.2; Table S2.1). The RM-ANOVA did not show a difference in default-*B* subnetwork connectivity between conditions (Table 2.1). However, statistical significance was reached in the RM-ANOVA for the default-*C* subnetwork ($p < 0.001$), with between-condition pairwise comparisons identifying significant connectivity differences when the Movie condition was compared to Eyes-Open ($p = 0.042$) and Eyes-Closed-Number ($p = 0.019$) conditions (Table 2.1).

2.3.3 – Dorsal Attention Network (DAN)

RM-ANOVA revealed a significant difference between conditions in the connectivity of the dorsal-attention-*A* subnetwork, see Table 2.1 ($p < 0.001$). In this subnetwork, a significant difference in pairwise comparisons was found in the Eyes-Open condition versus both Eyes-

Closed-Number ($p < 0.001$) and Eyes-Closed conditions ($p = 0.005$). Additionally, our results show that the Movie condition did not significantly differ from any other condition for this network (Table 2.1). We observed three connections exhibiting a difference in the comparison between Eyes-Open and Eyes-Closed, as well as five connections driving the connectivity changes seen between Eyes-Open and Eyes-Closed-Number conditions (Figure 2.2; Table S2.2). However, RM-ANOVA revealed significant changes in functional connectivity of the dorsal-attention-*B* subnetwork across conditions (Table 2.1).

2.3.4 – Limbic Network

RM-ANOVAs did not reveal significant differences in either the limbic-temporal-pole or limbic-orbitofrontal subnetworks between conditions (Table 2.1).

2.3.5 – Salience/Ventral Attention Network

Significant differences ($p \leq 0.001$) in connectivity in the salience/ventral-attention-*A* subnetwork were observed between conditions (Table 2.1). Subsequent pairwise comparisons further revealed significantly lower connectivity when watching a movie compared to the Eyes-Open ($p < 0.001$), Eyes-Closed ($p < 0.001$), and Eyes-Closed-Number ($p \leq 0.002$) conditions (Figure 2.3; Table S2.3). Functional connectivity in Eyes-Open, Eyes-Closed, and Eyes-Closed-Number conditions did not differ significantly for this subnetwork (Table 2.1). Of the three, Eyes-Closed-Number had the fewest connections that differed from the Movie condition, with five connections driving the observed differences (Table S2.3). Moreover, Eyes-Open vs Movie and Eyes-Closed vs Movie had 11 and 13 significant connections respectively (Table S2.3). Additionally, RM-ANOVA showed a trend level difference ($p = 0.005$ before Bonferroni correction) in salience/ventral-attention-*B* subnetwork functional connectivity (Table 2.1).

2.3.6 – Somatomotor Network

Functional connectivity was significantly different in the somatomotor-*A* subnetwork between conditions ($p = 0.002$). We observed significantly decreased subnetwork connectivity in the Movie condition compared to the Eyes-Open ($p = 0.02$), Eyes-Closed ($p = 0.005$) and Eyes-Closed-Number ($p = 0.002$) conditions (Table 2.1). RM-ANOVA also revealed a similar effect in the somatomotor-*B* subnetwork throughout conditions ($p \leq 0.001$). The somatomotor-*B* subnetwork shows a significant decrease in connectivity in the Movie condition compared to the Eyes-Closed and Eyes-Closed-Number conditions ($p \leq 0.001$) (Table 2.1). We observed 15 connections that significantly drove differences between the Movie and Eyes-Closed conditions, and 14 that drove the differences observed when comparing the Movie and Eyes-Closed-Number conditions (Figure 2.3; Table S2.4). Additionally, we found significantly decreased connectivity in the somatomotor-*B* subnetwork in the Eyes-Open condition compared to the Eyes-Closed condition ($p = 0.004$). As shown in Table S2.4, this was mostly driven by the connection between the left central sulcus and right auditory region ($p = 0.014$), however, there was a trend level effect between the left auditory and left central sulcus ($p = 0.09$).

2.3.7 – Auditory Network

We observed significant differences in temporal-parietal subnetwork connectivity across conditions ($p = 0.002$). Pairwise comparisons of network connectivity revealed a significant increase in the Movie condition compared to the Eyes-Open condition ($p \leq 0.001$) (Table 2.1). We also observed a slight increase in connectivity in both Eyes-Closed and Eyes-Closed-Number conditions relative to Eyes-Open. However, these comparisons did not reach significance following Bonferroni correction.

2.3.8 – Visual Network

RM-ANOVA revealed a significant difference in the visual-central subnetwork across conditions ($p \leq 0.001$). Pairwise comparisons showed its connectivity to be significantly higher in the Eyes-Open condition compared to the Movie ($p = 0.001$) and Eyes-Closed ($p = 0.007$) conditions (Table 2.1). One connection, between the right striate and right extrastriate, was found to drive the significant differences observed in the visual-central subnetwork between the Eyes-Open and Eyes-Closed conditions (Figure 2.4; Table S2.5). Comparing Eyes-Open to the Movie condition, we observed increased subnetwork functional connectivity of the Eyes-Open condition, which was driven by three individual connections (Table S2.5). Of these, two bilateral connections of the visual-central subnetwork were shown to significantly decline in connectivity in the Movie condition compared to Eyes-Open; these included the connections between the left and right striate cortices ($p \leq 0.001$) and between the left and right extrastriate regions ($p \leq 0.001$).

Finally, our analyses demonstrated a significant difference in the visual-peripheral subnetwork between conditions ($p = 0.001$). Pairwise comparisons revealed a significant decrease in average subnetwork functional connectivity in the Movie condition compared to Eyes-Open conditions ($p = 0.004$), Eyes-Closed ($p = 0.021$), and Eyes-Closed-Number ($p = 0.001$) (Table 2.1). Comparing the Eyes-Open and Movie conditions revealed the most connections with significant changes in functional connectivity (Figure 2.4; Table S2.6). The bilateral connection between the left and right striate of the visual-peripheral subnetwork was especially susceptible to changes in resting-state connectivity, showing significance in all comparisons other than Eyes-Closes versus Eyes-Closed-Number (Table S2.6). Connections between left and right inferior extrastriate ($p \leq 0.001$), as well as left superior extrastriate and right superior extrastriate ($p \leq 0.001$), were significantly increased during the Eyes-Closed-Number condition exclusively when compared to the Movie condition (Table S2.6).

2.4 – Discussion

In this study, we compared the effect of four different rest conditions (Eyes-Closed, Eyes-Closed-Number, Eyes-Open, and Movie) on functional connectivity measures. Each condition carried varying levels of cognitive load, which allowed for the investigation of network-specific susceptibility to environmental stimuli. We carried out comprehensive analyses on all cortical RSNs using Yeo's 17 network parcellation, and below we discuss the observed changes in global connectivity as well as each RSN (14).

2.4.1 – Overall Connectivity

The global average of absolute between-node connectivity, global average of within-network connectivity and between-network connectivity were all significantly affected by rest conditions. The Movie condition in general showed more effect on functional connectivity than other conditions. The Movie condition showed a significant average within-network decrease in functional connectivity relative to Eyes-Open, Eyes-Closed, and Eyes-Closed-Number conditions. This finding is consistent with a recent study showing that movie-watching can change the functional organization of whole-brain connectivity (106). Kim and colleagues concluded that in a movie condition, functional connections of RSNs are reorganized to form new connections involving brain regions that are more adherent to the cognitive demands of movie-watching. None of the other three conditions elicited a significant change in global average of absolute between-node connectivity and global average within-network connectivity when compared to one another. This suggests that whole-brain and global average within-network resting-state connectivity is relatively stable throughout rest conditions unless excessive stimulation is present. Based on this result, watching a movie during rs-fMRI can lead to large variations in RSN connectivity overall, which violates the pretense of a "rest" condition.

2.4.2 – Frontoparietal Control Network (FPN)

Although it did not reach significance, control-*A* connectivity was slightly decreased while movie-watching, which could be explained by the FPN's role in mediating activity between the dorsal attention network and the DMN in the presence of excess external stimulation (134). However, control-*B* and -*C* subnetworks were shown to be relatively unaffected by changes in rest conditions, as their connectivity pattern did not seem to be significantly influenced by the condition.

2.4.3 – Default-Mode Network (DMN)

In Yeo's network parcellation, the default-*A* subnetwork is most like the commonly recognized DMN. A decrease in connectivity was expected in this subnetwork as the subject's focus was diverted from self to the surrounding external stimuli. Indeed, we show several connections drive lower subnetwork connectivity in the Movie condition compared to the Eyes-Closed, Eyes-Closed-Number, and Eyes-Open conditions. The changes in default-*A* connectivity appear to be mainly attributed to the long-range anterior-posterior connections, with the largest decrease occurring when the Movie was compared to every other condition (Figure 2.2; Table S2.1). This finding is consistent with previous studies regarding event-related, task-induced deactivation of this network (15,39). Additionally, we show a slight increase in default-*A* subnetwork functional connectivity in the Eyes-Open condition compared to the Eyes-Closed condition (Table 2.1). This finding would suggest our observations are similar to existing literature, which showed an Eyes-Open condition to be well-suited to capture the default-mode connectivity (19,109). Looking at the functional connectivity of Yeo's default-*B* subnetwork, it seems to be largely unaffected by the differences between conditions tested here. Whereas Yeo's default-*C* subnetwork displays connectivity changes in the Movie condition compared to the Eyes-Open and Eyes-Closed-Number conditions. The changes in subnetwork connectivity across conditions suggest some level of susceptibility of default-*C* to connectivity alterations and

should warrant caution for future studies on the amount of external stimulation present in the rest condition.

2.4.4 – Dorsal Attention Network (DAN)

The changes in dorsal-attention-*A* connectivity between conditions appear to be mainly attributed to the interhemispheric connections, with the largest decrease occurring in both Eyes-Closed and Eyes-Closed-Number when compared to the Eyes-Open condition (Figure 2.2; Table S2.2). Our data demonstrated that connectivity was impacted mostly by whether subjects had their eyes open, with both eyes-closed conditions eliciting a significant decrease in network connectivity. There also appeared to be a slight increase in connectivity in the Movie condition relative to both the Eyes-Closed and Eyes-Closed-Number conditions, though not reaching significance. Overall, our results support previous findings that show DAN resting-state functional connectivity differences between Eyes-Open and both eyes-closed conditions (19).

However, there was no significant difference in functional connectivity of the dorsal-attention-*B* subnetwork between conditions. This may be due to the lack of an engaging task resulting in stable connections between regions of this subnetwork throughout conditions (113). Here, the Movie condition did not elicit significant connectivity alterations when compared to any other condition in either of the DAN subnetworks. This differs from recent work which showed the DAN to functionally reorganize to accommodate movie-watching and could be due to differences in parcellation strategies (106).

2.4.5 – Limbic Network

The differences in environmental stimulation between conditions were not found to drive significant alterations in the limbic subnetworks. This finding could be explained by the fact that the current study did not include conditions with a task that would invoke emotion strong enough to drive changes in RSN connectivity within our demographic (115,121,135). It is also important

to note that each limbic subnetwork only contains a single bilateral connection in Yeo's parcellation, which limits a fine-grained analysis of this network and thus may have impacted the results.

2.4.6 – Salience/Ventral Attention Network (VAN)

The changes in salience/ventral-attention-A connectivity between conditions appear to be mainly attributed to the interhemispheric connections, with the largest decrease occurring when the Movie was compared to every other condition (Figure 2.3; Table S2.3). This is consistent with previous findings, which show salience network connectivity to be highly impacted by movie-watching (136).

Although comparisons did not reach significance, the salience/ventral-attention-*B* subnetwork presented a similar trend (p = 0.005 before Bonferroni correction) in functional connectivity as salience/ventral-attention-*A* between conditions. This could be explained by the partially overlapping functions between these subnetworks (122). The trend-level decrease in functional connectivity of salience/ventral-attention-*B* in the Movie condition compared to other conditions may suggest that movie-watching violated the "rest" requirement. A follow-up investigation of the interaction between VAN functional connectivity and eye movements could bring more clarity(137). Overall, our findings warrant caution on the effects of movie-watching on RSN functional connectivity of both the salience network and the VAN.

2.4.7 – Somatomotor Network

The somatomotor-*A* subnetwork exhibits decreased connectivity in the Movie condition relative to Eyes-Open, Eyes-Closed, and Eyes-Closed-Number conditions. While somatomotor-*A* is comprised of only a single connection between the left and right central sulci, its connectivity appears susceptible to alterations in conditions with higher levels of environmental stimulation. In the Movie condition, subjects seemed to be more focused on the movie, rather than their body

position or action planning, which presumably lead to decreased somatomotor subnetwork functional connectivity (127,138). These connectivity differences can be further explained by a restructuring of functional network organization to better suit the processing of actions presented on the screen in the Movie condition (106).

The functional connectivity alterations we observed in the somatomotor-*B* subnetwork can be explained by a similar rationale. This subnetwork exhibited decreased connectivity in most connections in the Movie condition compared to both the Eyes-Closed and Eyes-Closed-Number conditions, as well as relatively higher connectivity when the Eyes-Closed was compared to the Eyes-Open condition (Figure 2.3; Table S2.4). Previous work has shown that when subjects close their eyes, they are likely to imagine voluntary movements, or plan to make movements, which can stimulate regions of the somatomotor-*B* subnetwork, such as the secondary somatosensory cortical region (139). We observe decreased somatomotor-*B* subnetwork connectivity in the Movie condition compared to the Eyes-Closed and Eyes-Closed-Number conditions. Additionally, the somatomotor-*B* subnetwork had the most connections of any network that were significantly affected by differences between conditions.

However, one difference between the somatomotor-*A* and -*B* subnetworks was that connectivity in the Eyes-Open condition compared to Eyes-Closed was significantly reduced for somatomotor-*B* (Table 2.1). This difference was driven by increased connectivity between the left central sulcus and right auditory regions in the Eyes-Closed condition (Figure 2.3; Table S2.4). Overall, our findings confirm and expand on previous research that shows the somatomotor subnetwork's susceptibility to decreased connectivity in the Movie condition compared to rest conditions with closed eyes, as well as lower connectivity in somatomotor-*B* in Eyes-Open relative to Eyes-Closed conditions (19,106).

2.4.8 – Auditory Network

In concordance with current literature, it was expected that the audio presented during the movie would invoke increased connectivity of auditory regions compared to the other rest conditions (106,108). Congruently, we observed significantly stronger connectivity of the temporal-parietal subnetwork in the Movie condition compared to the Eyes-Open condition. This recapitulates the findings of Kim et al. comparing RSN connectivity while movie-watching to an eyes-open rest condition (106). However, the same effect was not revealed comparing the Movie condition with the Eyes-Closed and Eyes-Closed-Number conditions. The observed higher auditory connectivity in both eyes-closed conditions compared to Eyes-Open was consistent with the previously reported by Patriat and colleagues (2013). While this difference was not significant in the current study, the slight increase could be attributed to subjects more intently focusing on the sounds of the scanner when their eyes were closed (17,130). Nonetheless, the slightly increased connectivity in both eyes-closed conditions lacks significance in pairwise comparisons involving the high-connectivity levels seen in the Movie condition. Overall, our results expand on the findings of Kim et al., showing a significant effect of movie-watching on the auditory network compared to the Eyes-Open condition, however not reaching significance compared to Eyes-Closed and Eyes-Closed-Number conditions (106).

2.4.9 – Visual Network

There were two significant differences in functional connectivity of Yeo's visual-central subnetwork comparing the different conditions. First, in line with Patriat's findings on the visual RSN, there was an increase in visual-central subnetwork connectivity, mainly due to the stronger anterior-posterior connections (Figure 2.4; Table S2.5), in the Eyes-Open condition compared to the Eyes-Closed condition (19). Second, we identified a significant decrease in this subnetwork connectivity in the Movie condition compared to the Eyes-Open condition. This corroborates the findings of Kim et al., as the decreased visual-central subnetwork connectivity in the Movie

condition could be indicative of network adaptations to better meet the cognitive demands of natural vision (106).

In addition to processing images of the human body, it has been shown that regions of the extrastriate cortex may be involved in the planning of body movements as part of dorsal visuomotor processing (138,140). Here, this effect seemed to be evident in the visual-peripheral subnetwork, as its connectivity alteration between conditions was similar to connectivity changes observed with the somatomotor-*A* subnetwork (Table 2.1). As such, visuomotor processing may have been impacted as the extrastriate cortex regions appeared to be the primary driver for changes seen in the visual-peripheral subnetwork (Table S2.6). Specifically, we found significantly decreased connectivity in the Movie condition, mainly due to the weaker interhemispheric connections (Figure 2.4; Table S2.6), compared to Eyes-Open, Eyes-Closed, and Eyes-Closed-Number conditions. No other comparison between Eyes-Open, Eyes-Closed, and Eyes-Closed-Number conditions revealed a difference in visual network connectivity, which further resembled the results of the somatomotor-*A* subnetwork. This could potentially be a result of an attentional shift to the movie rather than planning body movements in the Movie condition and should be addressed in further studies. Overall, given the observed connectivity differences between the visual-peripheral and the visual-central subnetworks between conditions, visual subnetworks should be investigated separately (131,140).

2.4.10 – General Discussion/Summary

Overall, whole-brain and within-network functional connectivity was affected most by the Movie condition compared to every other condition. Importantly, each of our scans was completed in a single session which allowed for our investigation of individual RSN stability between conditions. Some subnetworks (control-*A*, control-*B*, control-*C*, default-*B*, dorsal-attention-*B*, limbic-orbitofrontal, limbic-temporal-pole, and salience/ventral-attention-*B*)

demonstrate connections that are less susceptible to changes between rest conditions, including the Movie condition.

The remaining networks (default-*A*, default-*C*, dorsal-attention-*A*, salience/ventral-attention-*A*, somatomotor-*A*, somatomotor-*B*, temporal-parietal, visual-central, and visual-peripheral) were significantly altered between conditions in unique ways that may be explained by their specific functions. We confirm and expand upon previous findings by utilizing the complete cortical parcellation presented in Yeo's work (14,19,106). We corroborate that Eyes-Open and Eyes-Closed conditions yield functional connectivity profiles that differ in subnetworks of DMN, DAN and visual RSNs (19). We show the only subnetworks to elicit higher levels of connectivity in either eyes-closed condition relative to the Eyes-Open condition were the somatomotor-*B* subnetwork, as well as the temporal-parietal subnetwork, although only at the trend level (Tables 2.1 and S2.5). Both subnetworks contained auditory regions (Figure 2.1), which reproduces prior reports that auditory RSN exhibit relatively higher levels of connectivity in eyes-closed rest conditions (19).

There can be a general concern that differential mental processing occurs during the full rs-fMRI scan, which may lead to differential functional connectivity effects. To address this concern, we equally split the time course of each node, and conducted paired t-tests between the first and second halves of the resting-state scans for each network. We found no significant functional connectivity differences in any of the Yeo's 17 networks in any condition. While these divided time courses are rather short for reliable functional connectivity estimations, these non-significant findings strengthen our primary results. There also can be a concern of possible cross-over effects from a prior scanning condition. This possibility is much reduced with our experimental procedure. There were 1-min breaks before and between the 7-min rs-fMRI scans, with each scan at one rest condition. During the breaks, the MR operator verbally asked the subject to relax and press the button if he/she was ready for the new scan. This intervention

from the MR operator reduced the possible cross-over effects of movie-watching or the number remembering task.

A highlight of the findings is that no significant differences were found between Eyes-Closed-Number and Eyes-Closed conditions in whole-brain functional connectivity, global average within-network functional connectivity, and functional connectivity in all individual 17 networks as well as between-network functional connectivity. These non-significant findings suggest that internal cognitive process, including random and specific thoughts and memory rehearsal, will not affect functional connectivity. A follow-up study with a longer string of numbers can be interesting to understand the effect of memory rehearsal. On the other hand, the 4-number string has already placed a reasonable demand on memory rehearsal. Based on subject responses, all engaged in memory rehearsal. The non-significant findings in all comparisons let us speculate that a longer string of numbers will not significantly change the functional connectivity.

In our supplementary analyses, some individual between-network functional connectivity was also found significantly affected by rest conditions, suggesting a change of relationship between networks. Specific functional connectivity differences have been shown while watching a movie compared to an eyes-open rest condition (106). Moreover, a recent study has found that the affective experience of movie-watching can evoke altered connectivity patterns that are influenced by subject partiality toward the movie (141). Thus, between-subject variability in RSN connectivity is expected in movie conditions, although this was not explored in the present study. We did observe functional connectivity patterns that could be indicative of subnetwork interaction in some comparisons between conditions. Indeed, we observed a slight increase in mean connectivity of dorsal-attention-*A* along with a decrease in default-*A* when comparing the movie condition with both Eyes-Closed and Eyes-Closed Number conditions, a phenomenon

similarly reported by Fox et al., 2005 (Table 2.1). This finding may highlight the opposing roles of DAN and DMN when processing external stimulation.

Additionally, the visual-central subnetwork appears to operate in contrast to the temporal-parietal subnetwork. To illustrate, in comparisons with the Movie condition with the Eyes-Open condition we observe opposing changes of functional connectivity in the temporal-parietal and visual-central subnetworks. This seemingly represents a compensatory decrease in visual-central subnetwork connectivity to accommodate an attentional shift to the movie dialogue (Table 2.1). Finally, we observed slightly increased temporal-parietal subnetwork connectivity in both the Eyes-Closed and Eyes-Closed-Number conditions relative to Eyes-Open, which may represent the shift in subject focus to acoustic scanner noise in eyes-closed conditions. Similarly, the increase in visual-central subnetwork functional connectivity in Eyes-Open versus the Eyes-Closed condition may represent shifts in attention from visual input (e.g., fixation cross) to background auditory input in the Eyes-Open condition. In future studies, it may be beneficial to ask subjects to recall what they focused on to disentangle these subnetwork relationships.

2.4.11 – Study Limitations

While we attempted a comprehensive evaluation of all cortical networks based on the reliable cerebral cortical parcellation by Yeo and colleagues (14), Yeo's networks excluded subcortical regions and the cerebellum. The inclusion of subcortical regions could provide a more thorough understanding of RSN functional connectivity between rest conditions. Another limitation is the potential effect of rest condition sequence on functional connectivity. Future studies may want to compare the effects of condition order on functional connectivity. Finally, the number of conditions to evaluate in the current study was limited by potential subject fatigue. The comparison between Eyes-Open-Number and Eyes-Open conditions could also provide an interesting insight. However, to reduce subject fatigue, we decided to only compare the Eyes-Closed-Number with the Eyes-Closed condition. This choice also reduced the potential variation

of external visual stimulation that could not be controlled when the eyes were open. We speculate that internal processes, such as random thoughts and specific memory rehearsal, would not affect the functional connectivity, regardless of if subjects have their eyes open or closed.

2.4.12 – Conclusions

Overall, conditions that provide more external stimulation during resting-state fMRI will lead to more changes in connectivity. Watching a movie can lead to global changes in fMRI connectivity and should be avoided as a rest condition. The other conditions (Eyes-Open, Eyes-Closed, and Eyes-Closed-Number) did not show significant differences between one another at the average within-network level, but some variation did exist at the individual network level. We did not find significant differences in the frontoparietal-control-*B* and -*C,* limbic, and ventral attention subnetwork connectivity profiles between conditions, not even when comparing to the highly stimulative Movie condition. Finally, significant differences were not found between Eyes-Closed and Eyes-Closed-Number conditions in the functional connectivity between-nodes globally, within-network globally, between networks, or within the individual RSNs. This suggests cognitive engagement, if it is internal, and not related to external stimulation, does not significantly alter resting-state connectivity measurements. This suggests careful instruction on what to think during rs-fMRI is not necessary. However, we could not fully conclude whether the subjects should have their eyes open or closed during rs-fMRI. In sum, the presented comprehensive analyses will aid in designing rest conditions suited for the study of global and specific networks.

2.5 – Experimental Procedures

2.5.1 – Participants

Twenty-two healthy college students (12 females, 22 ± 4 years old) participated in this study. All participants were screened for neurological disorders of which none were reported. This study was approved by the Michigan State University Institutional Review Board. All subjects signed consent forms approved by the Michigan State University Institutional Review Board before participation.

2.5.2 – Imaging Acquisition

This experiment was conducted on a GE 3T Signa® HDx MR scanner (GE Healthcare, Waukesha, WI) with an 8-channel head coil. During each session, the first and higher-order shimming procedures were carried out to improve magnetic field homogeneity. To study resting-state brain function, echo-planar images, starting from inferior to superior regions of the brain, were acquired for 7 minutes using the following parameters: 36 contiguous 3-mm axial slices in an interleaved order, time of echo (TE) = 27.7 ms, time of repetition (TR) = 2500 ms, flip angle = 80°, field of view (FOV) = 22 cm, matrix size = 64 × 64, and ramp sampling. The first four data points were discarded to achieve a steady image signal. Each volume was acquired 164 times while the subjects were asked to adhere to each of the four previously described rest conditions (Eyes-Open, Eyes-Closed, Eyes-Closed-Number, and Movie). High-resolution isotropic (1 mm^3) T_1-weighted inversion recovery fast spoiled gradient-recalled (IR FSPGR) anatomical images with cerebrospinal fluid suppressed were obtained to cover the whole brain. These images were used within FreeSurfer to parcellate RSN regions.

2.5.3 – Resting-State fMRI Analysis

Individual Subject Pre-Processing: The "afni_proc.py" routine in AFNI (142) was used to generate the scripts to preprocess the rs-fMRI data. For each subject, signal time course spikes were first detected and removed. Data points with excess motion were identified (normalized motion derivative > 0.5 or voxel outliers > 10%) and modeled as regressors in subsequent processing. Then, acquisition timing differences across slice locations were corrected. The functional images were aligned to T_1-weighted high-resolution anatomical images, using the third volume as reference. Rigid-body motion correction was applied in three translational and three rotational directions. Translational and rotational estimates, as well as their derivatives, were modeled as regressors for the subsequent noise regression step. For each subject, spatial blurring with a full-width half-maximum of 4 mm was used to reduce random noise.

For the time course at each voxel location, the "3dDeconvolve" routine in AFNI (142) was used to remove temporal noise contributions due to motion, baseline, and system-induced signal trends (up to the 4^{th} order). The mean signal time courses of CSF and white matter regions as well as a temporal band-pass filter with a range of 0.009 Hz – 0.08 Hz were also modeled as regressors during the "3dDeconvolve" step. The pre-processed voxel time courses were then used in subsequent correlation analyses.

Subject-Level rs-fMRI Network Analyses: For each subject, T_1-weighted images were segmented via the FreeSurfer standard processing pipeline "recon-all" (143). The cortical nodes of the 17 networks derived by Yeo and colleagues (14) were identified in the subject native space using FreeSurfer segmentation (143). Pearson correlation between two rs-fMRI time courses of each pair of nodes in each network was performed in Matlab (MATLAB Version R2020a). The mean correlation was calculated for all node-pairs in each network to represent the connectivity of each network. The overall average within-network connectivity (correlation) is the mean of the connectivity values (correlations) of all 17 networks. In assessing the whole-

brain connectivity, due to the cancellation effect of positive and negative correlations, notably between networks that are known to be anticorrelated (i.e. task-negative vs. task-positive networks), we took the global average of the absolute *r* values between all nodes to represent the whole-brain connectivity. In this perspective, we consider a connection with a high negative *r* value to be highly connected, although in a negative way. To further investigate between-network connectivity, we first calculated the mean time course for each network across its nodes, then we calculated the pairwise correlations between networks to represent between-network connectivity.

Group Analyses on functional connectivity: To prepare for statistical analyses, all correlation coefficients of each subject were first Fisher's Z-transformed. Using SPSS (IBM SPSS Statistics for Windows, Version 26.0), RM-ANOVAs were conducted on these Fisher Z-transformed r-value distributions across the rest conditions of these subjects on the global average of absolute between-node connectivity, global average of within-network connectivity, the connectivity of the 17 RSNs, as well as between-network connectivity, followed by paired *t*-tests between different conditions. We also explored the differences of specific connections via paired *t*-tests within each network between conditions, to investigate connections driving overall changes in each individual RSN that was found significantly affected by the rest conditions based on RM-ANOVA. Correlation coefficients were obtained between each pair of nodes in each network to construct a correlation matrix for all RSNs in each condition. The correlation matrix of each RSN was compared between conditions to locate the connections that showed significant differences following paired *t*-tests. Statistical significance was set at $p \leq 0.05$ for all statistical analyses. RM-ANOVAs at the global level did not require multiple comparison correction. Bonferroni correction was applied in all multiple comparison corrections. Bonferroni correction was applied to the RM-ANOVAs on the 17 networks by setting a $p \leq 0.00294$ to obtain a corrected $p \leq 0.05$. After a network was found significantly affected by the rest conditions, Bonferroni correction was

applied to the six paired *t*-tests on the rest conditions by setting $p \leq 0.00833$ to obtain a corrected $p \leq 0.05$. Bonferroni correction was applied to a between-node connection by setting a *p* threshold less than 0.05 divided by the total number of between-node connections in a network to obtain a corrected $p \leq 0.05$.

REFERENCES

1. Attwell D, Laughlin SB. An Energy Budget for Signaling in the Grey Matter of the Brain. 2001.
2. Nation DA, Sweeney MD, Montagne A, Sagare AP, D'Orazio LM, Pachicano M, et al. Blood–brain barrier breakdown is an early biomarker of human cognitive dysfunction. Nat Med. 2019 Feb 1;25(2):270–6.
3. Zlokovic B V. Neurovascular mechanisms of Alzheimer's neurodegeneration. Vol. 28, Trends in Neurosciences. Elsevier Ltd; 2005. p. 202–8.
4. Nippert AR, Biesecker KR, Newman EA. Mechanisms Mediating Functional Hyperemia in the Brain. Vol. 24, Neuroscientist. SAGE Publications Inc.; 2018. p. 73–83.
5. Iadecola C. Neurovascular regulation in the normal brain and in Alzheimer's disease. Vol. 5, Nature Reviews Neuroscience. Nature Publishing Group; 2004. p. 347–60.
6. Heeger DJ, Ress D. What does fMRI tell us about neuronal activity? Vol. 3, Nature Reviews Neuroscience. 2002. p. 142–51.
7. Ogawa S, Lee TM, Kay AR, Tank DW. Brain magnetic resonance imaging with contrast dependent on blood oxygenation (cerebral blood flow/brain metabolism/oxygenation) [Internet]. Vol. 87. 1990. Available from: https://www.pnas.org
8. Linden D, Prvulovic D, Formisano E, Vollinger M, Friedhelm Z, Goebel R, et al. The Functional Neuroanatomy of Target Detection: An fMRI Study of Visual and Auditory Oddball Tasks. Cerebral Cortex. 1999;9(8):815–23.
9. Biswal B, Zerrin Yetkin F, Haughton VM, Hyde JS. Functional connectivity in the motor cortex of resting human brain using echo-planar mri. Magn Reson Med. 1995;34(4):537–41.
10. Golanov E V, Yamamoto S, Reis DJ. Spontaneous waves of cerebral blood flow associated with a pattern of electrocortical activity. Journal of American Physiology. 1994;266:204–14.
11. Shirer WR, Ryali S, Rykhlevskaia E, Menon V, Greicius MD. Decoding subject-driven cognitive states with whole-brain connectivity patterns. Cerebral Cortex. 2012 Jan;22(1):158–65.
12. Fox MD, Raichle ME. Spontaneous fluctuations in brain activity observed with functional magnetic resonance imaging. Nature Reviews Neuroscience. 2007.
13. Damoiseaux J, Rombouts S, Scheltens P, Stam CJ, Smith SM, Beckmann CF. Consistent resting-state networks across healthy subjects. Proc Natl Acad Sci U S A [Internet]. 2006 [cited 2012 May 7];(2). Available from: http://www.pnas.org/content/103/37/13848.short
14. Yeo BT, Krienen FM, Sepulcre J, Sabuncu MR, Lashkari D, Hollinshead M, et al. The organization of the human cerebral cortex estimated by intrinsic functional connectivity. J Neurophysiol. 2011 Sep;106(3):1125–65.

15. Fox MD, Snyder AZ, Vincent JL, Corbetta M, Essen DC Van, Raichle ME. The human brain is intrinsically organized into dynamic, anticorrelated functional networks. Proc Natl Acad Sci U S A [Internet]. 2005 Jul;102(27):9673–8. Available from: http://dx.doi.org/10.1073/pnas.0504136102

16. Mazoyer B, Zago L, Mellet E, Bricogne S, Etard O, Houde O, et al. Cortical networks for working memory and executive functions sustain the conscious resting state in man. Brain Res. 2001;54(3):287–98.

17. Kilpatrick LA, Suyenobu BY, Smith SR, Bueller JA, Goodman T, Creswell JD, et al. Impact of mindfulness-based stress reduction training on intrinsic brain connectivity. Neuroimage [Internet]. 2011;56(1):290–8. Available from: http://dx.doi.org/10.1016/j.neuroimage.2011.02.034

18. Kawagoe T, Onoda K, Yamaguchi S. Different pre-scanning instructions induce distinct psychological and resting brain states during functional magnetic resonance imaging. European Journal of Neuroscience. 2018 Jan 1;47(1):77–82.

19. Patriat R, Molloy EK, Meier TB, Kirk GR, Nair VA, Meyerand ME, et al. The effect of resting condition on resting-state fMRI reliability and consistency: A comparison between resting with eyes open, closed, and fixated. Neuroimage. 2013 Sep;78:463–73.

20. Hurd MD, Martorell P, Delavande A, Mullen KJ, Langa KM. Monetary Costs of Dementia in the United States. New England Journal of Medicine. 2013 Apr 4;368(14):1326–34.

21. Nichols E, Steinmetz JD, Vollset SE, Fukutaki K, Chalek J, Abd-Allah F, et al. Estimation of the global prevalence of dementia in 2019 and forecasted prevalence in 2050: an analysis for the Global Burden of Disease Study 2019. Lancet Public Health. 2022 Feb 1;7(2):e105–25.

22. Brookmeyer R, Evans DA, Hebert L, Langa KM, Heeringa SG, Plassman BL, et al. National estimates of the prevalence of Alzheimer's disease in the United States. Alzheimer's and Dementia. 2011 Jan;7(1):61–73.

23. Association A. Alzheimer ' s disease facts and figures. 2013;12:459–509.

24. McKhann GM, Knopman DS, Chertkow H, Hyman BT, Jack CR, Kawas CH, et al. The diagnosis of dementia due to Alzheimer's disease: Recommendations from the National Institute on Aging-Alzheimer's Association workgroups on diagnostic guidelines for Alzheimer's disease. Alzheimer's and Dementia. 2011;7(3):263–9.

25. Serrano-Pozo A, Frosch MP, Masliah E, Hyman BT. Neuropathological alterations in Alzheimer disease. Cold Spring Harb Perspect Med. 2011 Sep;1(1).

26. Deture MA, Dickson DW. The neuropathological diagnosis of Alzheimer's disease. Vol. 14, Molecular Neurodegeneration. BioMed Central Ltd.; 2019.

27. Aisen PS, Cummings J, Jack CR, Morris JC, Sperling R, Frölich L, et al. On the path to 2025: Understanding the Alzheimer's disease continuum. Vol. 9, Alzheimer's Research and Therapy. BioMed Central Ltd.; 2017.

28. Petersen RC, Lopez O, Armstrong MJ, Getchius TSD, Ganguli M, Gloss D, et al. Practice guideline update summary: Mild cognitive impairment report of theguideline development, dissemination, and implementation. Neurology. 2018 Jan 1;90(3):126–35.

29. Slot RER, Sikkes SAM, Berkhof J, Brodaty H, Buckley R, Cavedo E, et al. Subjective cognitive decline and rates of incident Alzheimer's disease and non–Alzheimer's disease dementia. Alzheimer's and Dementia. 2019 Mar 1;15(3):465–76.

30. Schmand B, Jonker C, Hooijer C, Lindenboom J. Subjective Memory Complaints May Announce Dementia. Neurology . 1996;46(1):121–5.

31. Mitchell AJ, Beaumont H, Ferguson D, Yadegarfar M, Stubbs B. Risk of dementia and mild cognitive impairment in older people with subjective memory complaints: Meta-analysis. Acta Psychiatr Scand. 2014 Dec 1;130(6):439–51.

32. Pfannmöller J, Lotze M. Review on biomarkers in the resting-state networks of chronic pain patients. Brain Cogn. 2019 Apr 1;131:4–9.

33. Zhu DC, Covassin T, Nogle S, Doyle S, Russell D, Pearson RL, et al. A potential biomarker in sports-related concussion: Brain functional connectivity alteration of the default-mode network measured with longitudinal resting-state fMRI over thirty days. J Neurotrauma. 2015;32(5):327–41.

34. Wolf RC, Sambataro F, Vasic N, Depping MS, Thomann PA, Landwehrmeyer GB, et al. Abnormal resting-state connectivity of motor and cognitive networks in early manifest Huntington's disease. Psychol Med. 2014 Nov 12;44(15):3341–56.

35. Varangis E, Habeck CG, Razlighi QR, Stern Y. The Effect of Aging on Resting State Connectivity of Predefined Networks in the Brain. Front Aging Neurosci. 2019 Sep 4;11.

36. Simic G, Babic M, Borovecki F, Hof PR. Early failure of the default-mode network and the pathogenesis of Alzheimer's disease. Vol. 20, CNS Neuroscience and Therapeutics. Blackwell Publishing Ltd; 2014. p. 692–8.

37. Shulman G, Fiez J, Corbetta M, Buckner R, Miezin F, Raichle M, et al. Common Blood Flow Changes across visual Tasks: II. Decreases in Cerebral Cortex. J Cogn Neurosci. 1997;9(5):648–63.

38. Binder JR, Frost JA, Hammeke TA, Bellgowan PSF, Rao SM, Cox RW. Conceptual Processing during the Conscious Resting State: A Functional MRI Study. J Cogn Neurosci [Internet]. 1999;11(1):1–14. Available from: papers2://publication/uuid/4EB1DEEA-D766-4D1B-A36D-072AE45D2B3C

39. Buckner RL, Andrews-Hanna JR, Schacter DL. The brain's default network: Anatomy, function, and relevance to disease. Ann N Y Acad Sci. 2008;1124:1–38.

40. Ekhtiari H, Nasseri P, Yavari F, Mokri A, Monterosso J. Neuroscience of drug craving for addiction medicine: From circuits to therapies. In: Progress in Brain Research. Elsevier B.V.; 2016. p. 115–41.

41. Desgranges B, Mevel K, Chételat G, Eustache F. The default mode network in healthy aging and Alzheimer's disease. International Journal of Alzheimer's Disease. 2011.

42. Greicius MD, Menon V. Default-mode activity during a passive sensory task: Uncoupled from deactivation but impacting activation. J Cogn Neurosci. 2004;16(9):1484–92.

43. Grothe MJ, Teipel SJ. Spatial patterns of atrophy, hypometabolism, and amyloid deposition in Alzheimer's disease correspond to dissociable functional brain networks. Hum Brain Mapp. 2016;37(1):35–53.

44. Hohenfeld C, Werner CJ, Reetz K. Resting-state connectivity in neurodegenerative disorders: Is there potential for an imaging biomarker? Neuroimage Clin [Internet]. 2018;18(March 2018):849–70. Available from: https://doi.org/10.1016/j.nicl.2018.03.013

45. Sperling RA, LaViolette PS, O'Keefe K, O'Brien J, Rentz DM, Pihlajamaki M, et al. Amyloid Deposition Is Associated with Impaired Default Network Function in Older Persons without Dementia. Neuron. 2009 Jul 30;63(2):178–88.

46. Han F, Liu X, Mailman RB, Huang X, Liu X. Resting-state global brain activity affects early β-amyloid accumulation in default mode network. Nat Commun [Internet]. 2023 Nov 27;14(1):7788. Available from: https://www.nature.com/articles/s41467-023-43627-y

47. Scheel N, Tarumi T, Tomoto T, Cullum CM, Zhang R, Zhu DC. Resting-state functional MRI signal fluctuation amplitudes are correlated with brain amyloid-β deposition in patients with mild cognitive impairment. Journal of Cerebral Blood Flow and Metabolism. 2022 May 1;42(5):876–90.

48. Sharma N, Murari G, Vandermorris S, Verhoeff NPLG, Herrmann N, Chen JJ, et al. Functional Connectivity between the Posterior Default Mode Network and Parahippocampal Gyrus Is Disrupted in Older Adults with Subjective Cognitive Decline and Correlates with Subjective Memory Ability. Journal of Alzheimer's Disease. 2021;82(1):435–45.

49. Badhwar AP, Tam A, Dansereau C, Orban P, Hoffstaedter F, Bellec P. Resting-state network dysfunction in Alzheimer's disease: A systematic review and meta-analysis. Alzheimer's and Dementia: Diagnosis, Assessment and Disease Monitoring. 2017;8:73–85.

50. Li R, Wu X, Fleisher AS, Reiman EM, Chen K, Yao L. Attention-related networks in Alzheimer's disease: A resting functional MRI study. Hum Brain Mapp. 2012 May;33(5):1076–88.

51. Noh JH, Kim JH, Yang HD. Classification of Alzheimer's Progression Using fMRI Data. Sensors. 2023 Jul 1;23(14).

52. Guo H, Zhang Y. Resting State fMRI and Improved Deep Learning Algorithm for Earlier Detection of Alzheimer's Disease. IEEE Access. 2020;8:115383–92.

53. Yamashita KI, Uehara T, Taniwaki Y, Tobimatsu S, Kira JI. Long-Term Effect of Acetylcholinesterase Inhibitors on the Dorsal Attention Network of Alzheimer's Disease Patients: A Pilot Study Using Resting-State Functional Magnetic Resonance Imaging. Front Aging Neurosci. 2022 Apr 5;14.

54. Koch W, Teipel S, Mueller S, Benninghoff J, Wagner M, Bokde ALW, et al. Diagnostic power of default mode network resting state fMRI in the detection of Alzheimer's disease. Neurobiol Aging. 2012 Mar;33(3):466–78.

55. Long JM, Holtzman DM. Alzheimer Disease: An Update on Pathobiology and Treatment Strategies. Cell [Internet]. 2019;179(2):312–39. Available from: https://doi.org/10.1016/j.cell.2019.09.001

56. Santisteban MM, Iadecola C. Hypertension, dietary salt and cognitive impairment. Journal of Cerebral Blood Flow and Metabolism. 2018;38(12):2112–28.

57. De la Torre JC. Hemodynamic consequences of deformed microvessels in the brain in Alzheimer's disease. In: Annals of the New York Academy of Sciences. Blackwell Publishing Inc.; 1997. p. 75–91.

58. Suter OC, Sunthorn T, Kraftsik R, Straubel J, Darekar P, Khalili K, et al. Cerebral hypoperfusion generates cortical watershed microinfarcts in Alzheimer disease. Stroke. 2002;33(8):1986–92.

59. de la Torre J. The Vascular Hypothesis of Alzheimer's Disease: A Key to Preclinical Prediction of Dementia Using Neuroimaging. Vol. 63, Journal of Alzheimer's disease : JAD. NLM (Medline); 2018. p. 35–52.

60. Tini G, Scagliola R, Monacelli F, La Malfa G, Porto I, Brunelli C, et al. Alzheimer's Disease and Cardiovascular Disease: A Particular Association. Vol. 2020, Cardiology Research and Practice. Hindawi Limited; 2020.

61. Farnsworth Von Cederwald B, Josefsson M, Wåhlin A, Nyberg L, Karalija N. Association of Cardiovascular Risk Trajectory With Cognitive Decline and Incident Dementia. Neurology. 2022 May 17;98(20):E2013–22.

62. Ungvari Z, Toth P, Tarantini S, Prodan CI, Sorond F, Merkely B, et al. Hypertension-induced cognitive impairment: from pathophysiology to public health. Vol. 17, Nature Reviews Nephrology. Nature Research; 2021. p. 639–54.

63. Shang X, Hill E, Zhu Z, Liu J, Ge BZ, Wang W, et al. The Association of Age at Diagnosis of Hypertension With Brain Structure and Incident Dementia in the UK Biobank. Hypertension. 2021 Nov 1;78(5):1463–74.

64. Iadecola C, Gottesman RF. Neurovascular and Cognitive Dysfunction in Hypertension: Epidemiology, Pathobiology, and Treatment. Circ Res. 2019;124(7):1025–44.

65. Toth P, Tarantini S, Csiszar A, Ungvari Z. Functional vascular contributions to cognitive impairment and dementia: Mechanisms and consequences of cerebral autoregulatory dysfunction, endothelial impairment, and neurovascular uncoupling in aging. Am J Physiol Heart Circ Physiol. 2017;312(1):H1–20.

66. Dai W, Lopez OL, Carmichael OT, Becker JT, Kuller LH, Gach HM. Abnormal regional cerebral blood flow in cognitively normal elderly subjects with hypertension. Stroke. 2008;39(2):349–54.

67. Sierra C. Hypertension and the Risk of Dementia. Front Cardiovasc Med. 2020;7(January):1–7.

68. Bu L, Huo C, Xu G, Liu Y, Li Z, Fan Y, et al. Alteration in brain functional and effective connectivity in subjects with hypertension. Front Physiol. 2018;9(MAY):1–12.

69. Greicius MD, Srivastava G, Reiss AL, Menon V, Raichle ME. Default-mode network activity distinguishes Alzheimer's disease from healthy aging: Evidence from functional MRI [Internet]. 2004. Available from: www.fmridc.org

70. Son SJ, Kim J, Lee E, Park JY, Namkoong K, Hong CH, et al. Effect of hypertension on the resting-state functional connectivity in patients with Alzheimer's disease (AD). Arch Gerontol Geriatr [Internet]. 2015;60(1):210–6. Available from: http://dx.doi.org/10.1016/j.archger.2014.09.012

71. Forette F. The Prevention of Dementia With Antihypertensive Treatment<subtitle>New Evidence From the Systolic Hypertension in Europe (Syst-Eur) Study</subtitle>. Arch Intern Med [Internet]. 2002 Oct 14;162(18):2046. Available from: http://archinte.jamanetwork.com/article.aspx?doi=10.1001/archinte.162.18.2046

72. Hsu CY, Huang CC, Chan WL, Huang PH, Chiang CH, Chen TJ, et al. Angiotensin-receptor blockers and risk of alzheimer's disease in hypertension population - A nationwide cohort study. Circulation Journal. 2013;77(2):405–10.

73. Cunningham E, Todd S, Passmore P, Bullock R, Mcguinness B. Pharmacological treatment of hypertension in people without prior cerebrovascular disease for the prevention of cognitive impairment and dementia (Review). 2021;

74. The SPRINT Research Group, Wright JT, Williamson JD, Whelton PK, Snyder JK, SinkS KM, et al. A Randomized Trial of Intensive versus Standard Blood-Pressure Control. New England Journal of Medicine. 2015;373(22):2103–16.

75. O'Connor PJ, Venkat Narayan KM, Anderson R, Feeney P, Fine L, Ali MK, et al. Effect of intensive versus standard blood pressure control on depression and health-related quality of life in type 2 diabetes: The ACCORD trial. Diabetes Care. 2012;35(7):1479–81.

76. Supiano MA, Williamson JD. New Guidelines and SPRINT Results: Implications for Geriatric Hypertension. Vol. 140, Circulation. Lippincott Williams and Wilkins; 2019. p. 976–8.

77. Williamson JD, Pajewski NM, Auchus AP, Bryan RN, Chelune G, Cheung AK, et al. Effect of Intensive vs Standard Blood Pressure Control on Probable Dementia: A Randomized Clinical Trial. In: JAMA - Journal of the American Medical Association. American Medical Association; 2019. p. 553–61.

78. Fox N, Warrington EK, Seiffer AL, Agnew SK, Rossor MN. Presymptomatic cognitive deficits in individuals at risk of familial Alzheimer's disease. Brain. 1998;121:1631–9.

79. Szabo-Reed AN, Vidoni E, Binder EF, Burns J, Cullum CM, Gahan WP, et al. Rationale and methods for a multicenter clinical trial assessing exercise and intensive vascular risk reduction in preventing dementia (rrAD Study). Contemp Clin Trials [Internet]. 2019;79(March):44–54. Available from: https://doi.org/10.1016/j.cct.2019.02.007

80. Dassanayake S, Sole G, Wilkins G, Skinner M. Exercise: a therapeutic modality to treat blood pressure in resistant hypertension. Physical Therapy Reviews [Internet]. 2020;25(3):149–58. Available from: https://doi.org/10.1080/10833196.2020.1733781

81. Juraschek SP, Blaha MJ, Whelton SP, Blumenthal R, Jones SR, Keteyian SJ, et al. Physical fitness and hypertension in a population at risk for cardiovascular disease: The Henry Ford ExercIse Testing (FIT) Project. J Am Heart Assoc. 2014;3(6):1–10.

82. Kim JM, Stewart R, Bae KY, Kim SW, Yang SJ, Park KH, et al. Role of BDNF val66met polymorphism on the association between physical activity and incident dementia. Neurobiol Aging [Internet]. 2011;32(3):551.e5-551.e12. Available from: http://dx.doi.org/10.1016/j.neurobiolaging.2010.01.018

83. Hashimoto M, Araki Y, Takashima Y, Nogami K, Uchino A, Yuzuriha T, et al. Hippocampal atrophy and memory dysfunction associated with physical inactivity in community-dwelling elderly subjects: The Sefuri study. Brain Behav. 2017;7(2):1–8.

84. García-Mesa Y, Pareja-Galeano H, Bonet-Costa V, Revilla S, Gómez-Cabrera MC, Gambini J, et al. Physical exercise neuroprotects ovariectomized 3xTg-AD mice through BDNF mechanisms. Psychoneuroendocrinology. 2014;45:154–66.

85. McDaniel MA, Binder EF, Bugg JM, Waldum ER, Dufault C, Meyer A, et al. Effects of cognitive training with and without aerobic exercise on cognitively demanding everyday activities. Psychol Aging. 2014;29(3):717–30.

86. Beckmann CF, Smith SM. Probabilistic Independent Component Analysis for Functional Magnetic Resonance Imaging. IEEE Trans Med Imaging. 2004;23(2):137–52.

87. Harrison SJ, Woolrich MW, Robinson EC, Glasser MF, Beckmann CF, Jenkinson M, et al. Large-scale probabilistic functional modes from resting state fMRI. Neuroimage. 2015 Apr 1;109:217–31.

88. Mazziotta J, Toga A, Evans A, Fox P, Lancaster J. A probabilistic Atlas of the Human Brain: Theory and Rationale for Its Development. The International Consortium for Brain Mapping (ICBM). 1995;2(2):89–101.

89. Damoiseaux JS. Effects of aging on functional and structural brain connectivity. Neuroimage. 2017 Oct 15;160:32–40.

90. Raz N, Gunning F, Head D, Dupuis J, McQuain J, Briggs S, et al. Selective Aging of the Human Cerebral Cortex Observed in Vivo: Differential Vulnerability of the Prefrontal Gray Matter. Cerebral Cortex. 1997;7(3):268–82.

91. Doucet GE, Labache L, Thompson PM, Joliot M, Frangou S. Atlas55+: Brain Functional Atlas of Resting-State Networks for Late Adulthood. Cerebral Cortex. 2021 Mar 1;31(3):1719–31.

92. Deery HA, Di Paolo R, Moran C, Egan GF, Jamadar SD. The older adult brain is less modular, more integrated, and less efficient at rest: A systematic review of large-scale resting-state functional brain networks in aging. Vol. 60, Psychophysiology. John Wiley and Sons Inc; 2023.

93. Ashburner J. A fast diffeomorphic image registration algorithm. Neuroimage. 2007 Oct 15;38(1):95–113.

94. Beckmann CF, DeLuca M, Devlin JT, Smith SM. Investigations into resting-state connectivity using independent component analysis. Philosophical Transactions of the Royal Society B: Biological Sciences. 2005;360(1457):1001–13.

95. Shinn AK, Baker JT, Lewandowski KE, Öngür D, Cohen BM. Aberrant cerebellar connectivity in motor and association networks in schizophrenia. Front Hum Neurosci. 2015;9(MAR).

96. Liu T, Wang Y, Yan T. Preclinical Stages of Alzheimer's Disease Classification by a Rs-fMRI Study. 2018 11th International Congress on Image and Signal Processing, BioMedical Engineering and Informatics (CISP-BMEI). 2018;1–6.

97. Uddin LQ, Supekar K, Menon V. Typical and atypical development of functional human brain networks: Insights from resting-state fMRI. Front Syst Neurosci. 2010;4(MAY):1–12.

98. Bolton TAW, Morgenroth E, Preti MG, Van De Ville D. Tapping into Multi-Faceted Human Behavior and Psychopathology Using fMRI Brain Dynamics. Trends Neurosci. 2020;43(9):667–80.

99. Zhu DC, Majumdar S, Korolev IO, Berger KL, Bozoki AC. Alzheimer's disease and amnestic mild cognitive impairment weaken connections within the default-mode network: A multi-modal imaging study. Journal of Alzheimer's Disease. 2013;34(4):969–84.

100. Chang SE, Zhu DC. Neural network connectivity differences in children who stutter. Brain. 2013;136(12):3709–26.

101. Anderson JS, Ferguson MA, Lopez-Larson M, Yurgelun-Todd D. Reproducibility of single-subject functional connectivity measurements. American Journal of Neuroradiology. 2011;32(3):548–55.

102. Ding K, Tarumi T, Wang C, Vernino S, Zhang R, Zhu DC. Central autonomic network functional connectivity: correlation with baroreflex function and cardiovascular variability in older adults. Brain Struct Funct. 2020;225(5):1575–85.

103. Roy AK, Shehzad Z, Margulies DS, Kelly AMC, Uddin LQ, Gotimer K, et al. Functional connectivity of the human amygdala using resting state fMRI. Neuroimage. 2009;45(2):614–26.

104. Vanderwal T, Kelly C, Eilbott J, Mayes LC, Castellanos FX. Inscapes: A movie paradigm to improve compliance in functional magnetic resonance imaging. Neuroimage. 2015;122:222–32.

105. Bolton TAW, Tarun A, Sterpenich V, Schwartz S, Van De Ville D. Interactions between Large-Scale Functional Brain Networks are Captured by Sparse Coupled HMMs. IEEE Trans Med Imaging. 2018;37(1):230–40.

106. Kim D, Kay K, Shulman GL, Corbetta M. A new modular brain organization of the bold signal during natural vision. Cerebral Cortex. 2018;28(9):3065–81.

107. Betti V, DellaPenna S, de Pasquale F, Mantini D, Marzetti L, Romani GL, et al. Natural scenes viewing alters the dynamics of functional connectivity in the human brain. Neuron. 2013;79(4):782–97.

108. Arbabshirani MR, Havlicek M, Kiehl KA, Pearlson GD, Calhoun VD. Functional network connectivity during rest and task conditions: A comparative study. Hum Brain Mapp. 2013 Nov;34(11):2959–71.

109. Yan C, Liu D, He Y, Zou Q, Zhu C, Zuo X, et al. Spontaneous brain activity in the default mode network is sensitive to different resting-state conditions with limited cognitive load. PLoS One. 2009 May 29;4(5).

110. Gordon EM, Laumann TO, Adeyemo B, Huckins JF, Kelley WM, Petersen SE. Generation and Evaluation of a Cortical Area Parcellation from Resting-State Correlations. Cerebral Cortex. 2016;26(1):288–303.

111. Smith SM, Fox PT, Miller KL, Glahn DC, Fox PM, Mackay CE, et al. Correspondence of the brain's functional architecture during activation and rest. Proc Natl Acad Sci U S A. 2009;106(31):13040–5.

112. Cole MW, Reynolds JR, Power JD, Repovs G, Anticevic A, Braver TS. Multi-task connectivity reveals flexible hubs for adaptive task control. Nat Neurosci. 2013;16(9):1348–55.

113. Corbetta M, Shulman GL. Control of goal-directed and stimulus-driven attention in the brain. Nat Rev Neurosci. 2002;3(3):201–15.

114. Osher DE, Brissenden JA, Somers DC. Predicting an individual's dorsal attention network activity from functional connectivity fingerprints. J Neurophysiol. 2019;122(1):232–40.

115. Mega MS, Cummings JL, Salloway S, Malloy P. The limbic system: An anatomic, phylogenetic, and clinical perspective. Journal of Neuropsychiatry and Clinical Neurosciences. 1997;9(3):315–30.

116. Xue W, Kang J, Bowman FD, Wager TD, Guo J. Identifying functional co-activation patterns in neuroimaging studies via poisson graphical models. Biometrics. 2014;70(4):812–22.

117. Zhang XF, He X, Wu L, Liu CJ, Wu W. Altered Functional Connectivity of Amygdala with the Fronto-Limbic-Striatal Circuit in Temporal Lobe Lesion as a Proposed Mechanism for Poststroke Depression. Am J Phys Med Rehabil. 2019;98(4):303–10.

118. O'Doherty JP, Cockburn J, Pauli WM. Learning, Reward, and Decision Making. Annu Rev Psychol. 2017;68:73–100.

119. O'Doherty J, Rolls ET, Francis S, Bowtell R, McGlone F, Kobal G, et al. Sensory-specific satiety-related olfactory activation of the human orbitofrontal cortex. Neuroreport. 2000;11(2):399–403.

120. Howard JD, Kahnt T. Identity-specific reward representations in orbitofrontal cortex are modulated by selective devaluation. Journal of Neuroscience. 2017;37(10):2627–38.

121. Pruessner JC, Dedovic K, Khalili-Mahani N, Engert V, Pruessner M, Buss C, et al. Deactivation of the Limbic System During Acute Psychosocial Stress: Evidence from Positron Emission Tomography and Functional Magnetic Resonance Imaging Studies. Biol Psychiatry. 2008;63(2):234–40.

122. Seeley WW, Menon V, Schatzberg AF, Keller J, Glover GH, Kenna H, et al. Dissociable intrinsic connectivity networks for salience processing and executive control. Journal of Neuroscience. 2007;27(9):2349–56.

123. Shulman GL, D'Avossa G, Tansy AP, Corbetta M. Two attentional processes in the parietal lobe. Cerebral Cortex. 2002;12(11):1124–31.

124. Farrant K, Uddin LQ. Asymmetric development of dorsal and ventral attention networks in the human brain. Dev Cogn Neurosci [Internet]. 2015;12:165–74. Available from: http://dx.doi.org/10.1016/j.dcn.2015.02.001

125. Deen B, Pitskel NB, Pelphrey KA. Three systems of insular functional connectivity identified with cluster analysis. Cerebral Cortex. 2011;21(7):1498–506.

126. Cramer SC, Finklestein SP, Schaechter JD, Bush G, Rosen BR. Activation of distinct motor cortex regions during ipsilateral and contralateral finger movements. J Neurophysiol. 1999;81(1):383–7.

127. Martin T, Houck JM, Bish JP, Kičić D, Woodruff CC, Moses SN, et al. MEG reveals different contributions of somatomotor cortex and cerebellum to simple reaction time after temporally structured cues. Hum Brain Mapp. 2006;27(7):552–61.

128. Friederici AD. The brain basis of language processing: From structure to function. Physiol Rev. 2011;91(4):1357–92.

129. Puschmann S, Steinkamp S, Gillich I, Mirkovic B, Debener S, Thiel CM. The right temporoparietal junction supports speech tracking during selective listening: Evidence from concurrent EEG-fMRI. Journal of Neuroscience. 2017;37(47):11505–16.

130. Langers DRM, Van Dijk P. Robustness of intrinsic connectivity networks in the human brain to the presence of acoustic scanner noise. Neuroimage. 2011;55(4):1617–32.

131. Levy I, Hasson U, Avidan G, Hendler T, Malach R. Center-periphery organization of human object areas. Nat Neurosci. 2001;4(5):533–9.

132. Nir Y, Hasson U, Levy I, Yeshurun Y, Malach R. Widespread functional connectivity and fMRI fluctuations in human visual cortex in the absence of visual stimulation. Neuroimage. 2006;30(4):1313–24.

133. Xia M, Wang J, He Y. BrainNet Viewer: A Network Visualization Tool for Human Brain Connectomics. PLoS One. 2013;8(7).

134. Spreng RN, Sepulcre J, Turner GR, Stevens WD, Schacter DL. Intrinsic architecture underlying the relations among the default, dorsal attention, and frontoparietal control networks of the human brain. J Cogn Neurosci. 2013;25(1):74–86.

135. Olson IR, Plotzker A, Ezzyat Y. The Enigmatic temporal pole: A review of findings on social and emotional processing. Brain. 2007;130(7):1718–31.

136. Campbell KL, Shafto MA, Wright P, Tsvetanov KA, Geerligs L, Cusack R, et al. Idiosyncratic responding during movie-watching predicted by age differences in attentional control. Neurobiol Aging. 2015;36(11):3045–55.

137. Agtzidis I, Meyhöfer I, Dorr M, Lencer R. Following Forrest Gump: Smooth pursuit related brain activation during free movie viewing. Neuroimage. 2020;216(January).

138. Zimmermann M, Meulenbroek RGJ, De Lange FP. Motor planning is facilitated by adopting an action's goal posture: An fMRI study. Cerebral Cortex. 2012;22(1):122–31.

139. De Pasquale F, Sabatini U, Della Penna S, Sestieri C, Caravasso CF, Formisano R, et al. The connectivity of functional cores reveals different degrees of segregation and integration in the brain at rest. Neuroimage. 2013;69:51–61.

140. Zimmermann M, Mars RB, de Lange FP, Toni I, Verhagen L. Is the extrastriate body area part of the dorsal visuomotor stream? Brain Struct Funct. 2018;223(1):31–46.

141. Chen PHA, Jolly E, Cheong JH, Chang LJ. Intersubject representational similarity analysis reveals individual variations in affective experience when watching erotic movies. Neuroimage. 2020;216(February):116851.

142. Cox J.S. RW; H. AFNI: Software for analysis and visualization of functional magnetic resonance neuroimages. Computers and Biomedical Research. 1996;29(29):162–73.

143. Fischl B. FreeSurfer. Neuroimage. 2012;62(2):774–81.

APPENDIX

FIGURES

Figure 2.1: (Top Row) AFNI software depiction using an underlay MNI152 standardized brain with a color coded overlay of Yeo's 17 Networks (available at http://surfer.nmr.mgh.harvard.edu/fswiki/CorticalParcellation_Yeo2011). (Below Top Row) Complete listing of the names of Yeo's 17 networks along with corresponding common network names and the cortical ROIs that belong to each network.

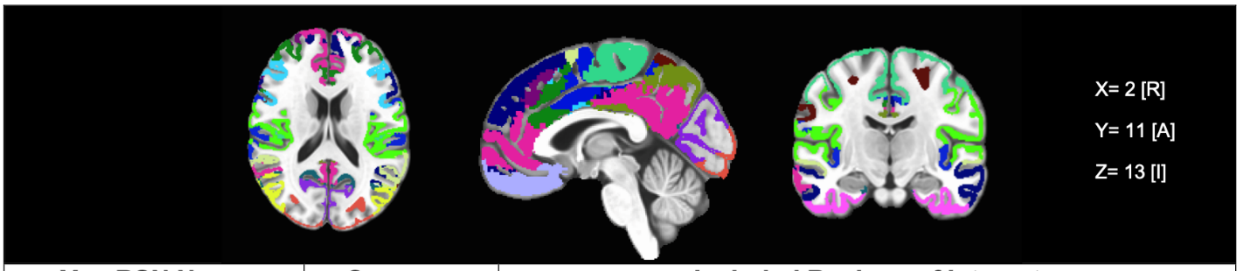

Yeo RSN Name (Yeo et al., 2011)	Common Network Resemblance	Included Regions of Interest
Control-*A*	Frontoparietal Control	Intraparietal sulcus (IPS); lateral prefrontal (PFCl); posterior temporal (Temp); lateral ventral prefrontal (PFClv); anterior cingulate (Cinga); dorsal prefrontal (PFCd).
Control-*B*		Inferior parietal (IPL); dorsal prefrontal (PFCd); lateral prefrontal (PFCl); lateral ventral prefrontal (PFClv); medial posterior prefrontal (PFCmp); temporal (Temp); lateral dorsal prefrontal (PFCld).
Control-*C*		Posterior cingulate (Cingp); precuneus (pCun).
Default-*A*	Default Mode	Inferior parietal (IPL); posterior cingulate cortex (PCC); dorsal prefrontal (PFCd); medial prefrontal (PFCm); temporal (Temp).
Default -*B*		Inferior parietal (IPL); dorsal prefrontal (PFCd); lateral prefrontal (PFCl); ventral prefrontal (PFCv); temporal (Temp); anterior temporal (AntTemp).
Default -*C*		Inferior parietal (IPL); parahippocampal (PHC); retrosplenial (Rsp).
Dorsal Attention-*A*	Dorsal Attention	Parietal occipital (ParOcc); superior parietal (SPL); temporal occipital (TempOcc).
Dorsal Attention-*B*		Frontal eye field (FEF); postcentral gyrus (PostC); precentral ventral (PrCv); temporal occipital (TempOcc).
Limbic Orbitofrontal	Limbic	Orbitofrontal (Limbic_OFC).
Limbic Temporal-Pole		Temporal pole (Limbic_TempPole).
Salience/Ventral Attention-*A*	Salience	Parietal operculum (ParOper); medial parietal (ParMed); medial frontal (FrMed); precentral frontal ventral (PrCv); insula (Ins); precentral frontal (PrC).
Salience/Ventral Attention-*B*	Ventral Attention	Medial posterior prefronal (PFCmp); ventral prefrontal (PFCv); lateral central prefrontal (PFClv); anterior cingulate (Cinga); inferior parietal (IPL); dorsal prefrontal (PFCd); lateral prefrontal (PFCl); Orbitofrontal (OFC).
Somatomotor-*A*	Somatomotor	Central Sulcus (SomMotA).
Somatomotor-*B*		Central sulcus (Cent); secondary somatosensory (S2); insula (Ins); auditory (Aud).
Temporal Parietal	Auditory	Temporal parietal (TempPar).
Visual Central	Visual	Extrastriate (ExStr); Striate.
Visual Peripheral		Inferior extrastriate (ExStrInf); superior extrastriate (ExStrSup); Striate.

Figure 2.2: Brain Net Viewer graphical visualization of connectivity within RSNs that showed a significant difference in functional connectivity between conditions following repeated-measures ANOVAs ($p \leq 0.05$). The strength of each connection is denoted by both its size (larger diameter denoting stronger connection) and color (scale). Each node is labeled with a number coding for each region of interest. **Default-Mode Network *-A*** (Top**)**: (1) IPL, (2) IPL, (3) PCC, (4) PCC, (5) PFCd, (6) PFCd, (7) PFCm, (8) PFCm, and (9) Temp. **Dorsal-Attention Network *-A*** (Bottom): (1) TempOcc, (2) TempOcc, (3) ParOcc, (4) ParOcc, (5) SPL, and (6) SPL (For abbreviations, see Figure 2.1).

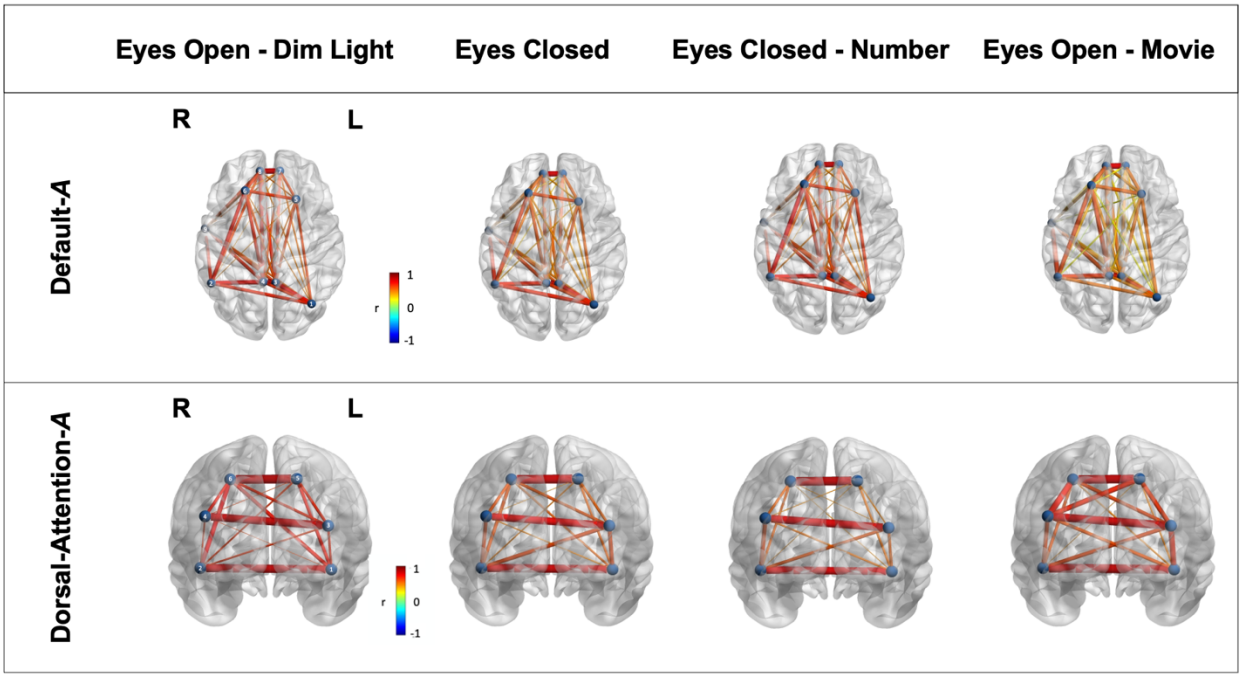

Figure 2.3: Brain Net Viewer graphical visualization of connectivity within RSNs that showed a significant difference in functional connectivity between conditions following repeated-measures ANOVAs ($p \leq 0.05$). The strength of each connection is denoted by both its size (larger diameter denoting stronger connection) and color (scale). Each node is labeled with a number coding for each region of interest. **Salience/Ventral-Attention Network *-A* (**Top**)**: (1) Ins, (2) Ins, (3) PrCv, (4) PrCv, (5) ParOper, (6) ParOper, (7) FrMed, (8) FrMed, (9) ParMed, (10) ParMed, and (11) PrC. **Somatomotor Network *-B*** (Bottom): (1) Aud, (2) Aud, (3) Ins, (4) Ins, (5) S2, (6) S2, (7) Cent, and (8) Cent (For abbreviations, see Figure 2.1).

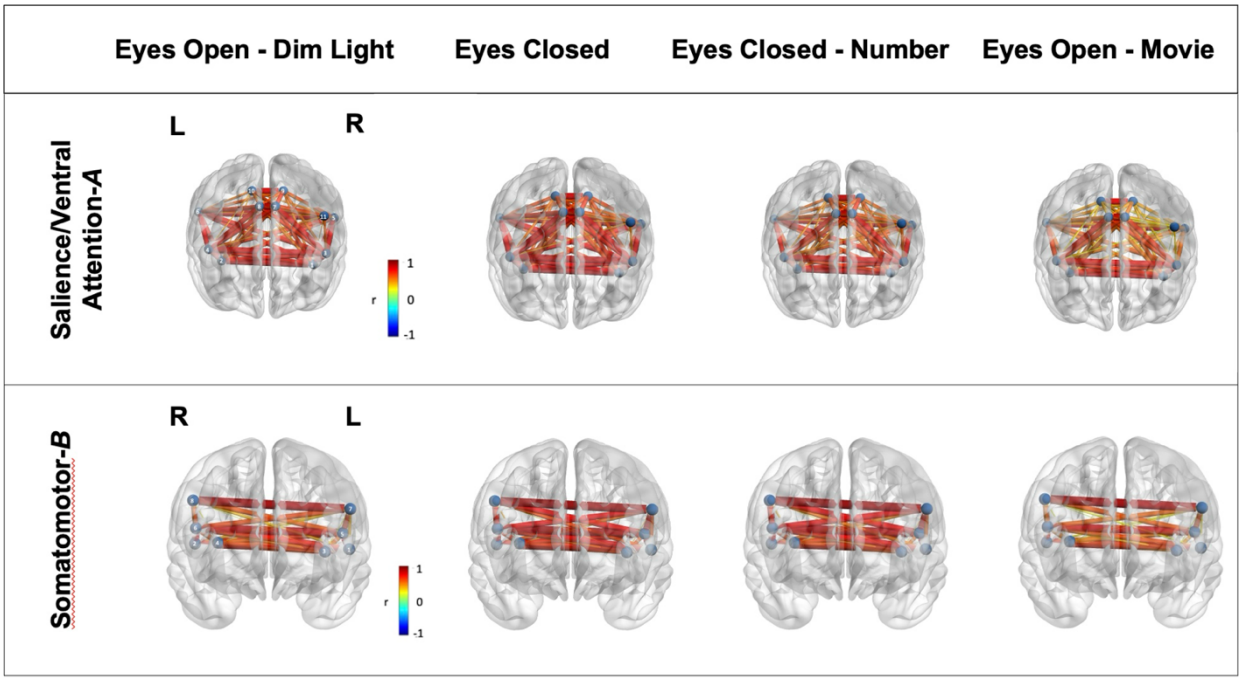

Figure 2.4: Brain Net Viewer graphical visualization of connectivity within RSNs that showed a significant difference in functional connectivity between conditions following repeated-measures ANOVAs ($p \leq 0.05$). The strength of each connection is denoted by both its size (larger diameter denoting stronger connection) and color (scale). Each node is labeled with a number coding for each region of interest. **Central Visual Network** (Top): (1) Striate, (2) Striate, (3) ExStr, and (4) ExStr. (Bottom) **Peripheral Visual Network** (Bottom): (1) ExStrInf, (2) ExStrInf, (3) Striate, (4) Striate, (5) ExStrSup, (6) ExStrSup (For abbreviations, see Figure 2.1).

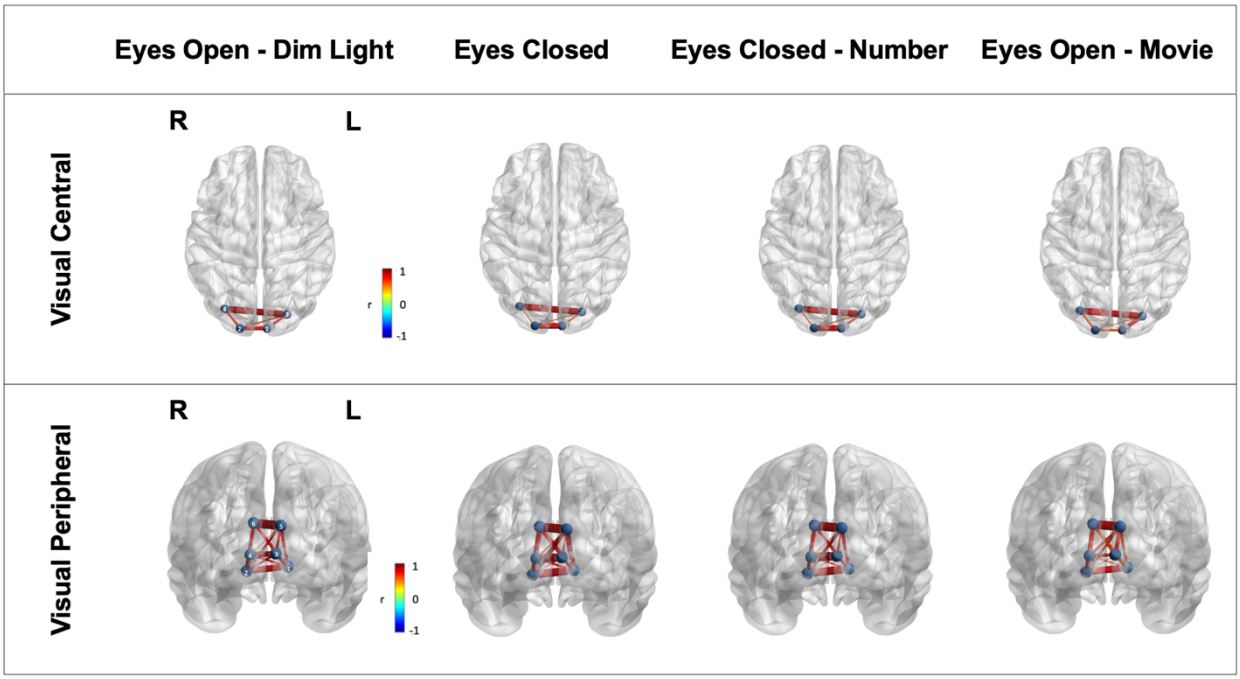

TABLES

Table 2.1. Resting-State Functional Connectivity at Different Conditions: *Significant comparisons after Bonferroni correction are indicated in **bold**. The first two rows in the "ANOVA" column did not require correction for multiple comparisons, as it is a global measurement. The "ANOVA" column (excluding the first two rows) shows uncorrected *p*-values with significance set at $p < 0.00294$. The "Pairwise *t*-test" columns show corrected *p*-values with significance set at $p \leq 0.05$. The *p*-values greater than 1 following Bonferroni correction are shown as "1". **Abbreviations:** Eyes-Open (EO); Eyes-Closed (EC); Eyes-Closed-Number (ECN); Movie (M).

Network	Mean Connectivity (*r* value)				ANOVA (*p* value)	Pairwise *t*-test (*p-value*)					
	Eyes Open	Eyes Closed	Eyes Closed Number	Movie		EO v. EC	EO v. ECN	EC v. ECN	EO v. M	EC v. M	ECN v. M
Global Average of Absolute between-Node Connectivity	0.28 ± 0.03	0.31 ± 0.04	0.29 ± 0.03	0.27 ± 0.02	**<0.001**	0.105	1	1	0.652	**0.002**	**0.02**
Global Average of Within-Network Connectivity	0.75 ± 0.31	0.75 ± 0.33	0.74 ± 0.33	0.68 ± 0.31	**<0.001**	1	1	1	**<0.001**	**<0.001**	**<0.001**
Control-*A*	0.45 ± 0.09	0.43 ± 0.12	0.43 ± 0.10	0.37 ± 0.11	0.008						
Control-*B*	0.46 ± 0.08	0.45 ± 0.11	0.47 ± 0.07	0.40 ± 0.07	0.050						
Control-*C*	0.62 ± 0.16	0.64 ± 0.13	0.64 ± 0.14	0.64 ± 0.11	0.950						
Default-*A*	0.60 ± 0.10	0.53 ± 0.10	0.58 ± 0.09	0.45 ± 0.10	**<0.001**	**0.012**	1	0.179	**<0.001**	**0.013**	**<0.001**
Default-*B*	0.51 ± 0.09	0.52 ± 0.11	0.50 ± 0.10	0.51 ± 0.10	0.860						
Default-*C*	0.55 ± 0.10	0.51 ± 0.12	0.53 ± 0.11	0.53 ± 0.11	**<0.001**	1	1	1	**0.042**	0.113	**0.019**
Dorsal Attention-*A*	0.70 ± 0.10	0.58 ± 0.13	0.55 ± 0.12	0.63 ± 0.10	**<0.001**	**0.005**	**<0.001**	1	0.111	1	0.258
Dorsal Attention-*B*	0.52 ± 0.10	0.50 ± 0.13	0.45 ± 0.12	0.50 ± 0.11	0.110						
Limbic Temporal-Pole	0.71 ± 0.10	0.77 ± 0.87	0.75 ± 0.13	0.73 ± 0.12	0.150						
Limbic Orbitofrontal	0.64 ± 0.20	0.69 ± 0.10	0.62 ± 0.18	0.66 ± 0.18	0.750						
Salience/Ventral Attention-*A*	0.60 ± 0.09	0.62 ± 0.08	0.58 ± 0.10	0.48 ± 0.10	**<0.001**	1	1	0.327	**<0.001**	**<0.001**	**0.002**
Salience/Ventral Attention-*B*	0.37 ± 0.10	0.37 ± 0.10	0.35 ± 0.09	0.30 ± 0.09	0.005						
Somatomotor-*A*	0.78 ± 0.15	0.81 ± 0.20	0.83 ± 0.14	0.70 ± 0.15	**0.002**	0.934	1	1	**0.02**	**0.005**	**0.002**
Somatomotor-*B*	0.54 ± 0.11	0.63 ± 0.14	0.60 ± 0.12	0.46 ± 0.08	**<0.001**	**0.004**	0.650	0.597	0.11	**<0.001**	**<0.001**
Temporal-Parietal	0.70 ± 0.12	0.77 ± 0.13	0.77 ± 0.12	0.83 ± 0.11	**0.002**	0.312	0.070	1	**0.001**	0.229	0.111
Visual Central	0.75 ± 0.09	0.63 ± 0.14	0.66 ± 0.18	0.63 ± 0.11	**<0.001**	**0.007**	0.757	1	**0.001**	1	1
Visual Peripheral	0.77 ± 0.11	0.75 ± 0.12	0.77 ± 0.11	0.67 ± 0.10	**0.001**	1	1	1	**0.004**	**0.021**	**0.001**

CHAPTER 3: DEFINING A FUNCTIONAL ATLAS OF RESTING-STATE NETWORKS FOR OLDER HYPERTENSIVE ADULTS WITHIN THE rrAD420 ANATOMICAL SPACE

This chapter was adapted from: Fernandez, Z.*, Scheel, N.*, Keller,J, Binder, E., Vidoni, E., Burns, J., Stowe, A., Kerwin, D., Vongpatanasin., W., Cullum, M., Zhang, R., & Zhu, D. C. (2022). Introducing rrAD420, an anatomical template and multi-modal atlas for older adults. (In Preparation)

3.1 – Abstract

Risk Reduction for Alzheimer's Disease (rrAD) is a recently completed randomized clinical trial designed to investigate the effects of improved cardiovascular health on neurocognitive function as well as brain structure and connectivity ((1)). The rrAD sample is comprised of 420 hypertensive older adults (60 to 84 years, 68.8±5.9) with a family history of dementia or subjective cognitive decline that underwent aerobic exercise training and/or intensive pharmacological interventions. This trial collected anatomical and resting-state functional MRI (rs-fMRI) scans at baseline and two years following intervention for all subjects across five different 3T MRI scanners.

Current rs-fMRI atlases, such as those developed by Yeo (2), Shirer (3), and Damoiseaux (4), were based on young and healthy populations. While being used to study resting-state networks (RSNs) in older adults, these atlases do not account for age-related brain atrophy and changes in RSN connectivity. Here, our goal is to use the rrAD baseline rs-fMRI scans to create a robust rs-fMRI atlas that is better-suited to study older populations. Using SPM12's DARTEL registration (5) we created a cohort-specific MNI-adjacent anatomical template space, namely rrAD420. Using the data-driven approaches of temporally concatenated group independent component analysis (GICA) (6) and probabilistic functional mode decomposition (PROFUMO) (7), we created an rs-fMRI atlas that more adequately describes RSN functional connectivity of our cohort, including different modes of major networks. We expect the rrAD420 rs-fMRI atlas to

be applicable to study the functional connectivity of older populations in general, which could lead to more reliable biomarker detection.

3.2 – Introduction

Functional magnetic resonance imaging (fMRI) offers a noninvasive measurement of hemodynamic changes in the blood oxygenation level-dependent (BOLD) response to infer brain function (8). Until recently, fMRI studies have mostly focused on the task-evoked BOLD signals of specific brain regions to gauge regional neuronal activation while subjects are presented with a specific stimulus or task compared to baseline. However, there is an ever-growing interest towards resting-state fMRI (rs-fMRI), a model-free approach that does not require a specific task or stimulus. Rs-fMRI concentrates on the spontaneous fluctuations of BOLD signals at low frequencies (0.01 - 0.1 Hz) at rest. These fluctuations have been shown to preserve the synchronized configurations of functionally connected brain regions found using task-based fMRI (9). Spatially, distinct brain regions that share a common BOLD signal time-course are believed to be functionally connected. They are typically grouped together and collectively referred to as a resting-state network (RSN). Previous work has revealed a consistent organization of RSNs, and the complete collection of all RSNs in a single parcellation can be described as a functional atlas (2,4,10,11).

Typically, rs-fMRI research is conducted by characterizing RSNs through either seed-based or data-driven approaches, or by using existing atlases that are well-matched for the demographics of the population of interest for a given study. Seed-based approaches can be considered hypothesis-driven, as the experimenter must choose each optimal seed region in order to generate the corresponding RSNs of interest one at a time (9,12,13). This method cross-correlates the BOLD time course of voxels within the chosen seed region with all other voxels throughout the rest of the brain and estimates the spatial map of regions that share similar spontaneous BOLD signal fluctuations throughout the time course. Whereas data-driven

methods are thought to be more exploratory, as this type of approach attempts to summarize the entire dataset between a set number of separate components, or modes, and provide multiple spatial configurations that resemble known RSNs simultaneously (6,7,14–16) Independent component analysis (ICA) is regarded as the current standard data-driven blind source separation technique to decompose raw rs-fMRI data into components that are maximally spatially independent from one another, such that each individual piece of the data belongs to a single component (6). Recently, probabilistic functional modes (PROFUMO) also emerged as a data-driven tool to extract RSNs in groups and individuals without the requirement of spatial independence (7,16). Regardless of the strategy used to characterize RSNs, the general concept is the same: brain regions that are integrated together within the same RSN are thought to be more functionally connected to each other than regions that do not belong to the same RSN. Currently, there is no consensus on the exact number of distinguishable RSNs present in the brain, and RSN configuration can differ between functional atlases depending on the strategies used to define RSNs. Although these slight variations exist between functional atlases, major RSNs such as the default mode network (DMN), executive control network (ECN), salience network, visual network, and somatomotor network (SMN) have been represented throughout multiple functional atlases (9,10,17–23).

The demographics of the individuals which functional atlases are based on can also lead to differences in RSN configuration. Most of the existing functional atlases are focused on healthy and often younger populations, and the same can be said about the anatomical standard images used to normalize group-based results (24). However, the brain experiences age-related structural and functional changes that should be accounted for when using a functional atlas in older populations (25). For example, brain atrophy and ventricular enlargement are common in aged populations, leading to substantial deviations from the standard MNI152 and MNI305 coordinates which are based on much younger subjects, 25.02 ± 4.9 and 23.4 ± 4.1 years of

age respectively (26,27). These anatomical differences are problematic as they might cause severe artifacts when transforming non-normative brains into MNI space via volumetric non-linear normalization pipelines (28). Furthermore, fMRI studies have demonstrated functional connectivity to change throughout the lifespan, even in normal nonpathological aging (24,29). Indeed, a study by Doucet and colleagues found that major RSNs, including DMN, ECN, SMN, visual and salience networks, had a different spatial composition in older adults compared to younger adults (24). Their results highlight the importance of age-appropriate functional atlases and present the first functional atlas derived from older adults, namely the Atlas55+. While the Atlas55+ provides a viable option to examine major RSNs in older adults through a network modeling approach, there are currently limited alternatives for other commonly studied RSNs that capture the expected anatomical and functional distinctions from younger populations. Examples of such other common RSNs include the language network, limbic network, and visuospatial network (2,11). The current study sought to provide a functional atlas for older adults that includes a comprehensive RSN parcellation, as well as an age-appropriate standard anatomical space, using the rs-fMRI and anatomical T1-weighted scan data from the Risk Reduction for Alzheimer's Disease (rrAD) study.

The rrAD study is a recently completed randomized controlled trial designed to assess the effects of aerobic exercise training and intensive pharmacological cardiovascular interventions on neurocognitive function in hypertensive older adults with a family history of dementia or subjective cognitive decline (1). The in-depth neuroimaging protocol included anatomical, functional, and physiological MRI scans, obtained at baseline and again after two years of intervention. 420 older subjects (60 to 84 years, 68.8±5.9) had baseline scans on five different 3T MRI scanners (two Siemens, two GE, and one Philips). Each scan underwent rigorous quality control directed by Dr. David Zhu (a trained MRI physicist).

Here, we utilize the data-driven group independent component analysis (GICA) (6) and probabilistic functional mode decomposition (PROFUMO) (7), together with seed-based connectivity maps of the pre-processed rs-fMRI data, to create a functional atlas tailored to older hypertensive adults. This sample provides a good number of older subjects with imaging data collected for each subject in a standardized manner across all testing locations. Additionally, because all subjects are demographically similar, our anatomical space and functional atlas will be optimized for future studies that wish to perform RSN modeling within hypertensive older adults. However, we also believe the provided templates and flow fields of our rrAD420 space will extend to better representing the RSNs of older adults in general. Using the high-quality baseline data of this study, we aim to integrate images from multiple modalities to create an accurate brain template and atlas that is better suited to represent older populations and can be used by researchers studying comparable cohorts.

3.3 – Methods

3.3.1 – Participants

Four-hundred-twenty hypertensive older adults (261 females, 68.8 ± 5.9 years old) with a family history of dementia or subjective memory complaints and a sedentary lifestyle participated in the rrAD study. They did not have significant cognitive impairment. All subjects were recruited from the Dallas, Baton Rouge, Kansas City, and St. Louis areas. This study was approved by the Human Subjects Committee at Pennington Biomedical Research Center (PBRC; n = 128), The University of Texas Southwestern Medical Center and Texas Health Presbyterian Hospital Dallas (UTSW/IEEM; GE scanner n = 56; Phillips scanner n = 44), University of Kansas Medical Center (KUMC; n = 103), and Washington University School of Medicine (WashU; n = 89). All participants met the strict inclusion criteria detailed in the recent rrAD rationale and methods paper and signed the necessary consent forms before participation (1).

3.3.2 – Imaging Acquisition

This experiment was conducted across five different 3T MRI scanners (UTSW using a Philips Achieva and a GE Discovery MR 750 W scanner, KUMC a Siemens Skyra scanner, WashU a Siemens Prisma scanner, and PBRC a GE Discovery MR 750 W scanner). To accommodate inter-scanner variability and harmonize the data collected between sites, each protocol was individually calibrated. All scanners utilized a 32-channel head coil, except for the UTSW GE system which used a 48-channel coil. For this current study, we focused on the rrAD neuroimaging data and specifically utilized the baseline rs-fMRI and T1-weighted anatomical images. The rs-fMRI scans were acquired with 2.5 s TR (time of repetition), 28 ms TE (time of echo), and a 64 x 64 matrix size with 3.4mm x 3.4mm pixels. A 3 mm slice thickness was used on all but the UTSW GE system, which instead used thicker slices of 3.4 mm to account for the reduced signal-to-noise ratio on the 48-channel coil. Each rs-fMRI scan lasted 12-minutes, during which subjects were asked to focus on a fixation cross to ensure a consistent rest condition across subjects, as our lab and others have shown RSNs are influenced by the condition subjects are exposed to during scan acquisition (30,31). For all subjects, the anatomical 3D 1-mm isotropic T1-weighted MPRAGE scans with cerebrospinal fluid suppressed were collected in accordance with the rrAD neuroimaging protocol using the following parameters: 176 sagittal slices, TE = 3.8–4 ms, TR of acquisition ≈ 8.6 ms, time of inversion (TI) = 830 ms, TR of inversion = 2,330 ms, flip angle = 8°, FOV (field of view) = 25.6 cm x 25.6 cm, matrix size = 256 x 256, slice thickness = 1 mm.

3.3.3 – Data Preprocessing

For processing the rs-fMRI data in subject space, we implemented the “afni_proc.py” routine in AFNI (32) to generate the script for a standard preprocessing pipeline. For each subject, spikes in the signal time course were first detected and removed. Data points with excess normalized motion derivatives or voxel outliers were identified and modeled as regressors in

subsequent processing. Slice-timing corrections were applied to account for acquisition time differences across slice locations. The functional images were co-registered to the T1-weighted high-resolution anatomical images, using the third volume as reference. Then, we applied rigid-body motion correction in three translational and three rotational directions. Translational and rotational estimates, and their derivatives, were modeled as regressors for the following noise regression step. Spatial blurring with a full-width half-maximum of 4 mm was also applied to each subject to reduce random noise and improve signal-to-noise ratios. Using the output from these initial preprocessing steps, we transformed the motion parameters from AFNI's motion correction into an FSL-compatible format to perform an aggressive ICA-AROMA to remove noise, such as subject motion, from the rs-fMRI data (33,34). We ran ICA-AROMA version 0.4 beta in MATLAB on the data in order to improve the resolution of smaller structures within the brain. First, we extracted the noise components from the rs-fMRI data that was blurred with a 6-mm full-width half-maximum kernel as suggested in previous work (36), then the time courses of these noise components were regressed out of the rs-fMRI data that was blurred with a 4-mm kernel (33,35). A comprehensive explanation for the rationale behind choosing aggressive ICA-AROMA for the removal of nuisance components on rrAD rs-fMRI data over other preprocessing techniques, such as standard censoring, censoring with global signal removal, non-aggressive ICA-AROMA, or the spatially organized component klassifikator (SOCK) has recently been published (36). In line with previous research, our lab found that while the other aforementioned techniques performed reasonably well aggressive ICA-AROMA showed the greatest level of data reproducibility (33,37). As a final preprocessing step, we applied a temporal band-pass filter in the range of 0.009 Hz – 0.08 Hz as part of the regression model.

After the T1-weighted high-resolution anatomical images were properly co-registered with the rs-fMRI images, the origin was manually reoriented to the anterior commissure for each subject to stabilize the following spatial normalization steps. Then, in order to create a cohort-

specific MNI-adjacent standard template, the reoriented images were used as inputs for SPM12's segmentation and non-linear DARTEL registration (5). We transformed the rs-fMRI images from the subjects' native space into the newly created standard space, referred to as the rrAD420 space. The rrAD420 normalized anatomical space captures the characteristics specific to the rrAD cohort and provides an excellent template to display the functional connectivity profiles extracted from the rs-fMRI data and later compare them between treatment groups through network modeling methods (Figure 3.1).

3.3.4 – Functional Data Decomposition

Using hypothesis-driven seed-based connectivity maps (9,12,38) in combination with data-driven approaches, temporally concatenated group independent component analysis (GICA) (6) and probabilistic functional mode decomposition (PROFUMO) (7), on the pre-processed rs-fMRI data, we created a functional atlas that describes the functional connectivity for the older adults in the rrAD cohort. Data-driven methods for blind source separation have the advantage of distinguishing sources of noise and signal, and later identify RSNs without having to define the model beforehand (6,7,38). One example of these techniques is GICA, which is the most frequently used temporal decomposition method in functional neuroimaging research.

GICA is a matrix factorization tool that unmixes the signals from rs-fMRI data, and groups spatially distinct brain regions of interest (ROIs) that share a common BOLD signal time-course into single components. Here, we employed FSL's MELODIC software to perform GICA on the entire sample by temporal concatenation (39). Through this approach, GICA reorganized the four-dimensional rs-fMRI data for each subject into a two-dimensional time x space matrix, with each row representing an individual voxel and each column representing an individual time point. The time x space matrices for all subjects were then concatenated in the temporal direction in order to identify components that relate to the entire group. GICA decomposes this large, group time x space matrix into two matrices; a spatial matrix that contains a topological

map for each group component that was identified and a temporal matrix with a time-course corresponding to each spatial component that was identified. Afterwards, MELODIC takes each row of the group spatial matrix and converts it back into a three-dimensional image to visualize each spatial component. GICA attempts to maximize spatial independence between each component based on the non-gaussianity of the data, and each component explains parts of the original input data by providing a map that represents either neural signals, noise, or a mixture of both (40). MELODIC uses negative entropy as a measure for non-gaussianity, and by maximizing the non-gaussianity of the unmixed signals it decreases the chance of identifying random noise as a component (41). Furthermore, these group spatial components were backtransformed to the individual subjects by performing the dual regression in FSL. This allows for the group spatial maps to be mapped to the subject time courses for later comparison between groups. Due to this step, GICA is considered unidirectional as it always builds the group spatial maps first and then applies them to the individual subjects. This unidirectionality in turn can limit the amount of inter-subject variation in functional connectivity that GICA can incorporate into the group spatial maps (42). In addition, because MELODIC does not allow spatial overlap between components, it does not represent the functional networks well when networks are in-fact overlapping (43). This may pose some issues when assigning an ROI that is potentially involved multiple RSNs to a single component. Recently, FSL released a new data-driven matrix factorization approach called Probabilistic Functional Mode decomposition (PROFUMO) to define RSNs within the brain. PROFUMO offers some advantage over GICA (7,16). In contrast to GICA, PROFUMO offers a bidirectional approach to simultaneously model the population and the individuals. This is achieved by using the group spatial maps to normalize the subject spatial maps through a top-down framework, while also using the subject spatial maps to continuously update the group spatial maps through a bottom-up framework. This process repeats iteratively until the group spatial maps best agree with the subject spatial maps. In doing so, these updated group spatial maps can better capture inter-subject variability

(44). Another difference to GICA is that PROFUMO does not assume spatial independence between modes, with modes being analogous to “components” in GICA. This allows for spatial repeats across modes, so a single multifunctional ROI can be included across multiple modes. Here, similar to GICA, we applied the approach using PROFUMO to unmix the preprocessed rs-fMRI data into individual modes comprised of ROIs that share a common BOLD signal time-course. PROFUMO does this by estimating a probability distribution for the spatial and temporal elements of the group and each individual subject and optimizing the estimated distribution through Bayesian inference (7). This probability distribution optimization is reached by using the initial estimates, referred to as priors, from the group modes to normalize the subject modes. The priors are then optimized for each subject until the final distribution estimates, referred to as posteriors, are obtained. These subject mode posteriors are subsequently used to update the group modes, and the process repeats until there is a convergence between the group and subject spatial maps.

3.3.5 – Atlas Creation

To create a hypothesis-driven map of the default mode network (DMN) for our functional atlas through traditional seed-based correlation analysis, we chose the isthmus of the posterior cingulate cortex as our seed region (45). We used Freesurfer segmentation output for each subject to identify and select the region to correlate BOLD time course of the seed region with every other voxel time course throughout the brain (46). We then transformed the structural images from each subject into rrAD420 standard space using the DARTEL transformation (5). Finally, we obtained our group-level DMN spatial maps through averaging all subject connectivity maps and thresholding through gaussian mixture modeling and ROI extraction (9).

Although the described data-driven techniques are powerful, it is difficult to determine how many true signal sources are present in the mixed signal. In addition, fMRI data is inherently noisy, and we must allow extra components to account for nuisance signals, and while ICA can

separate some of these noise components, it is inherently difficult to label some components as neuronal signals or noise (47). Therefore, we performed multiple iterations of both MELODIC and PROFUMO in order to find the best-fitting parcellation to use for our functional atlas. Specifically, we ran seven instances of GICA with the dimensionality hyperparameter set at 21, 35, 49, 63, 77, 91, and 105, and three instances of PROFUMO with 30, 50, and 80 dimensions. We chose to start with a 21-component parcellation for GICA as suggested by previous literature and incrementally increased the number of components with each iteration (6). We followed a similar reasoning when selecting the number of parcellations to use for PROFUMO. However, we had to limit the number of iterations due to the immense computational demand required to run PROFUMO. We then manually checked the output of each GICA and PROFUMO iteration separately and labeled each component as true signal or noise following the ICA hand classification protocol presented by Griffanti et al. (48). This protocol provides useful examples of spatial patterns observed in individual components to look for and assist in identifying the components with true neuronal signals versus those that capture signals of other origins such as subject motion, vessels, or artefacts. Also included in their protocol is the "innocent until proven guilty" flowchart which summarized their procedure and proved to be instrumental in labeling components and modes. Components and modes determined to be true signals were assigned a network designation based on the RSN each component or mode best resembled. To facilitate the labeling phase, we implemented an anatomical dual-regression approach, combining FreeSurfer segmentation and DARTEL normalization to create probabilistic representations of commonly used brain atlases, such as the automatic anatomical labeling (AAL) (49), Brodmann (50), Desikan (51), Destrieux (52), Yeo (2), and Shirer (11) from MNI into rrAD420 space, allowing conversions between rrAD420 and other atlases. We used these atlases in rrAD420 space to cross-reference with our own data and accurately label components and modes as the RSN they best aligned with through a manual two-rater system. This procedure required both raters to agree before assigning an RSN designation (Zac

Fernandez and Dr. Norman Scheel). Once all components were appropriately designated as signal or noise, we used metrics of RSN representation, RSN splitting, and RSN grouping as criteria to select the parcellation dimension with optimal separation of our data. RSN representation was decided based on the percentage of RSNs present relative to the 14 networks from the Shirer atlas (11). RSN splitting was quantified by tallying the number of networks present in each component, while RSN grouping was quantified by tallying the number of components that represented the same RSN. RSN splitting and RSN grouping describe issues associated with the problem of overfitting and underfitting the data, respectively (Figure 3.2). If the dimensionality hyperparameter is greater than the actual number of RSNs present in the data, then overfitting occurs and a single RSN can be split into subnetworks between multiple components or modes. Conversely, if the dimensionality hyperparameter is less than the actual number of RSNs present in the data, then underfitting occurs and multiple RSNs will be improperly grouped together within a single component or mode. After considering these metrics, we concluded the 49-component GICA parcellation and the 50-mode PROFUMO parcellation provided the best RSN separations for our functional atlas.

3.4 – Results

The rrAD420 template and functional atlas integrate multimodal neuroimaging data of older populations into a common space, accounting for cohort-specific distinctions, such as cortical atrophy and enlarged ventricles. It provides references to commonly used brain parcellations and completes these with functional and structural atlases created from the rrAD cohort, forming a comprehensive multimodal reference brain template.

3.4.1 – Seed-Based Correlation Analysis

Here, we provide a hypothesis-driven spatial map of DMN that was generated through a traditional seed-based approach (Figure 3.3). The results of our analysis found that an optimal

DMN spatial map comprised 24 ROIs, including the right posterior cingulum, left posterior cingulum, right precuneus/angular gyrus, left precuneus/angular gyrus, right medial frontal gyrus/medial orbital gyrus, left medial frontal gyrus/medial orbital gyrus, right superior frontal gyrus, left superior frontal gyrus, right anterior superior temporal sulcus, left anterior superior temporal sulcus, right medial prefrontal thalamus, left medial prefrontal thalamus, right hippocampus subiculum, left hippocampus subiculum, right parahippocampal place area, left parahippocampal place area, right inferior frontal gyrus (BA11), left inferior frontal gyrus (BA11), right medial cerebellum, left medial cerebellum, right cerebellar tonsil, left cerebellar tonsil, right posterior cerebellum, left posterior cerebellum.

3.4.2 – Group Independent Component Analysis

We examined the FSL MELODIC output of each of the seven GICA iterations with hyperparameters for the total number of components allowed set at 21, 35, 49, 63, 77, 91, and 105. Adhering to the hand-classification guide provided by Griffanti and colleagues, we categorized each component as either signal or noise (48). We found the 21-component parcellation yielded 9 components that represent true signal, and the remaining 12 noise components were of non-neuronal origin. Likewise, the 35-component parcellation yielded 15 components that were true signal and 20 noise components. The 49-component parcellation yielded 19 true signal components and 30 noise components. While the remaining 63-component 77-component, 91-component and 105-component parcellations respectively yielded 20, 27, 31 and 32 components that were derived from true signal. We then designated each component that was classified as true signal as the RSN it best represented for each iteration, using the 14 Shirer networks as a reference atlas (11). In instances where spatial maps of a component represented the true signal of an RSN that was not included in the Shirer atlas, such as the limbic network, we used additional functional atlases to supplement the labeling phase of the process. In order to decide which parcellation strategy was best for our

functional atlas, we assessed RSN representation, RSN splitting, and RSN grouping as defined in the methods section.

We found that all iterations represented all 14 of Shirer's networks in some capacity, either as a single network in a single component or as a secondary RSN in a component that groups one or more RSNs together (Figure 3.4). However, when only considering primary RSN representation in components, we found variance between parcellations. Specifically, the 21-component and 35-component parcellations did not identify as many primary network components as the other iterations. The 49-component parcellation was able to capture a primary representation of most RSNs, and there was a plateau effect as the 63-component, 77-component, and 91-component parcellations performed at the same level. The 105-component parcellation was the only iteration to show primary RSN representation for all RSNs in single components (Figure 3.5). The next metric we considered in our decision was RSN splitting. We found that although the 105-component parcellation captured all primary RSNs from the reference atlas, it also had the highest occurrence of splitting single RSNs between multiple components (Figure 3.6). Although this issue was not as extreme in other parcellations, there was a trend that as the hyperparameters allowed for more components, network splitting would become more common. Lastly, we considered RSN grouping and found the inverse of RSN splitting to be true. The 21-component and 35-component parcellations were shown to group more RSNs together within single components, which lowered the primary network representation for these iterations (Figure 3.7). Overall, we found the 49-component parcellation provided the best RSN separation in terms of network representation and the balance between RSN splitting and grouping. Therefore, we chose this parcellation solution to use as the GICA portion of our rrAD420 functional atlas.

Within the 49-component GICA parcellation solution of the rrAD420 functional atlas, we identified fifteen recognizable RSNs including: primary visual, sensorimotor (SMN), left

executive control (LECN), precuneus, dorsal attention/visuospatial (DAN/Vis), ventral default mode (vDMN), high visual, posterior salience, anterior salience, language, dorsal default mode (dDMN), right executive control (RECN), auditory, basal ganglia, and limbic networks. These RSNs were ordered in terms of spatial reproducibility with the primary visual network being the most reproducible and the limbic network being the most difficult to reproduce (33,34). A listing of the number and names of regions included for each RSN (Table 3.1) and visual representations for each RSN spatial map and a list of corresponding brain regions have been provided (Figure 3.8).

For the GICA portion of the rrAD420 functional atlas, the primary visual network spanned the medial occipital lobe and was comprised of the right superior middle occipital gyrus and left superior middle occipital gyrus. SMN was represented across two components which were combined for the purposes of the functional atlas to create a single SMN spatial map. The regions included in the finalized SMN spatial map were the right superior pre/postcentral gyrus, left superior pre/postcentral gyrus; right inferior precentral gyrus, and left inferior precentral gyrus. LECN included the left inferior parietal lobe, left middle/inferior frontal gyrus, left superior medial gyrus, left posterior middle cingulate cortex, left inferior/middle temporal gyrus, and right posterior cerebellum. The precuneus network included the right precuneus, left precuneus, right posterior/middle cingulate cortex, and left posterior/middle cingulate cortex. The DAN/Vis network contained a mixture of regions from the visuospatial network as presented in the Shirer atlas, as well as regions that belong to the DAN presented by Yeo and colleagues (2,11). Specifically, the DAN/Vis network included the right superior parietal cortex, right precuneus, left superior parietal cortex, left precuneus, right superior frontal cortex, left superior frontal cortex, right inferior frontal gyrus, left inferior frontal gyrus, right middle temporal gyrus, left middle temporal gyrus, and right inferior temporal gyrus. The vDMN contained the right precuneus, left precuneus, right frontal eye field, left frontal eye field, right middle occipital gyrus, left middle

occipital gyrus, right retrosplenial cortex, left retrosplenial cortex, right parahippocampal place area, and left parahippocampal place area. The high visual network covered regions of the lateral occipital lobe which consisted of a single bilateral connection between the right prestriate cortex and the left prestriate cortex. The posterior salience network was comprised of the right supramarginal gyrus, left supramarginal gyrus; right precuneus/middle cingulate cortex, left precuneus/middle cingulate cortex, right thalamus, left thalamus, right insula, left insula, right superior cerebellum, and left superior cerebellum. Regions of the anterior salience network were identified across four components and were subsequently combined into a single spatial map to capture the RSN in its entirety. The final anterior salience network map included the right superior frontal gyrus, left superior frontal gyrus, right middle frontal gyrus, left middle frontal gyrus, right dorsal anterior cingulate cortex, left dorsal anterior cingulate cortex, right superior frontal gyrus/pre-supplemental motor area, left superior frontal gyrus/pre-supplemental motor area, right insula, left insula, right superior cerebellum, left superior cerebellum, right inferior cerebellum, and left inferior cerebellum. We also observed the language network across two separate components, which were merged to create a finalized language network spatial map. The brain regions of the final language network spatial map included the right angular gyrus, left angular gyrus, right superior temporal gyrus, left superior temporal gyrus, right superior/middle temporal gyrus, left superior/middle temporal gyrus, right pars triangularis, left pars triangularis, right middle temporal gyrus, and left middle temporal gyrus. Two components of our GICA parcellation resembled the dDMN, these components were combined to create a single dDMN spatial map. The final dDMN spatial map contained the most brain regions of any RSN in the rrAD420 functional atlas. These regions included the right posterior cingulate cortex, left posterior cingulate cortex, right superior frontal gyrus, left superior frontal/medial gyrus, right angular gyrus, left angular gyrus, right superior medial gyrus, right basal ganglia, left basal ganglia, right anterior cingulate cortex, left anterior cingulate cortex, right inferior frontal gyrus, left inferior frontal gyrus, right hippocampus, left hippocampus, right middle temporal gyrus, left

middle temporal gyrus, right superior cerebellum, left superior cerebellum, right inferior cerebellum, left inferior cerebellum. The RECN also presented across two components that were combined to form a single spatial map to represent the complete RSN. The finalized RECN spatial map was comprised of the right inferior parietal lobe/angular gyrus, right middle/inferior frontal gyrus, right superior medial gyrus, right posterior middle cingulate cortex, right pars opercularis/inferior frontal gyrus, right middle frontal gyrus, right inferior/middle temporal gyrus, and left posterior cerebellum. The auditory network spanned the auditory cortex, which included a single bilateral connection between the right superior temporal gyrus/operculum and left superior temporal gyrus/operculum. The basal ganglia network was a simple RSN that contained the right basal ganglia and left basal ganglia. The final network for the GICA portion of our atlas was the limbic network, which involved the right temporal pole, left temporal pole, right pallidum, and left pallidum.

3.4.3 – Probabilistic Functional Modes

Following the same process detailed in the above GICA section, we examined the FSL PROFUMO output of each of the three PROFUMO iterations with the hyperparameters for the number of network modes set at 30, 50, and 80. Following the same hand-classification guidelines detailed above, we categorized each mode as either signal or noise (48). We found the 30-mode parcellation yielded 24 modes that represent true signal, and the remaining 6 modes were of non-neuronal origin and considered as noise. The 50-mode parcellation yielded 42 true signal modes and 30 noise modes, and the 80-mode parcellation had 65 modes derived from true signal and 15 modes from noise. Again, we assessed RSN representation, RSN splitting, and RSN grouping to determine which parcellation solution would provide the best RSN separation. In terms of RSN representation, we found that each iteration captured all RSNs of the reference functional atlas presented by Shirer and colleagues (11) (Figure 3.5).

However, the 50-mode parcellation showed the most promise as the basis for our functional atlas when considering RSN splitting and grouping (Figure 3.6; Figure 3.7).

Within the 50-mode PROFUMO parcellation solution of the rrAD420 functional atlas, we identified thirteen “pure” RSNs including the precuneus, primary visual, LECN, SMN, high visual, RECN, vDMN, dDMN, posterior salience, visuospatial, anterior salience, limbic, and basal ganglia networks. In addition, some modes integrated elements of multiple RSNs together into a single spatial map. This occurred primarily due to PROFUMO’s allowance for multimodal brain regions to be represented across multiple modes, whereas GICA seeks to maximize spatial independence for each region between components. These modes were kept in our functional atlas as “combinatory” networks. We identified six RSNs of this type including the anterior ECN/dDMN (aECN/dDMN), language/dDMN, anterior salience/dorsal attention network (aSalience/DAN), language/temporoparietal, language/auditory/temporoparietal, and language/auditory networks. Also, in contrast to the GICA portion of our functional atlas, the PROFUMO parcellation yielded some cases in which multiple modes captured elements of the same RSN. In these instances, all modes were kept as subnetworks for their respective RSNs. Nine RSNs of our functional atlas include subnetworks, namely the primary visual, SMN, high visual, vDMN, dDMN, posterior salience, visuospatial, anterior salience, and limbic networks, as well as the language/DMN combinatory network. We assigned the mode that best captured the reference spatial map of its respective RSN as the primary representative subnetwork. As such, the primary representative subnetwork was listed first for each RSN with subnetworks in our functional atlas (i.e. “PROFUMO X.1” in Table 3.2 and Figure 3.9).

For the “pure” networks in the PROFUMO portion of the rrAD420 functional atlas, we identified the precuneus network in a single mode with regions composed of the right precuneus, left precuneus, right posterior/middle cingulate cortex, and left posterior/middle cingulate cortex. The primary visual network was represented by three modes which were kept

separately as subnetworks because each mode captured distinct features of the primary visual network. The first subnetwork included the right and left superior middle occipital gyri. This closely resembles the analogous primary visual network spatial map from the GICA section. The second primary visual subnetwork was comprised of the right inferior occipital gyrus and left inferior occipital gyrus. While the third subnetwork was comprised of the right middle occipital gyrus and left middle occipital gyrus, with some anticorrelated regions that survived thresholding, the right superior occipital gyrus and left superior occipital gyrus. The LECN spanned the frontal and parietal cortices which included the left inferior parietal lobe/angular gyrus, left medial/inferior frontal cortex, left superior medial frontal cortex, left inferior/medial temporal cortex, left posterior middle cingulate cortex, right inferior semilunar lobule of the cerebellum, and right posterior cerebellum. Five modes each resembled portions of the sensorimotor network and were defined as subnetworks. The first sensorimotor subnetwork included the right superior pre/postcentral gyrus and left superior pre/postcentral gyrus. The second subnetwork was comprised of the right inferior precentral gyrus and left inferior precentral gyrus. Next, the third subnetwork was comprised of the right middle precentral gyrus and left middle precentral gyrus. Cerebellar regions of the sensorimotor network were identified in the fourth subnetwork, and specifically included the bilateral anterior portions of the cerebellum. The final sensorimotor subnetwork involved the medial portions of the right superior pre/postcentral gyrus and left superior pre/postcentral gyrus. Subnetworks of the high visual network were identified between three modes. The first subnetwork best resembled the GICA high visual network and included the right and left prestriate cortex. The second subnetwork covered the right and left inferior occipital gyrus, while the final high visual subnetwork contained the right and left superior occipital gyrus. For the RECN, a single mode resembled the network in its entirety, consisting of the right inferior parietal lobe/angular gyrus, right medial/inferior frontal cortex, right superior medial frontal cortex, right inferior/medial temporal cortex, right posterior middle cingulate cortex, left inferior posterior cerebellum, and left

posterior cerebellum. Two subnetworks of the vDMN were identified between two modes. The first subnetwork was most consistent with the vDMN spatial map in the GICA portion, as it contained the right precuneus, left precuneus, right frontal eye field, left frontal eye field, right middle occipital gyrus, left middle occipital gyrus, right retrosplenial cortex, left retrosplenial cortex, right parahippocampal place area, and left parahippocampal place area. While the second vDMN subnetwork contained a single connection between the left and right precuneus. For our atlas, we identified four modes that were labeled as dDMN subnetworks. The first subnetwork best maintained the typical configuration expected of the dDMN, which included the right posterior cingulate cortex, left posterior cingulate cortex, right angular gyrus, left angular gyrus, right superior frontal gyrus, left superior frontal gyrus, right medial prefrontal cortex, left medial prefrontal cortex, right middle temporal lobe, and left middle temporal lobe. Cerebellar regions of the dDMN were included in the second subnetwork, namely the right posterior cerebellum and left posterior cerebellum. The third dDMN subnetwork included a single connection between the left and right prefrontal cortex. While the fourth dDMN subnetwork captured the right anterior cingulate cortex, left anterior cingulate cortex, right middle cingulate cortex and left middle cingulate cortex. The posterior salience network was represented by two modes, which were both included in our atlas as subnetworks. The first posterior salience subnetwork was comprised of the right supramarginal gyrus, left supramarginal gyrus, right precuneus/middle cingulate cortex, left precuneus/middle cingulate cortex, right superior middle frontal gyrus, left middle frontal gyrus, right inferior frontal gyrus, left inferior frontal gyrus, right inferior middle frontal gyrus, left inferior middle frontal gyrus, and right middle temporal gyrus. The second subnetwork contained only two regions, the right superior parietal lobule and left superior parietal lobule. Regions of the visuospatial network were identified across six modes, which were all included as individual subnetworks. The primary representative subnetwork included the right superior parietal cortex/precuneus, left superior parietal cortex/precuneus, right superior frontal cortex, left superior frontal cortex, right inferior

frontal gyrus, left inferior frontal gyrus, right inferior temporal gyrus, and left inferior temporal gyrus. The second visuospatial subnetwork contained two large, mirrored regions that bilaterally spanned the inferior parietal cortex and superior parietal cortex/precuneus. Third, we identified a visuospatial subnetwork comprised of the right inferior parietal lobule, right pars opercularis, and right middle frontal gyrus. The fourth visuospatial subnetwork included the right inferior frontal gyrus and left inferior frontal gyrus. The fifth subnetwork included the right intraparietal sulcus and left intraparietal sulcus. While the sixth and final visuospatial subnetwork contained regions of the right superior parietal lobule and left superior parietal lobule. Three modes represented subnetworks of the anterior salience network. The primary subnetwork best captured features of the classic anterior salience network, which included the right superior/middle frontal gyrus, left middle frontal gyrus, right dorsal anterior cingulate cortex, left dorsal anterior cingulate cortex, right insula, and left insula. The second subnetwork contained the right middle frontal gyrus and left middle frontal gyrus. While the third subnetwork consisted of a single connection between the right and left secondary motor area. For our atlas, two modes of the rrAD420 PROFUMO parcellation resembled subnetworks of the limbic network. First, we identified a limbic subnetwork that contained the right and left orbitofrontal cortex. Our second limbic subnetwork included the right temporal pole and the left temporal pole. A single mode represented the basal ganglia network in its entirety, and this network included the left and right basal ganglia.

In addition to the individual “pure” networks listed above, the PROFUMO portion of the rrAD420 atlas also yielded six “combinatory” networks because multimodal regions were allowed to belong to more than one mode. The first combinatory network merged anterior regions of the ECN (aECN) and portions of the dDMN. Specifically, the aECN/dDMN network contained the right superior frontal sulcus, left superior frontal sulcus, right medial superior frontal gyrus and left medial superior frontal gyrus. Three modes represented subnetworks which combined regions of the language network and dDMN together in individual spatial maps.

The first language/dDMN subnetwork was comprised of the right angular gyrus, left angular gyrus, right middle temporal gyrus, left posterior cerebellum, right pars triangularis, right middle frontal gyrus, right dorsomedial prefrontal cortex, and right precuneus. The second language/dDMN subnetwork spanned the right posterior cerebellum, left angular gyrus, left middle temporal gyrus, left pars triangularis, left middle frontal gyrus, left dorsomedial prefrontal cortex, and left precuneus. While the final language/dDMN subnetwork contained a single connection between the right pars triangularis and left pars triangularis. Another combinatory network that emerged was the aSalience/DAN. This network consisted of two large regions that covered the right and left superior precentral gyrus. The PROFUMO portion of the rrAD420 atlas concludes with three combinatory networks that involve the language network. The first was the language network combined with the temporoparietal network presented by Yeo and colleagues (2). This network included the right and left middle temporal gyrus. Next, we found a mode that contained regions shared by the language network, auditory network and temporoparietal network. Specifically, this included two regions that span the right and left posterior middle temporal gyrus, and each contained some portions of the posterior superior temporal and posterior superior temporal gyri as well. Finally, we identified a mode that spanned over both the language and auditory networks, namely the right and left superior temporal gyrus. A listing of the number of modes for each network as well as the number and names of regions included for each mode (Table 3.2) and visual representations for each RSN spatial map, and a list of corresponding brain regions have been provided (Figure 3.9).

3.5 – Discussion

Changes in neuroplasticity and functional connectivity occurs with life experiences and age-related variables. Functional atlases based on younger adults may not necessarily be reliable in older adults as they do not account for these changes. The high number of subjects with a similar demographic background in the rrAD trial presented an opportunity to establish a

standard anatomical template for older adults. In addition, the harmonized rs-fMRI scan protocols between scanners used for the study allowed us to define a complete listing of RSNs identified within this standard space. Specifically, the rrAD420 template and functional atlas integrate multimodal neuroimaging data of older populations into a common space accounting for cohort-specific distinctions, such as cortical atrophy and enlarged ventricles. It provides references to commonly used brain parcellations and completes these with functional and structural atlases created from the rrAD cohort, forming a comprehensive multimodal reference brain template. Age-appropriate baseline functional atlases of late adulthood could offer more predictive power regarding age-related disease progression, prevention, and treatment effectiveness. Within our rrAD420 functional atlas, we supply multiple options for spatial maps that can be chosen based on the goals or data quality of an individual study. Major RSNs of interest such as the DMN, salience network, primary visual network, sensorimotor network, and ECN have shown potential as biomarkers of neurodegenerative disease (53). Both the GICA and PROFUMO portions of the rrAD420 functional atlas provide spatial distributions representing each major RSN to assist in the investigation of brain functional connectivity in late adulthood. In addition, RSNs that are not typically counted among the major RSNs such as the visuospatial network, basal ganglia network, and limbic network are also included to facilitate further identification of relevant imaging biomarkers for aging and age-related disease in future studies.

3.5.1 – Seed-based Correlation Analysis

The DMN is considered to be a task-negative RSN that shows higher activation in the absence of a task, and presents as anticorrelations when subjects are performing a task (54,55). Typically, the DMN includes brain regions such as the prefrontal cortex, precuneus, posterior cingulate cortex, hippocampus, inferior parietal lobule, and angular gyri (56). The role of DMN has since been associated with mind wandering, internally driven processing and

preparation for future tasks (57). Prior work has shown DMN functional connectivity to be reduced in older individuals relative to younger adults, and it is selectively vulnerable in early Alzheimer's Disease (29,56,58,59). In addition, PET studies have revealed that hyperphosphorylated tau and amyloid beta, established hallmarks of AD, aggregate within primary DMN regions including the precuneus and posterior cingulate cortex (60,61).

In the rrAD420 atlas, we provide a high-resolution seed-based spatial map of DMN containing twenty-four regions, the so-called DMN24. The DMN24 is tailored to older adults and will benefit researchers primarily concerned with the DMN in aging. In this map, the first eighteen regions listed are cortical, and the last six are defined in the cerebellum. The cerebellum often excluded in some studies because it falls outside the FOV due to factors such as head position or brain size. Our sample had enough subjects that included the full cerebellum to increase the power of our findings, as the inclusion of these regions in our spatial map was clear and substantiated by the existing literature (56). Although these six regions showed strong functional connectivity, the last six regions of the DMN24 can be excluded from the analysis if studies choose to ignore cerebellar regions.

3.5.2 – Group Independent Component Analysis

The GICA portion of the rrAD420 functional atlas provides a spatial distribution for all 15 RSNs identified across the whole brain. This method represents the current standard for data-driven RSN definition, and will be useful to investigate multiple independent RSNs simultaneously in older populations. The GICA parcellation would benefit studies that wish to identify changes in mean functional connectivity for the entire RSN(s) of interest. There are some drawbacks to this technique such as the unidirectionality of the method which does not explicitly account for inter-subject differences, and the limited ability to distinguish between overlapping RSNs.

3.5.3 – Probabilistic Functional Modes

The PROFUMO portion of the rrAD420 functional atlas expands on GICA by simultaneously modeling RSNs at the group and subject levels through Bayesian inference (7). The group-level modes are used to normalize subject-specific modes from top-down, and the subject-specific modes are used to update and normalize group-level modes from the bottom-up. This introduces a bidirectionality to the model that better accounts for subject variability. Compared to GICA, the PROFUMO portion of the rrAD420 functional atlas found a higher proportion of modes derived of true signal origin. This resulted in less modes being discarded as they represent meaningful information rather than random noise or artifact. PROFUMO also allowed for the grouping of multimodal regions into various subnetworks and combinatory networks. These factors may hold some advantage over GICA in some cases as it accommodates the study of specific RSN subdivisions that can vary in their susceptibility to connectivity disruptions of age-related disease (62,63). Namely, the primary visual, SMN, high visual, vDMN, dDMN, posterior salience, visuospatial, anterior salience, and limbic networks of the PROFUMO parcellation contained subnetworks. The subnetwork that best captured the primary representation of each RSN was listed first for each respective network. The primary representative subnetwork was well-matched to the GICA counterparts; however, they were not identical. Therefore, in future studies comparing mean functional connectivity that require all regions of a given RSN, the GICA portion may be favorable. In addition, the combinatory RSNs that were identified in the PROFUMO section include: the aECN/dDMN, language/dDMN, anterior salience/DAN, language/temporoparietal, language/auditory/temporoparietal, and language/auditory networks. These represent regions of overlapping RSNs that were highly correlated to each other and could warrant further study as potential biomarkers. For instance, the DMN has been shown to have interconnections with the language network (64). The DMN recruitment of language network regions such as the middle temporal gyrus and middle frontal

gyrus have been shown to be associated with inner speech, or internal, verbal thinking (65). Therefore, the language/dDMN RSNs of the PROFUMO parcellation may present an interesting opportunity to study these connections as biomarkers. While PROFUMO is a powerful tool that addresses some of the drawbacks of GICA, PROFUMO itself also has some downside. Primarily, PROFUMO is computationally expensive. Each iteration required an allocation of 4TB of RAM working memory, so it had to be run on a high-performance computation center (HPCC). However, the current version of PROFUMO employs additional dimensionality reduction algorithms to make it more computationally efficient (66).

3.5.4 – Limitations

While we attempted to use state-of-the-art neuroimaging techniques to define an age-appropriate structural template and functional atlas, some limitations of the current study are worth noting. All rrAD subjects were hypertensive which could alter the connectivity of some RSNs. However, hypertension is highly prevalent in older adults which could be useful in representing the population. Furthermore, all subjects had measures in place to control their blood pressure and they scored within the normal range for cognitive testing. Therefore, we predict our functional atlas will still be preferable over existing options for older subjects in general beyond the scope of the rrAD trial.

3.5.5 – Conclusion

Here, we present a functional atlas for older adults containing RSN spatial maps derived from both seed-based and data-driven approaches. While these spatial maps are intended for the direct assessment of rrAD trial outcomes, we expect our functional atlas will also be applicable options for the study of RSNs in older adults in future studies. We provide a seed-based map of the DMN that can be directly applied in aging studies and for biomarker detection in multiple neurodegenerative diseases. The data-driven GICA and PROFUMO sections

identified all group-level RSNs simultaneously. The standard GICA section presents each RSN with maximal spatial independence. While the PROFUMO section presents relevant subnetworks of RSNs, when applicable, and additional combinatory/overlapping RSNs that may be of interest to future studies investigating biomarkers of aging or neurodegenerative disease.

In addition to rs-fMRI data, the rrAD study included several other imaging modalities including T2 FLAIR images for white matter hyperintensity (WMH) quantification, arterial spin labeling (ASL) to estimate regional cerebral blood flow (CBF), and diffusion imaging for fiber tracking and structural connectivity analyses. These other modalities will later be transformed into rrAD420 space as well for future studies. The averages across subjects from the complete imaging dataset will incorporate cohort- and modality-specific templates for T1, T2 FLAIR, WMH distributions, CBF, and DTI fractional anisotropy, mean diffusivity, and free water. Through the rrAD420 template, longitudinal multi-modal image analyses can now be carried out using a template unique to this rrAD population. Our rrAD420 should also apply to older populations in general, facilitating analyses across different imaging modalities, data integration, and biomarker detection.

3.5.6 – Acknowledgements

This work has been supported by NIH grants (R01AG057571 and R01AG049749), the computational resources provided by the Institute for Cyber-Enabled Research at Michigan State University

REFERENCES

1. Szabo-Reed AN, Vidoni E, Binder EF, Burns J, Cullum CM, Gahan WP, et al. Rationale and methods for a multicenter clinical trial assessing exercise and intensive vascular risk reduction in preventing dementia (rrAD Study). Contemp Clin Trials. 2019 Apr 1;79:44–54.

2. Yeo BT, Krienen FM, Sepulcre J, Sabuncu MR, Lashkari D, Hollinshead M, et al. The organization of the human cerebral cortex estimated by intrinsic functional connectivity. J Neurophysiol. 2011 Sep;106(3):1125–65.

3. Shirer WR, Ryali S, Rykhlevskaia E, Menon V, Greicius MD. Decoding subject-driven cognitive states with whole-brain connectivity patterns. Cerebral Cortex. 2012 Jan;22(1):158–65.

4. Damoiseaux J, Rombouts S, Scheltens P, Stam CJ, Smith SM, Beckmann CF. Consistent resting-state networks across healthy subjects. Proc Natl Acad Sci U S A [Internet]. 2006 [cited 2012 May 7];(2). Available from: http://www.pnas.org/content/103/37/13848.short

5. Ashburner J. A fast diffeomorphic image registration algorithm. Neuroimage. 2007 Oct 15;38(1):95–113.

6. Beckmann CF, Smith SM. Probabilistic Independent Component Analysis for Functional Magnetic Resonance Imaging. IEEE Trans Med Imaging. 2004;23(2):137–52.

7. Harrison SJ, Woolrich MW, Robinson EC, Glasser MF, Beckmann CF, Jenkinson M, et al. Large-scale probabilistic functional modes from resting state fMRI. Neuroimage. 2015 Apr 1;109:217–31.

8. Ogawa S, Lee TM, Kay AR, Tank DW. Brain magnetic resonance imaging with contrast dependent on blood oxygenation (cerebral blood flow/brain metabolism/oxygenation) [Internet]. Vol. 87. 1990. Available from: https://www.pnas.org

9. Biswal B, Zerrin Yetkin F, Haughton VM, Hyde JS. Functional connectivity in the motor cortex of resting human brain using echo-planar mri. Magn Reson Med. 1995;34(4):537–41.

10. Fox MD, Raichle ME. Spontaneous fluctuations in brain activity observed with functional magnetic resonance imaging. Vol. 8, Nature Reviews Neuroscience. 2007. p. 700–11.

11. Shirer WR, Ryali S, Rykhlevskaia E, Menon V, Greicius MD. Decoding subject-driven cognitive states with whole-brain connectivity patterns. Cerebral Cortex. 2012 Jan;22(1):158–65.

12. Lowe MJ, Mock BJ, Sorenson JA. Functional Connectivity in Single and Multislice Echoplanar Imaging Using Resting-State Fluctuations 2. 1998.

13. Lalousis PA, Malaviya A, Upthegrove R, Heinze K, Diukova A, Auer D, et al. Trait related aberrant connectivity in clinically stable patients with schizophrenia: A seed based resting state fMRI study. Brain Imaging Behav. 2022 Dec 1;16(6):2705–14.

14. Damoiseaux JS, Rombouts SARB, Barkhof F, Scheltens P, Stam CJ, Smith SM, et al. Consistent resting-state networks across healthy subjects [Internet]. Vol. 103. 2006. Available from: www.pnas.orgcgidoi10.1073pnas.0601417103

15. Neha, Gandhi TK. Resting state fMRI analysis using seed based and ICA methods. INDIACom. 2016;3:2551–4.

16. Farahibozorg SR, Bijsterbosch JD, Gong W, Jbabdi S, Smith SM, Harrison SJ, et al. Hierarchical modelling of functional brain networks in population and individuals from big fMRI data. Neuroimage. 2021 Nov 1;243.

17. Fox MD, Snyder AZ, Vincent JL, Corbetta M, Van Essen DC, Raichle ME. The human brain is intrinsically organized into dynamic, anticorrelated functional networks [Internet]. Vol. 5, PNAS July. 2005. Available from: www.pnas.orgcgidoi10.1073pnas.0504136102

18. Binder JR, Frost JA, Hammeke TA, Bellgowan PSF, Rao SM, Cox RW. Conceptual Processing during the Conscious Resting State: A Functional MRI Study. J Cogn Neurosci [Internet]. 1999;11(1):1–14. Available from: papers2://publication/uuid/4EB1DEEA-D766-4D1B-A36D-072AE45D2B3C

19. Cole MW, Reynolds JR, Power JD, Repovs G, Anticevic A, Braver TS. Multi-task connectivity reveals flexible hubs for adaptive task control. Nat Neurosci. 2013;16(9):1348–55.

20. Shinn AK, Baker JT, Lewandowski KE, Öngür D, Cohen BM. Aberrant cerebellar connectivity in motor and association networks in schizophrenia. Front Hum Neurosci. 2015;9(MAR).

21. Seeley WW, Menon V, Schatzberg AF, Keller J, Glover GH, Kenna H, et al. Dissociable intrinsic connectivity networks for salience processing and executive control. Journal of Neuroscience. 2007;27(9):2349–56.

22. Cramer SC, Finklestein SP, Schaechter JD, Bush G, Rosen BR. Activation of distinct motor cortex regions during ipsilateral and contralateral finger movements. J Neurophysiol. 1999;81(1):383–7.

23. Smith SM, Fox PT, Miller KL, Glahn DC, Fox PM, Mackay CE, et al. Correspondence of the brain's functional architecture during activation and rest. Proc Natl Acad Sci U S A. 2009;106(31):13040–5.

24. Doucet GE, Labache L, Thompson PM, Joliot M, Frangou S. Atlas55+: Brain Functional Atlas of Resting-State Networks for Late Adulthood. Cerebral Cortex. 2021 Mar 1;31(3):1719–31.

25. Damoiseaux JS. Effects of aging on functional and structural brain connectivity. Neuroimage. 2017 Oct 15;160:32–40.

26. Atlason HE, Love A, Robertsson V, Blitz AM, Sigurdsson S, Gudnason V, et al. A joint ventricle and WMH segmentation from MRI for evaluation of healthy and pathological changes in the aging brain. PLoS One. 2022 Sep 1;17(9 September).

27. Raz N, Gunning F, Head D, Dupuis J, McQuain J, Briggs S, et al. Selective Aging of the Human Cerebral Cortex Observed in Vivo: Differential Vulnerability of the Prefrontal Gray Matter. Cerebral Cortex. 1997;7(3):268–82.

28. Mazziotta J, Toga A, Evans A, Fox P, Lancaster J. A probabilistic Atlas of the Human Brain: Theory and Rationale for Its Development. The International Consortium for Brain Mapping (ICBM). 1995;2(2):89–101.

29. Damoiseaux JS, Beckmann CF, Arigita EJS, Barkhof F, Scheltens P, Stam CJ, et al. Reduced resting-state brain activity in the “default network” in normal aging. Cerebral Cortex. 2008 Aug;18(8):1856–64.

30. Fernandez Z, Scheel N, Baker JH, Zhu DC. Functional connectivity of cortical resting-state networks is differentially affected by rest conditions. Brain Res. 2022 Dec 1;1796.

31. Patriat R, Molloy EK, Meier TB, Kirk GR, Nair VA, Meyerand ME, et al. The effect of resting condition on resting-state fMRI reliability and consistency: A comparison between resting with eyes open, closed, and fixated. Neuroimage. 2013 Sep;78:463–73.

32. Cox J.S. RW; H. AFNI: Software for analysis and visualization of functional magnetic resonance neuroimages. Computers and Biomedical Research [Internet]. 1996;29(29):162–73. Available from: https://ac-els-cdn-com.ezp-prod1.hul.harvard.edu/S0010480996900142/1-s2.0-S0010480996900142-main.pdf?_tid=c22bae7a-b8f5-4a8b-9dac-91c1ed841d53&acdnat=1549393398_e37181b8933a2ac88c2d7dc0eab14413

33. Pruim RHR, Mennes M, Buitelaar JK, Beckmann CF. Evaluation of ICA-AROMA and alternative strategies for motion artifact removal in resting state fMRI. Neuroimage. 2015 May 5;112:278–87.

34. Pruim RHR, Mennes M, van Rooij D, Llera A, Buitelaar JK, Beckmann CF. ICA-AROMA: A robust ICA-based strategy for removing motion artifacts from fMRI data. Neuroimage. 2015 May 5;112:267–77.

35. Scheel N, Keller JN, Binder EF, Vidoni ED, Burns JM, Thomas BP, et al. Evaluation of noise regression techniques in resting-state fMRI studies using data of 434 older adults. Front Neurosci. 2022 Oct 19;16.

36. Scheel N, Keller JN, Binder EF, Vidoni ED, Burns JM, Thomas BP, et al. Evaluation of noise regression techniques in resting-state fMRI studies using data of 434 older adults. Front Neurosci. 2022 Oct 19;16.

37. Scheel N, Keller JN, Binder EF, Vidoni ED, Burns JM, Thomas BP, et al. Evaluation of noise regression techniques in resting-state fMRI studies using data of 434 older adults. Front Neurosci. 2022 Oct 19;16.

38. Cole DM, Smith SM, Beckmann CF. Advances and pitfalls in the analysis and interpretation of resting-state FMRI data. Vol. 4, Frontiers in Systems Neuroscience. 2010.

39. Beckmann C, Mackay C, Filippini N, Smith S. Group comparison of resting-state FMRI data using multi-subject ICA and dual regression. Neuroimage. 2009 Jul 1;47:S148.

40. Mckeown MJ, Sejnowski TJ. Independent Component Analysis of fMRI Data: Examining the Assumptions. Vol. 6, Hum. Brain Mapping. 1998.

41. Hyvärinen A, Oja E. Independent Component Analysis: Algorithms and Applications. Vol. 13, Neural Networks. 2000.

42. Bijsterbosch JD, Woolrich MW, Glasser MF, Robinson EC, Beckmann CF, Van Essen DC, et al. The relationship between spatial configuration and functional connectivity of brain regions. 2018; Available from: https://doi.org/10.7554/eLife.32992.001

43. Diane Bijsterbosch J, Beckmann CF, Woolrich MW, Smith SM, Harrison SJ. The relationship between spatial configuration and functional connectivity of brain regions revisited. 2019; Available from: https://doi.org/10.7554/eLife.44890.001

44. Harrison SJ, Bijsterbosch JD, Segerdahl AR, Fitzgibbon SP, Farahibozorg SR, Duff EP, et al. Modelling subject variability in the spatial and temporal characteristics of functional modes. Neuroimage. 2020 Nov 15;222.

45. Zhu DC, Majumdar S, Korolev IO, Berger KL, Bozoki AC. Alzheimer's disease and amnestic mild cognitive impairment weaken connections within the default-mode network: A multi-modal imaging study. Journal of Alzheimer's Disease. 2013;34(4):969–84.

46. Fischl B. FreeSurfer. Neuroimage. 2012;62(2):774–81.

47. Bhaganagarapu K, Jackson GD, Abbott DF. An automated method for identifying artifact in independent component analysis of resting-state fMRI. Front Hum Neurosci. 2013 Jul 10;(JUL).

48. Griffanti L, Douaud G, Bijsterbosch J, Evangelisti S, Alfaro-Almagro F, Glasser MF, et al. Hand classification of fMRI ICA noise components. Neuroimage. 2017 Jul 1;154:188–205.

49. Tzourio-Mazoyer N, Landeau B, Papathanassiou D, Crivello F, Etard O, Delcroix N, et al. Automated anatomical labeling of activations in SPM using a macroscopic anatomical parcellation of the MNI MRI single-subject brain. Neuroimage. 2002;15(1):273–89.

50. Rasser PE, Johnston PJ, Ward PB, Thompson PM. A DEFORMABLE BRODMANN AREA ATLAS [Internet]. Available from: http://www.nisad.org.au.

51. Desikan RS, Ségonne F, Fischl B, Quinn BT, Dickerson BC, Blacker D, et al. An automated labeling system for subdividing the human cerebral cortex on MRI scans into gyral based regions of interest. Neuroimage. 2006 Jul 1;31(3):968–80.

52. Destrieux C, Fischl B, Dale A, Halgren E. Automatic parcellation of human cortical gyri and sulci using standard anatomical nomenclature. Neuroimage. 2010 Oct;53(1):1–15.

53. Hohenfeld C, Werner CJ, Reetz K. Resting-state connectivity in neurodegenerative disorders: Is there potential for an imaging biomarker? Neuroimage Clin [Internet]. 2018;18(March 2018):849–70. Available from: https://doi.org/10.1016/j.nicl.2018.03.013

54. Shulman G, Fiez J, Corbetta M, Buckner R, Miezin F, Raichle M, et al. Common Blood Flow Changes across visual Tasks: II. Decreases in Cerebral Cortex. J Cogn Neurosci. 1997;9(5):648–63.

55. Raichle ME, Macleod AM, Snyder AZ, Powers WJ, Gusnard DA, Shulman GL. A default mode of brain function [Internet]. National Academy of Sciences. 1996. Available from: www.pnas.org

56. Buckner RL, Andrews-Hanna JR, Schacter DL. The brain's default network: Anatomy, function, and relevance to disease. Ann N Y Acad Sci. 2008;1124:1–38.

57. Raichle ME. The Brain's Default Mode Network. Annu Rev Neurosci. 2015 Jul 8;38:433–47.

58. Andrews-Hanna JR, Snyder AZ, Vincent JL, Lustig C, Head D, Raichle MEE, et al. Disruption of Large-Scale Brain Systems in Advanced Aging. Neuron. 2007 Dec 6;56(5):924–35.

59. Greicius MD, Srivastava G, Reiss AL, Menon V, Raichle ME. Default-mode network activity distinguishes Alzheimer's disease from healthy aging: Evidence from functional MRI [Internet]. 2004. Available from: www.fmridc.org

60. Putcha D, Eckbo R, Katsumi Y, Dickerson BC, Touroutoglou A, Collins JA. Tau and the fractionated default mode network in atypical Alzheimer's disease. Brain Commun. 2022;4(2).

61. Sperling RA, LaViolette PS, O'Keefe K, O'Brien J, Rentz DM, Pihlajamaki M, et al. Amyloid Deposition Is Associated with Impaired Default Network Function in Older Persons without Dementia. Neuron. 2009 Jul 30;63(2):178–88.

62. Viviano RP, Hayes JM, Pruitt PJ, Fernandez ZJ, van Rooden S, van der Grond J, et al. Aberrant memory system connectivity and working memory performance in subjective cognitive decline. Neuroimage. 2019 Jan 15;185:556–64.

63. Xue C, Yuan B, Yue Y, Xu J, Wang S, Wu M, et al. Distinct Disruptive Patterns of Default Mode Subnetwork Connectivity Across the Spectrum of Preclinical Alzheimer's Disease. Front Aging Neurosci. 2019 Nov 13;11.

64. Gordon EM, Laumann TO, Marek S, Raut R V, Gratton C, Newbold DJ, et al. Default-mode network streams for coupling to language and control systems. Available from: www.pnas.org/cgi/doi/10.1073/pnas.2005238117

65. Alderson-Day B, Weis S, McCarthy-Jones S, Moseley P, Smailes D, Fernyhough C. The brain's conversation with itself: Neural substrates of dialogic inner speech. Soc Cogn Affect Neurosci. 2015 Mar 25;11(1):110–20.

66. Bijsterbosch JD, Farahibozorg SR, Glasser MF, Van Essen D, Snyder LH, Woolrich MW, et al. Evaluating functional brain organization in individuals and identifying contributions to network overlap. Imaging Neuroscience. 2023 Dec 8;1:1–19.

67. Yu T, Cai LY, Morgan VL, Goodale SE, Englot DJ, Chang CE, et al. SynBOLD-DisCo: Synthetic BOLD images for distortion correction of fMRI without additional calibration scans. Available from: https://doi.org/10.1101/2022.09.13.507794

APPENDIX

FIGURES

Figure 3.1: Comparison of standard MNI152 template (TOP) based on younger adults (25.02 ± 4.9) and the standard rrAD420 template based on 420 older adults (68.8 ± 5.9) in the rrAD study.

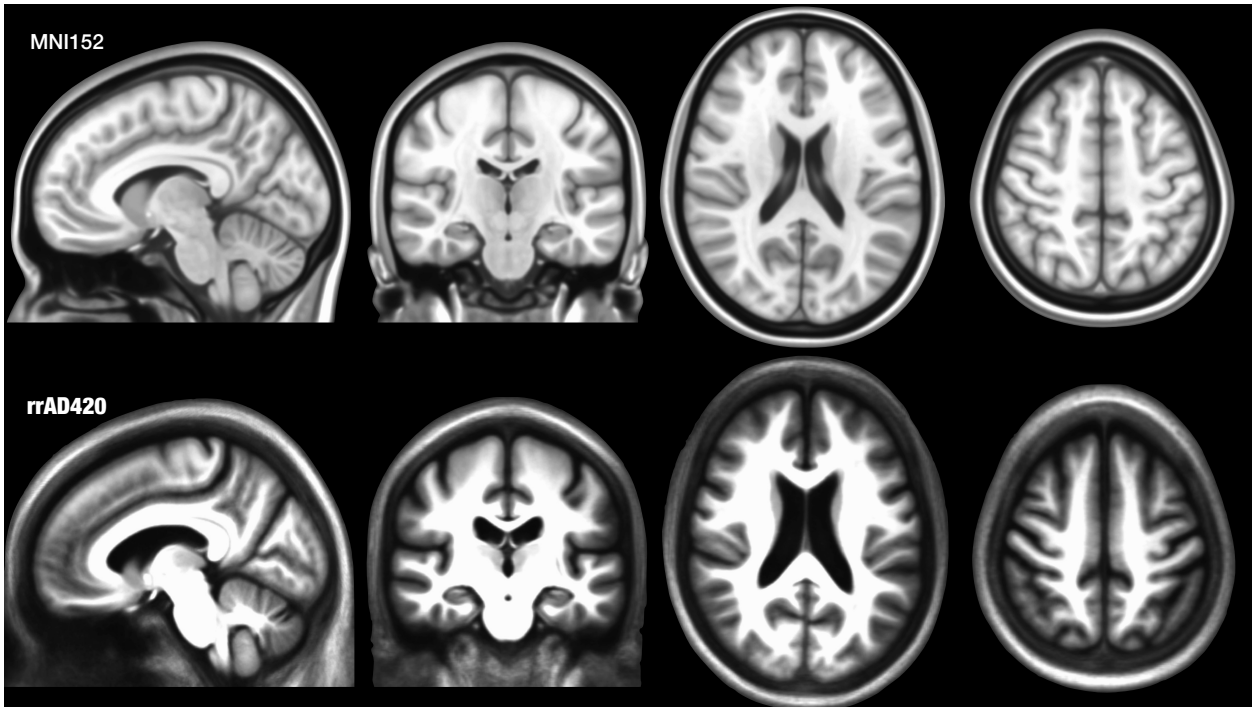

Figure 3.2: Basic schematic to explain the concept of overfitting and underfitting. The "ground truth" (LEFT) represents the desired grouping of connected regions that we want to capture using our model. Overfitting (TOP) occurs when the hyperparameters are set too high in the blind source separation model and leads to splitting a true network between multiple components. Underfitting (BOTTOM) occurs when the hyperparameters are set too low in the model and leads to grouping multiple networks into a single component.

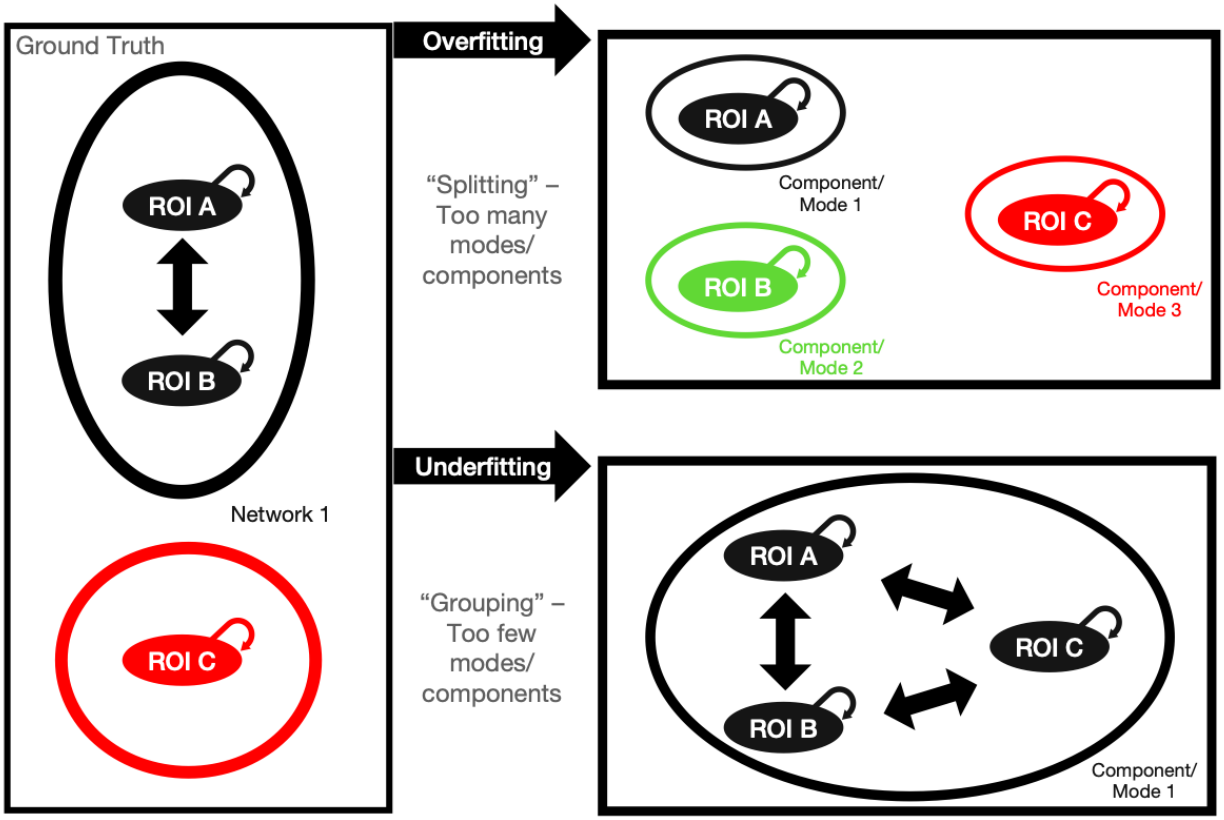

Figure 3.3: Representative images of the seed-based group spatial map of Default Mode Network (DMN24) based on 420 hypertensive older adults with a high familial risk of dementia or subjective cognitive decline that participated in the rrAD trial. The first 18 regions listed are cortical regions, while the remaining 6 are cerebellar regions.

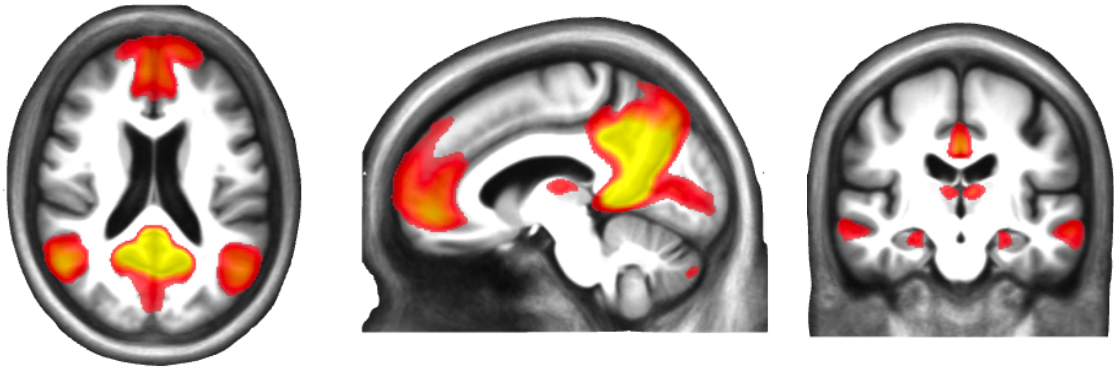

DMN24: Right posterior cingulum, left posterior cingulum, right precuneus/angular gyrus, left precuneus/angular gyrus, right medial frontal gyrus/medial orbital gyrus, left medial frontal gyrus/medial orbital gyrus, right superior frontal gyrus, left superior frontal gyrus, right anterior superior temporal sulcus, left anterior superior temporal sulcus, right medial prefrontal thalamus, left medial prefrontal thalamus, right hippocampus subiculum, left hippocampus subiculum, right parahippocampal place area, left parahippocampal place area, right inferior frontal gyrus (BA11), left inferior frontal gyrus (BA11), right medial cerebellum, left medial cerebellum, right cerebellar tonsil, left cerebellar tonsil, right posterior cerebellum, left posterior cerebellum.

Figure 3.4: Percentage of the 14 RSNs in the Shirer functional atlas, which served as our reference atlas, represented by each GICA and PROFUMO parcellation regardless of the designation of primary or secondary.

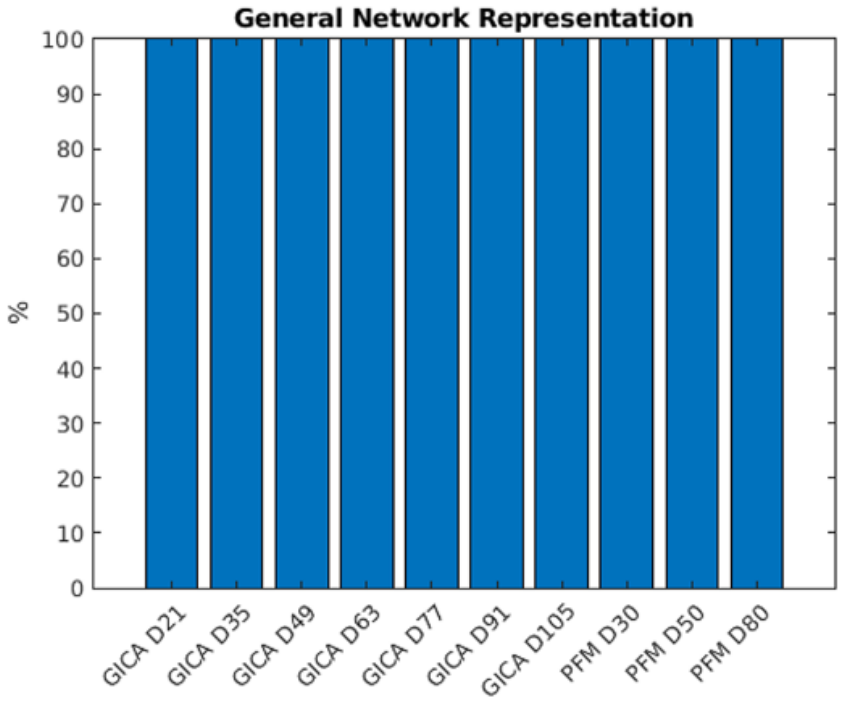

Figure 3.5: Percentage of the 14 RSNs in the Shirer functional atlas, which served as our reference atlas, represented by each GICA and PROFUMO parcellation that presented as a primary network.

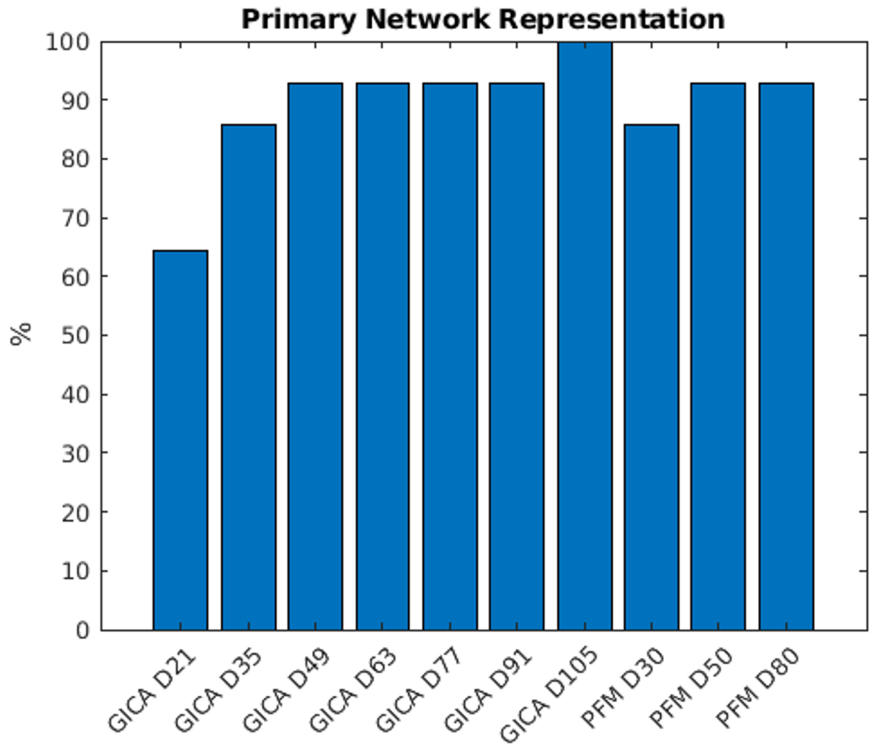

Figure 3.6: Percentage of the 14 RSNs in the Shirer functional atlas, which served as our reference atlas, dispersed between multiple components for each GICA and PROFUMO parcellation.

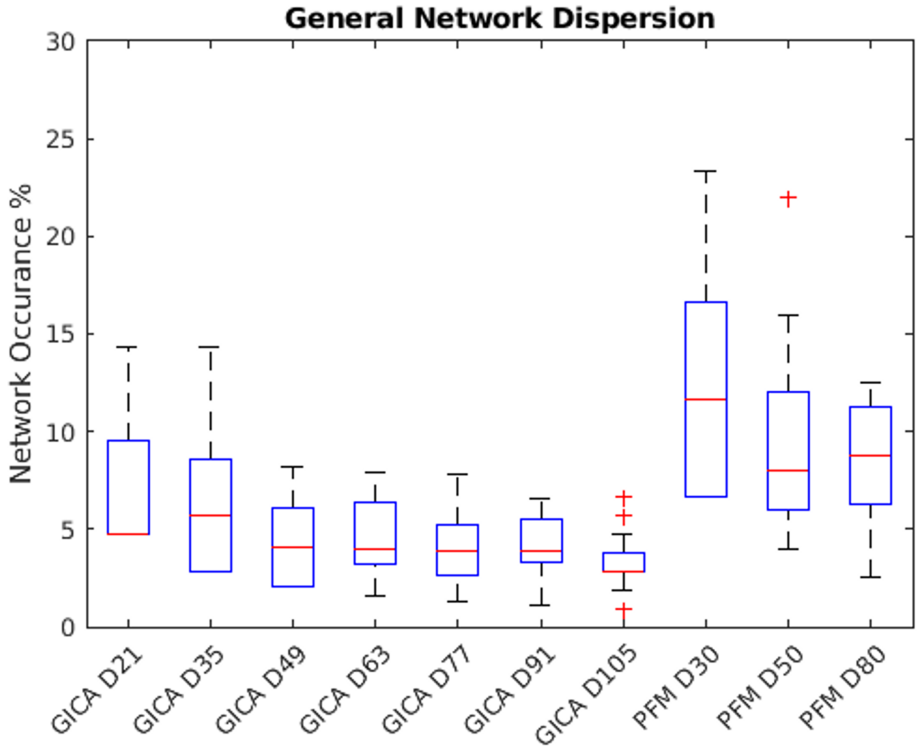

Figure 3.7: Percentage of the 14 RSNs in the Shirer functional atlas, which served as our reference atlas, grouped within a single component for each GICA and PROFUMO parcellation.

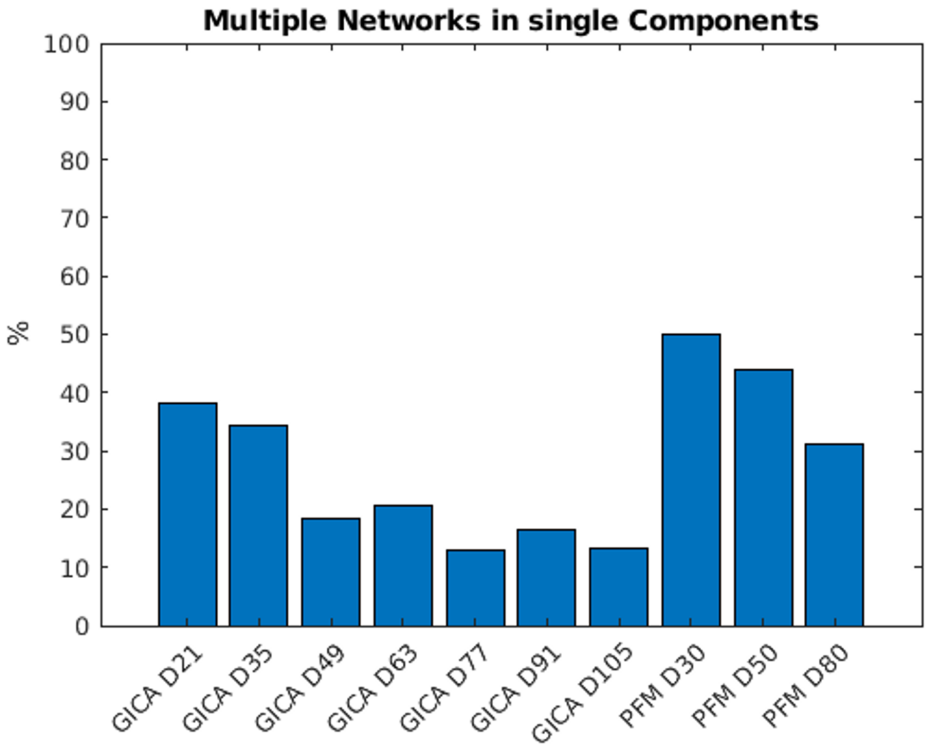

Figure 3.8: Representative images and list of brain regions for each group resting-state network based on 420 hypertensive older adults with a high familial risk of dementia or subjective cognitive decline that participated in the rrAD trial. We performed group independent component analysis (GICA) on rrAD subject resting-state fMRI data through FSL's MELODIC software. Here, we display resting-state networks from the 49-component parcellation, which showed the most ideal network separation from those tested.

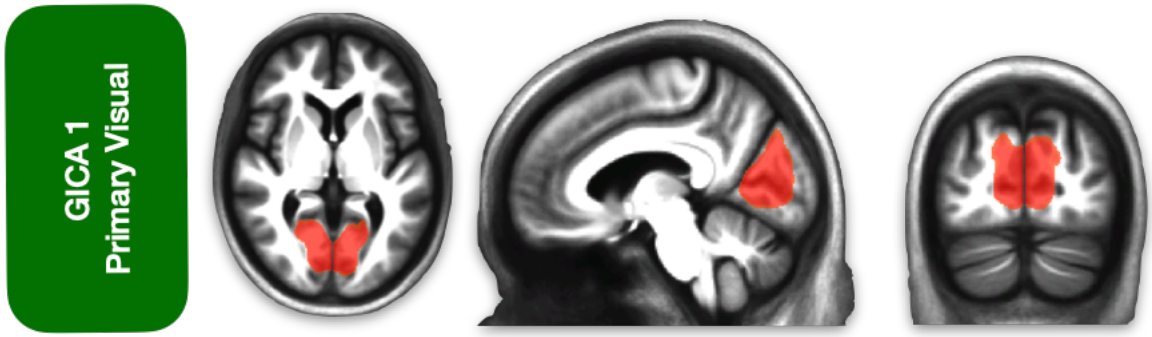

Primary Visual Network: Right superior middle occipital gyrus (striate); Left superior middle occipital gyrus (striate cortex).

Sensorimotor Network: Right superior pre/postcentral gyrus (Sensorimotor cortex); Left superior pre/postcentral gyrus (Sensorimotor cortex); Right inferior precentral gyrus (Sensorimotor cortex); Left inferior precentral gyrus (Sensorimotor cortex).

Figure 3.8 (cont'd):

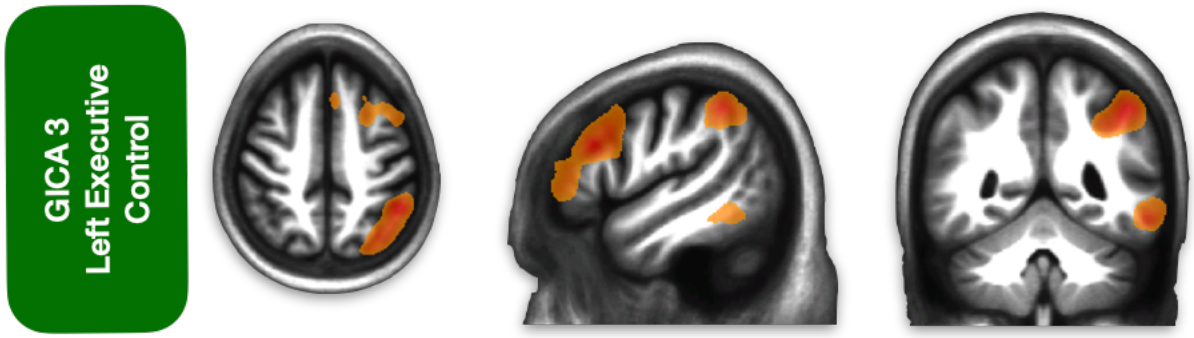

Left Executive Control Network (LECN): Left inferior parietal lobe/angular gyrus; Left middle/inferior frontal gyrus; Left superior medial gyrus; Left posterior middle cingulate cortex; Left inferior/middle temporal gyrus; Right posterior cerebellum.

Precuneus Network: Right precuneus; Left precuneus; Right posterior/middle cingulate cortex; Left posterior/middle cingulate cortex.

Figure 3.8 (cont'd):

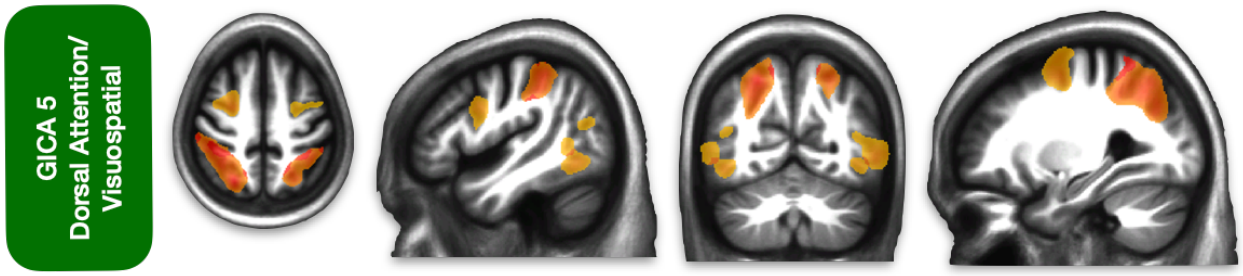

Dorsal Attention/Visuospatial Network: Right superior parietal cortex/precuneus; Left superior parietal cortex/precuneus; Right superior frontal cortex; Left superior frontal cortex; Right inferior frontal gyrus; Left inferior frontal gyrus; Right middle temporal gyrus; Left middle temporal gyrus; Right inferior temporal gyrus.

Ventral Default Mode Network (vDMN): Right precuneus; Left precuneus; Right frontal eye field; Left frontal eye field; Right middle occipital gyrus; Left middle occipital gyrus; Right retrosplenial cortex; Left retrosplenial cortex; Right parahippocampal place area; Left parahippocampal place area.

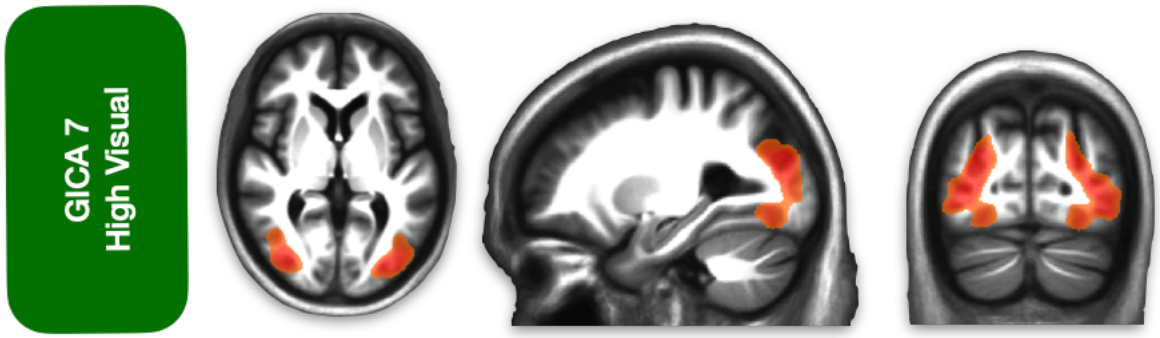

High Visual Network: Right prestriate; Left prestriate.

Figure 3.8 (cont'd):

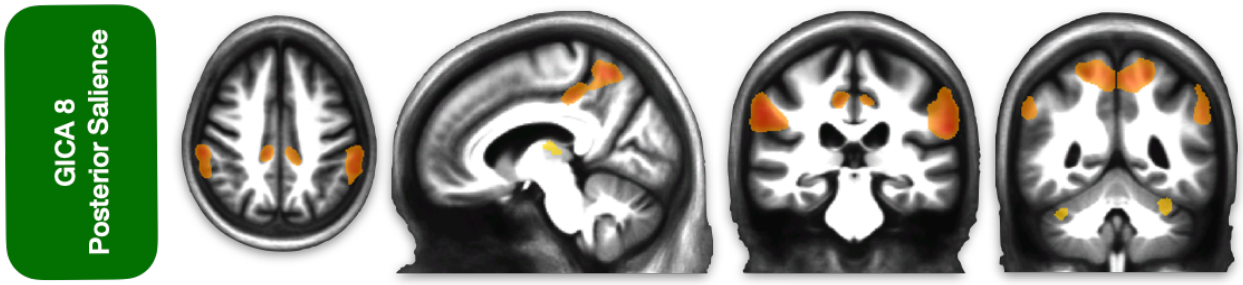

Posterior Salience Network: Right supramarginal gyrus; Left supramarginal gyrus; Right precuneus/middle cingulate cortex; Left precuneus/middle cingulate cortex; Right thalamus; Left thalamus; Right insula; Left insula; Right superior cerebellum; Left superior cerebellum.

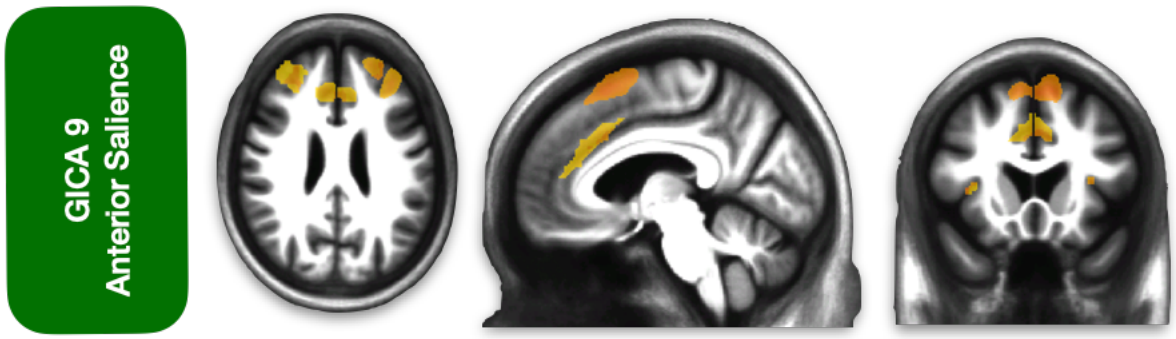

Anterior Salience Network: Right superior frontal gyrus; Left superior frontal gyrus; Right middle frontal gyrus; Left middle frontal gyrus; Right dorsal anterior cingulate cortex; Left dorsal anterior cingulate cortex; Right superior frontal gyrus/pre-supplemental motor area; Left superior frontal gyrus/pre-supplemental motor area; Right insula; Left insula; Right superior cerebellum; Left superior cerebellum; Right inferior cerebellum; Left inferior cerebellum.

Figure 3.8 (cont'd):

Language Network: Right angular gyrus; Left angular gyrus; Right superior temporal gyrus; Left superior temporal gyrus; Right superior/middle temporal gyrus; Left superior/middle temporal gyrus; Right pars triangularis; Left pars triangularis; Right middle temporal gyrus; Left middle temporal gyrus.

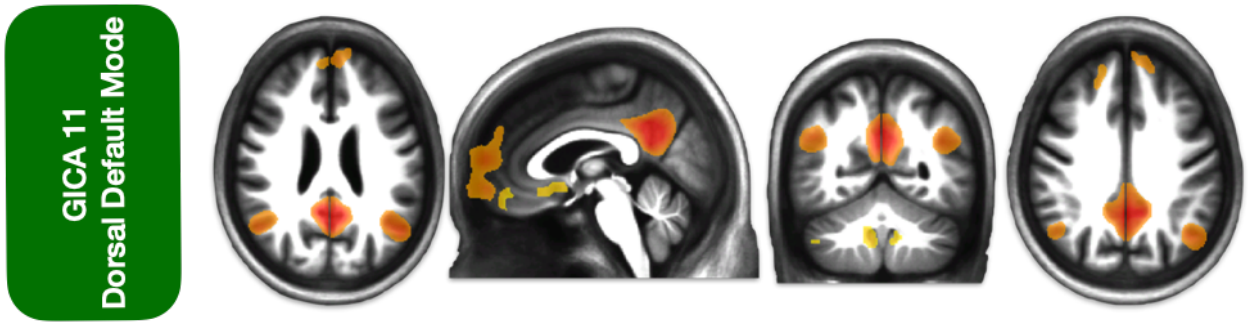

Dorsal Default Mode Network (dDMN): Right posterior cingulate cortex; Left posterior cingulate cortex; Right superior frontal gyrus; Left superior frontal/medial gyrus; Right angular gyrus; Left angular gyrus; Right superior medial gyrus; Right basal ganglia; Left basal ganglia; Right anterior cingulate cortex; Left anterior cingulate cortex; Right inferior frontal gyrus; Left inferior frontal gyrus; Right hippocampus; Left hippocampus; Right middle temporal gyrus; Left middle temporal gyrus; Right superior cerebellum; Left superior cerebellum; Right inferior cerebellum; Left inferior cerebellum.

Figure 3.8 (cont'd):

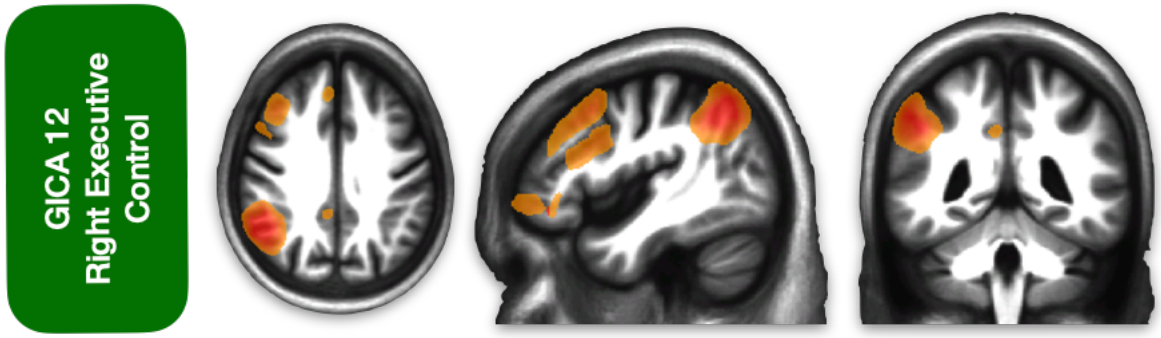

Right Executive Control Network (RECN): Right inferior parietal lobe/angular gyrus; Right middle/inferior frontal gyrus; Right superior medial gyrus; Right posterior middle cingulate cortex; Right pars opercularis/inferior frontal gyrus; Right middle frontal gyrus; Right inferior/middle temporal gyrus; Left posterior cerebellum.

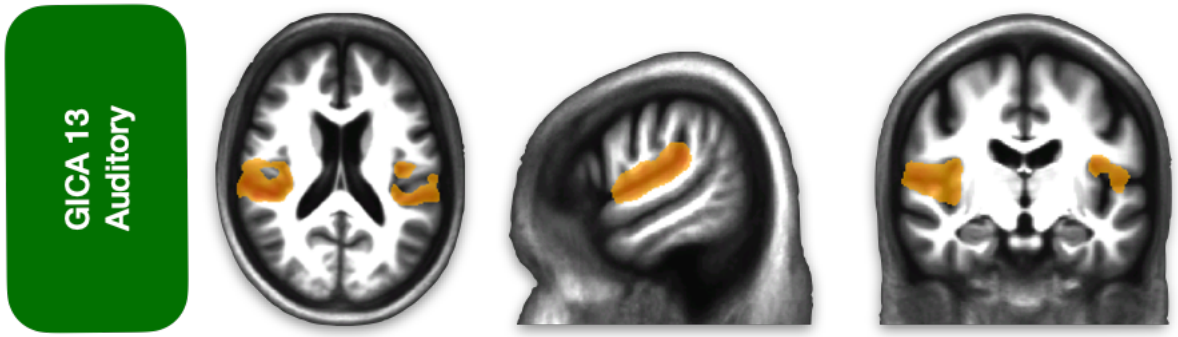

Auditory Network: Right superior temporal gyrus/operculum; Left superior temporal gyrus/operculum.

Figure 3.8 (cont'd):

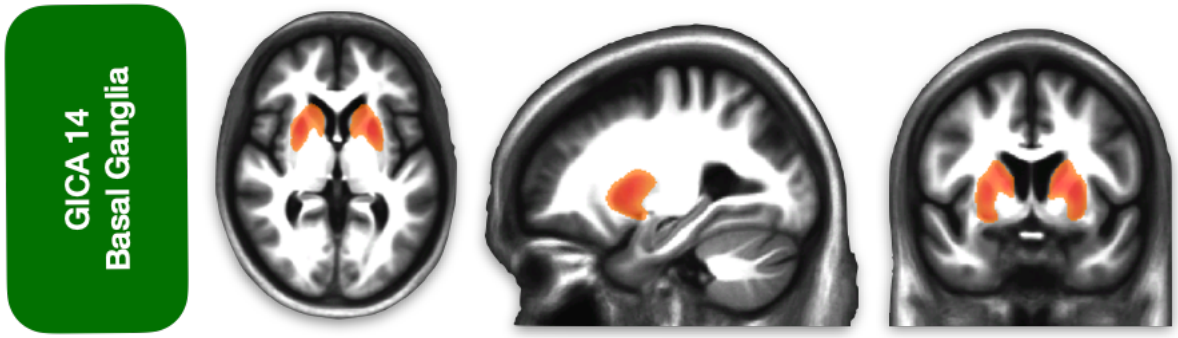

Basal Ganglia Network: Right basal ganglia; Left basal ganglia.

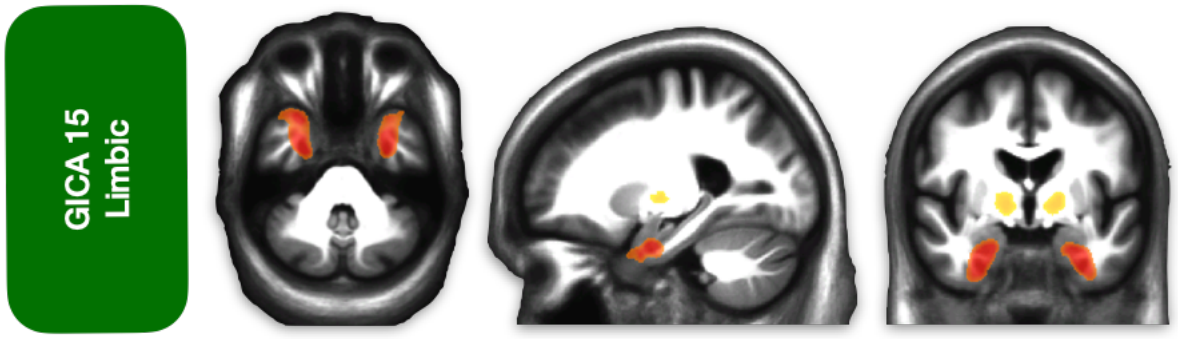

Limbic Network: Right temporal pole; Left temporal pole; Right pallidum; Left pallidum.

Figure 3.9: Representative images and list of brain regions for each group resting-state network based on 420 hypertensive older adults with a high risk of dementia that participated in the rrAD

trial. We performed Probabilistic Functional Modes (PROFUMO) on rrAD subject resting-state fMRI data through FSL's newly integrated PROFUMO software. Here, we display resting-state networks from the 50-mode parcellation, which showed the most ideal network separation from those tested.

Single Networks

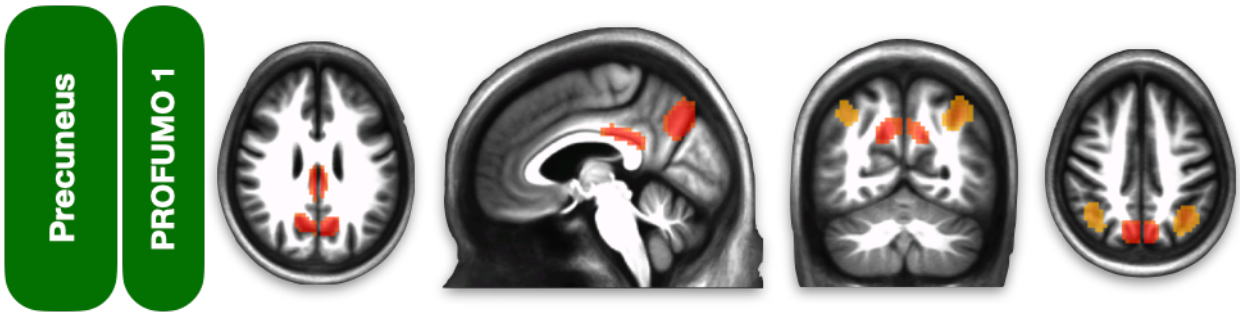

Precuneus Network: Right precuneus; Left precuneus; Right posterior/middle cingulate cortex; Left posterior/middle cingulate cortex.

Figure 3.9 (cont'd):

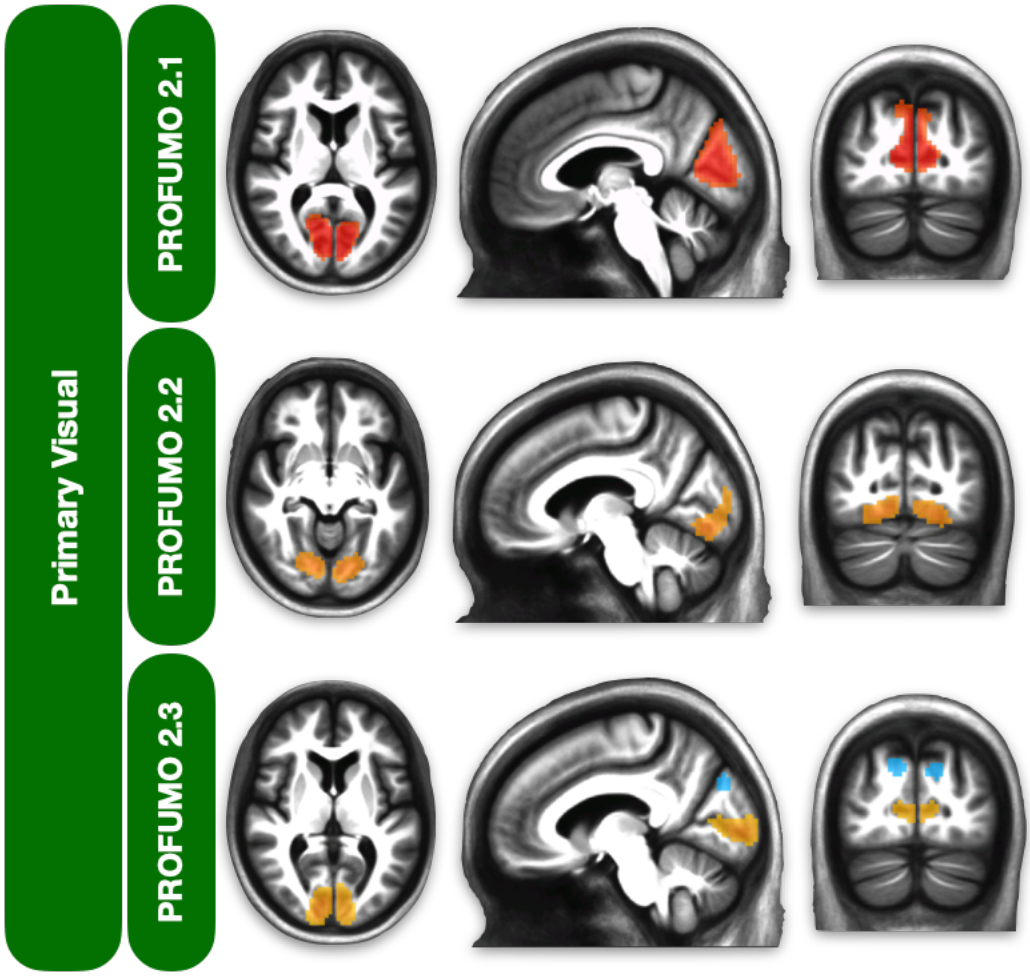

Primary Visual Network (2.1): Right superior middle occipital gyrus (striate); Left superior middle occipital gyrus (striate cortex).

Primary Visual Network (2.2): Right inferior occipital gyrus; Left inferior occipital gyrus.

Primary Visual Network (2.3): Right superior occipital gyrus; Left superior occipital gyrus; Right middle occipital gyrus; Left middle occipital gyrus.

Figure 3.9 (cont'd):

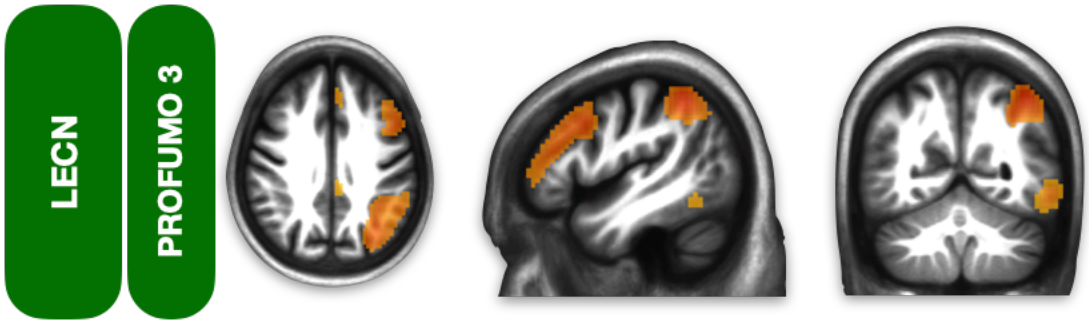

Left Executive Control Network (LECN): Left inferior parietal lobe/angular gyrus; Left medial/inferior frontal cortex; Left superior medial frontal cortex; Left inferior/medial temporal cortex; Left posterior middle cingulate cortex; Right inferior semilunar lobule of the cerebellum; Right posterior lobule of the cerebellum.

Figure 3.9 (cont'd):

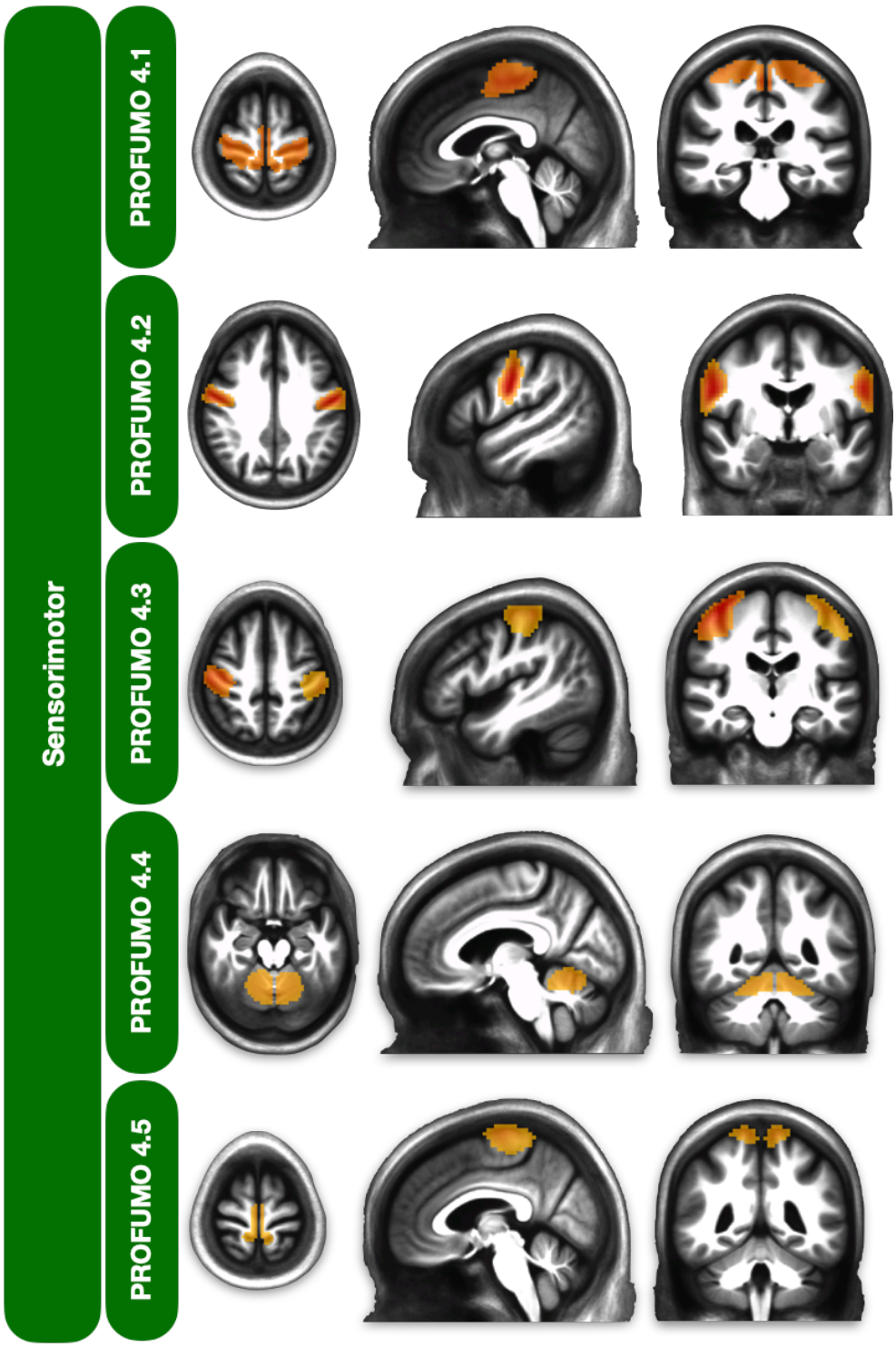

Sensorimotor Network (4.1): Right superior pre/postcentral gyrus (Sensorimotor cortex); Left superior pre/postcentral gyrus (Sensorimotor cortex).

Sensorimotor Network (4.2): Right inferior precentral gyrus (Sensorimotor cortex); Left inferior precentral gyrus (Sensorimotor cortex).

Figure 3.9 (cont'd):

Sensorimotor Network (4.3): Right middle precentral gyrus (Sensorimotor cortex); Left middle precentral gyrus (Sensorimotor cortex).

Sensorimotor Network (4.4): Right anterior cerebellum; Left anterior cerebellum.

Sensorimotor Network (4.5): Right superior pre/postcentral gyrus (Sensorimotor cortex); Left superior pre/postcentral gyrus (Sensorimotor cortex).

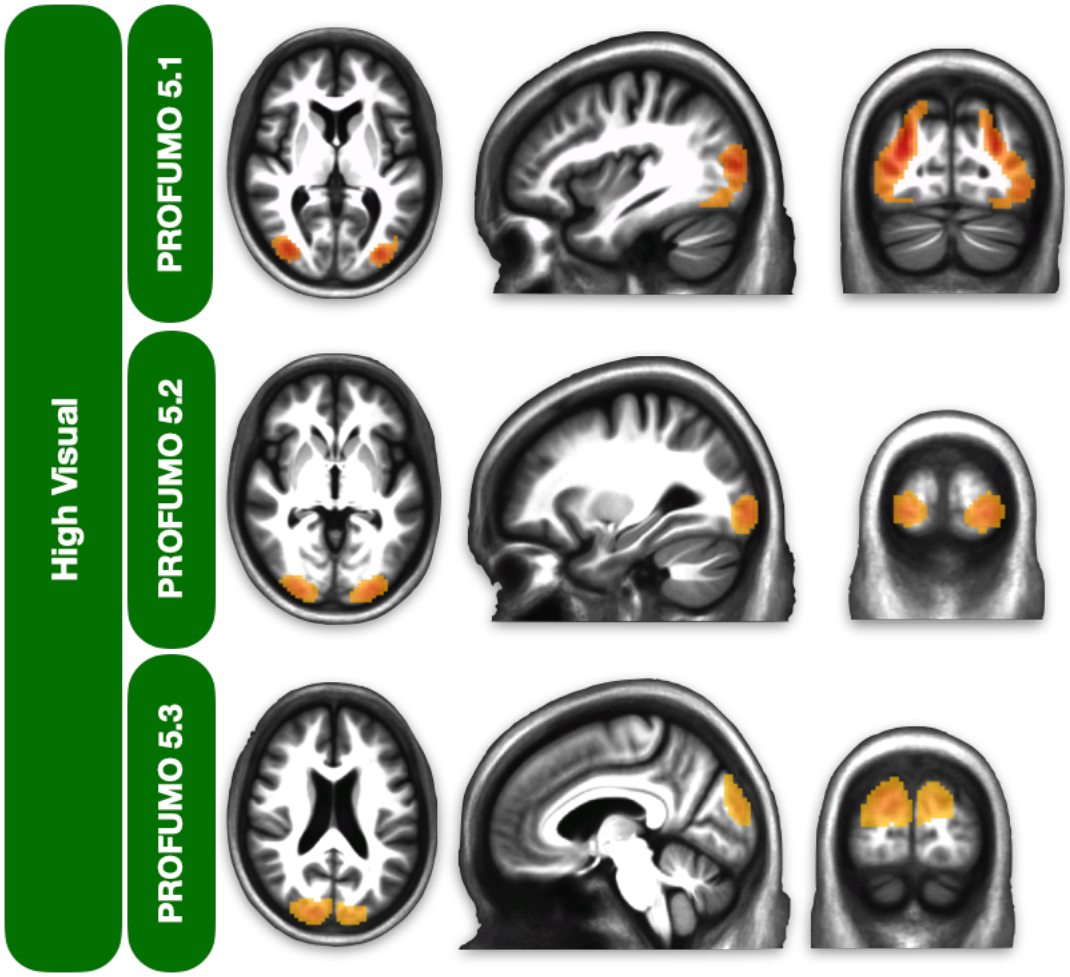

High Visual Network (5.1): Right prestriate cortex; Left prestriate cortex.

High Visual Network (5.2): Right inferior occipital lobe; Left inferior occipital lobe.

High Visual Network (5.3): Right superior occipital lobe; Left superior occipital lobe.

Figure 3.9 (cont'd):

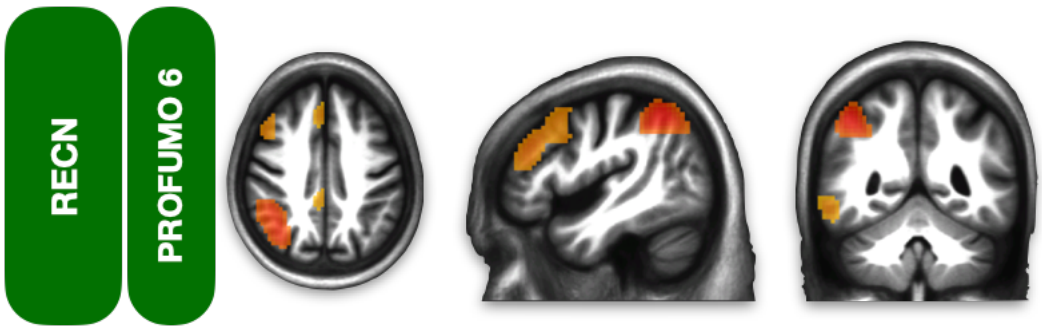

Right Executive Control Network (RECN): Right inferior parietal lobe/angular gyrus; Right medial/inferior frontal cortex; Right superior medial frontal cortex; Right inferior/medial temporal cortex; Right posterior middle cingulate cortex; Left inferior posterior cerebellum; Left posterior cerebellum.

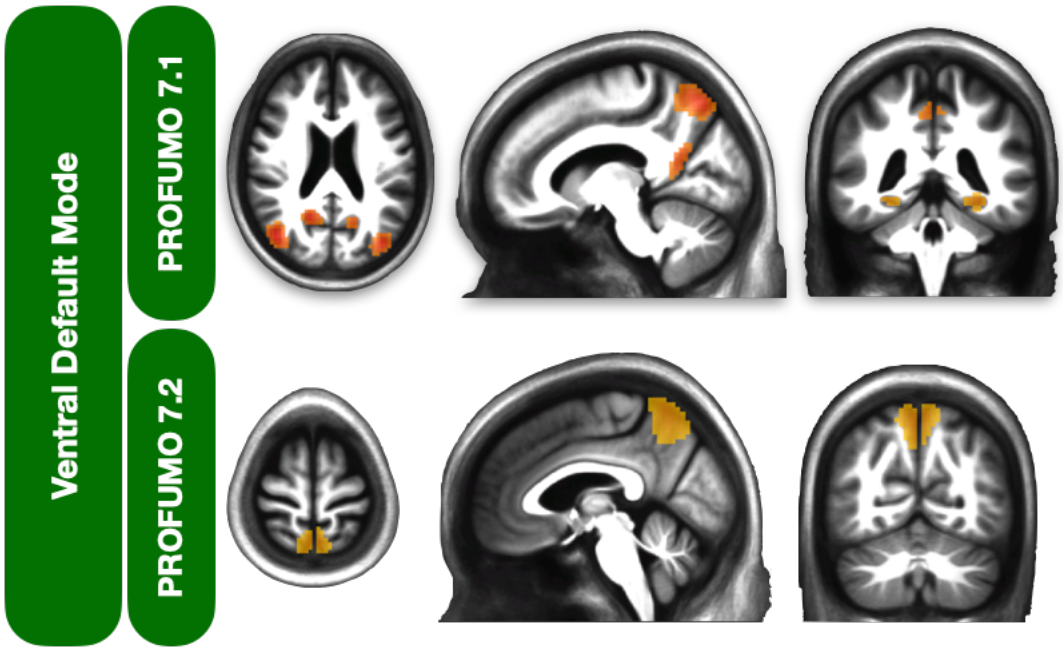

Ventral Default Mode Network (7.1): Right precuneus; Left precuneus; Right frontal eye field; Left frontal eye field; Right middle occipital gyrus; Left middle occipital gyrus; Right retrosplenial cortex; Left retrosplenial cortex; Right parahippocampal place area; Left parahippocampal place area.

Ventral Default Mode Network (7.2): Right precuneus; Left precuneus.

Figure 3.9 (cont'd):

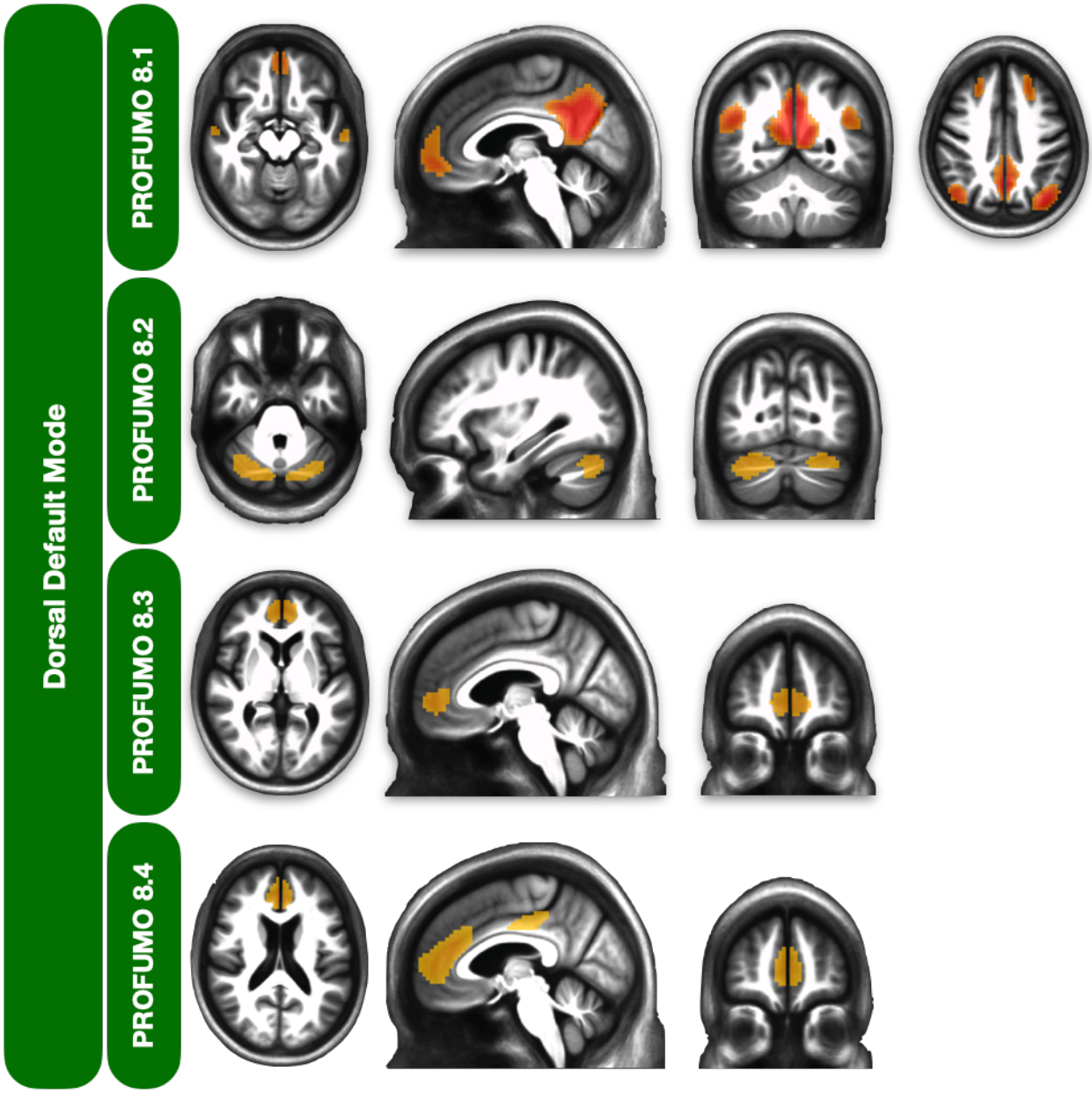

Dorsal Default Mode Network (8.1): Right posterior cingulate cortex; Left posterior cingulate cortex; Right angular gyrus; Left angular gyrus; Right superior frontal gyrus; Left superior frontal gyrus; Right medial prefrontal cortex; Left medial prefrontal cortex; Right middle temporal lobe; Left middle temporal lobe.

Dorsal Default Mode Network (8.2): Right posterior cerebellum; Left posterior cerebellum.

Dorsal Default Mode Network (8.3): Right prefrontal cortex; Left prefrontal cortex.

Dorsal Default Mode Network (8.4): Right anterior cingulate cortex; Left anterior cingulate cortex; Right cingulate cortex; Left middle cingulate cortex.

Figure 3.9 (cont'd):

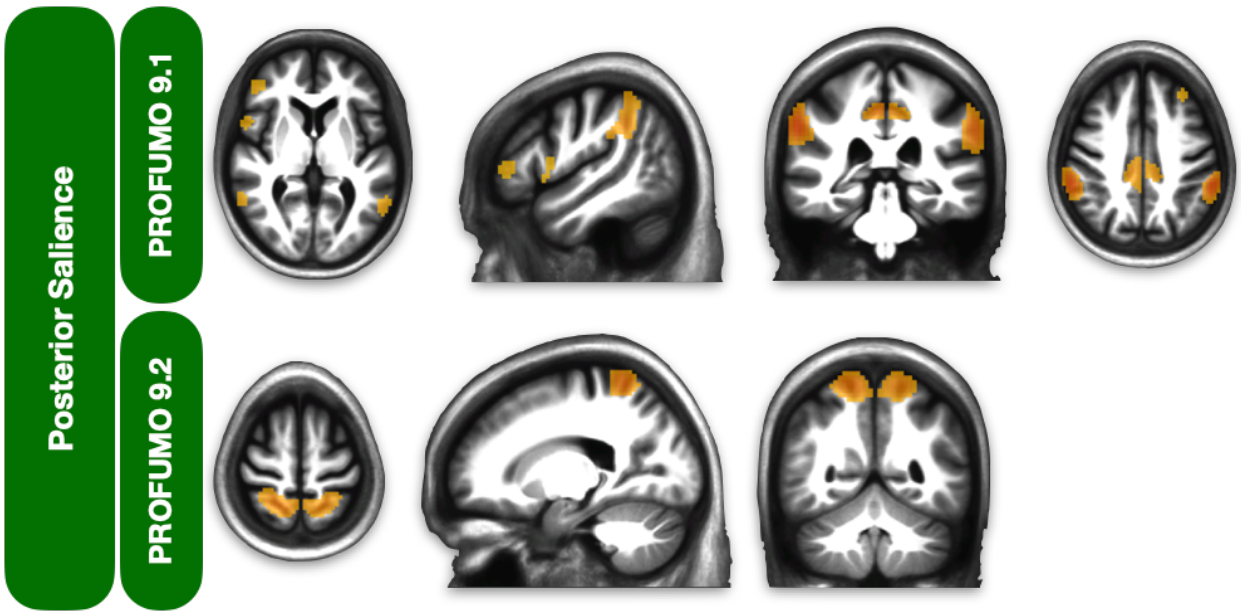

Posterior Salience Network (9.1): Right supramarginal gyrus; Left supramarginal gyrus; Right precuneus/middle cingulate cortex; Left precuneus/middle cingulate cortex; Right superior middle frontal gyrus; Left middle frontal gyrus; Right inferior frontal gyrus; Left inferior frontal gyrus; Right inferior middle frontal gyrus; Left inferior middle frontal gyrus; Right middle temporal gyrus.

Posterior Salience Network (9.2): Right superior parietal cortex; Left superior parietal cortex.

Figure 3.9 (cont'd):

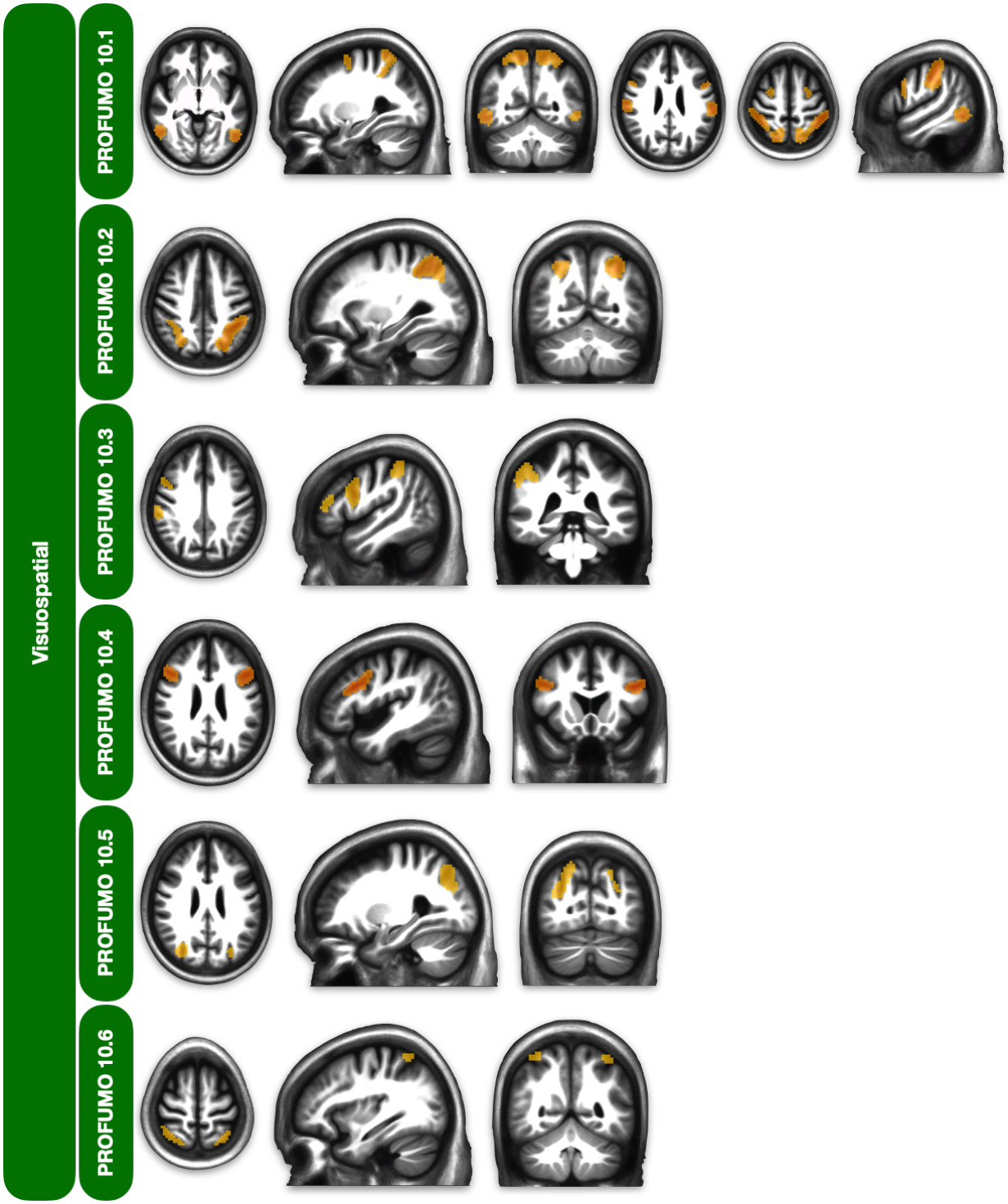

Visuospatial Network (10.1): Right superior parietal cortex/precuneus; Left superior parietal cortex/precuneus; Right superior frontal cortex; Left superior frontal cortex; Right inferior frontal gyrus; Left inferior frontal gyrus; Right inferior temporal gyrus; Left inferior temporal gyrus.

Figure 3.9 (cont'd):

Visuospatial Network (10.2): Right inferior parietal cortex and superior parietal cortex/precuneus; Left inferior parietal cortex and superior parietal cortex/precuneus.

Visuospatial Network (10.3): Right inferior parietal lobule; Right pars opercularis; Right middle frontal gyrus.

Visuospatial Network (10.4): Right inferior frontal gyrus; Left inferior frontal gyrus.

Visuospatial Network (10.5): Right intraparietal sulcus; Left intraparietal sulcus.

Visuospatial Network (10.6): Right superior parietal lobule; Left superior parietal lobule.

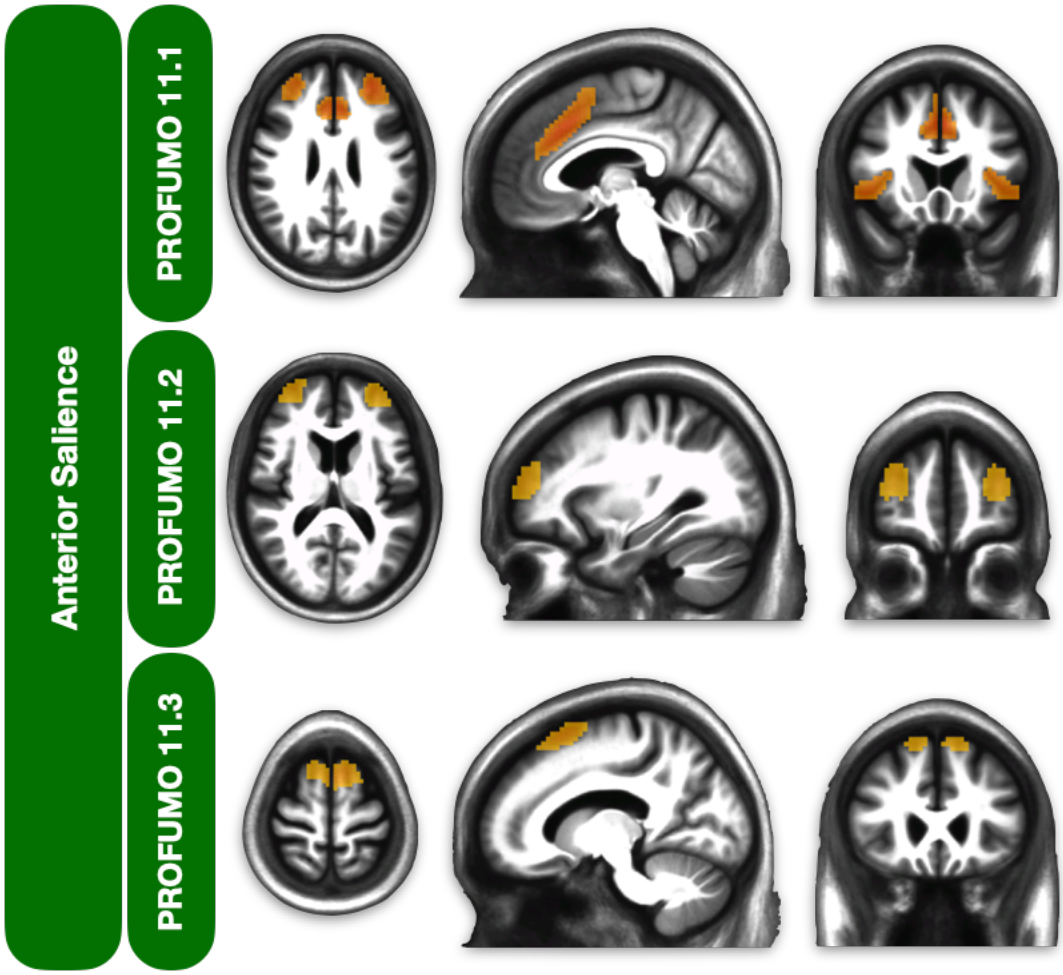

Anterior Salience Network (11.1): Right superior/middle frontal gyrus; Left middle frontal gyrus; Right dorsal anterior cingulate cortex; Left dorsal anterior cingulate cortex; Right insula; Left insula.

Anterior Salience Network (11.2): Right middle frontal gyrus; Left middle frontal gyrus.

Anterior Salience Network (11.3): Right secondary motor area (SMA); Left secondary motor area (SMA).

Figure 3.9 (cont'd):

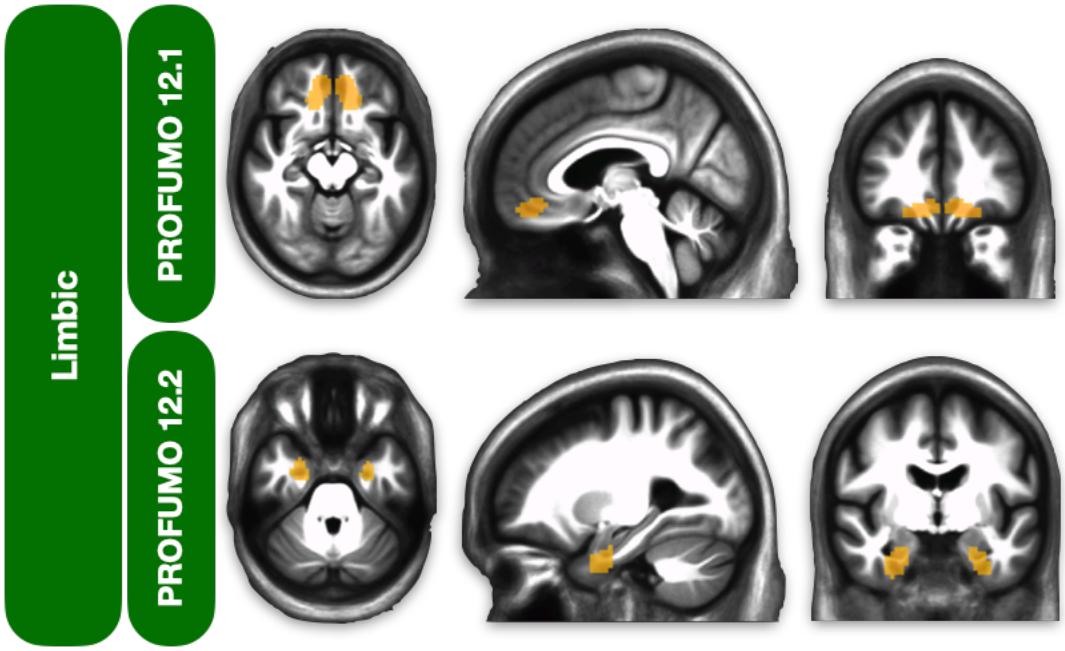

Limbic Network (12.1): Right orbitofrontal cortex; Left orbitofrontal cortex.

Limbic Network (12.2): Right temporal pole; Left temporal pole.

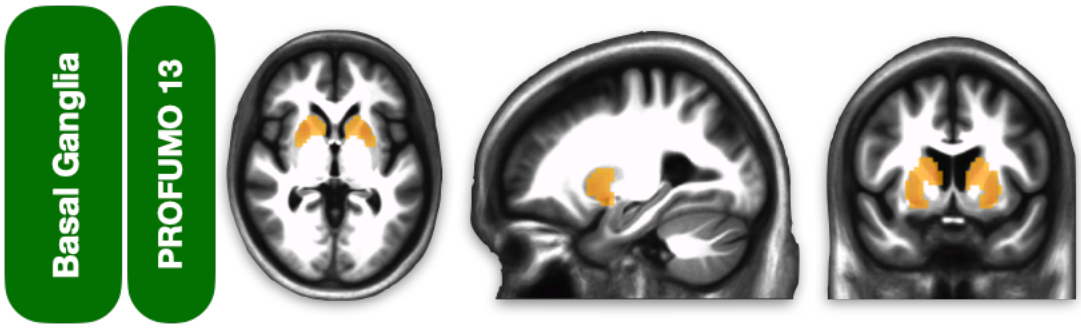

Basal Ganglia Network: Right basal ganglia; Left basal ganglia.

Figure 3.9 (cont'd):

Combinatory Networks

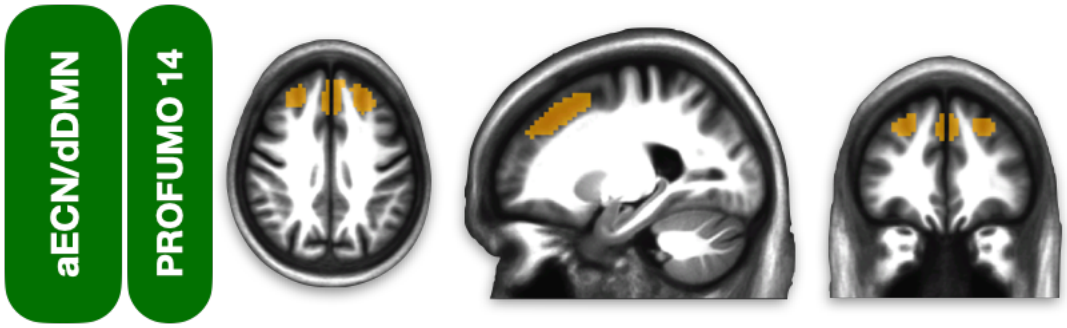

Anterior Executive Control Network (aECN)/Dorsal Default Mode Network (dDMN): Right superior frontal sulcus; Left superior frontal sulcus; Right medial superior frontal gyrus; Left medial superior frontal gyrus.

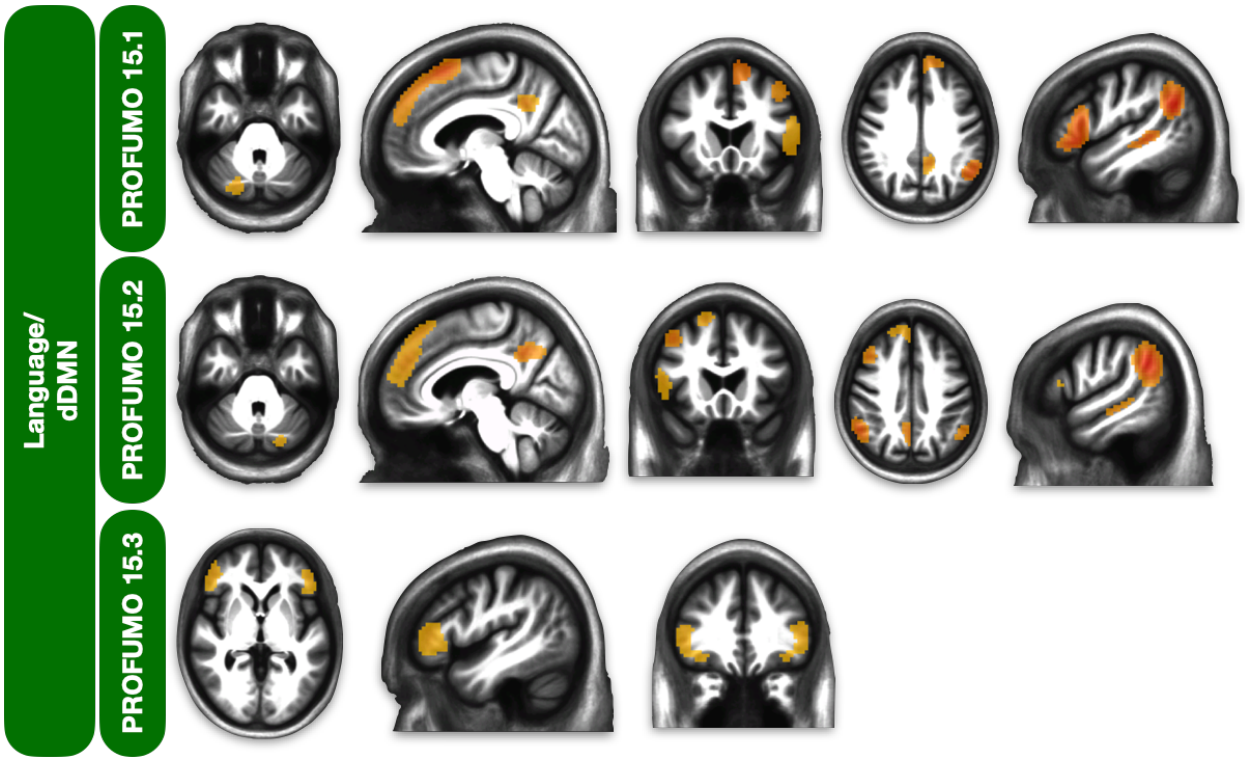

Language/Dorsal Default Mode Network (dDMN) (15.1): Right angular gyrus; Left angular gyrus; Right middle temporal gyrus; Left posterior cerebellum; Right pars triangularis; Right middle frontal gyrus; Right dorsomedial prefrontal cortex; Right precuneus.

Language/Dorsal Default Mode Network (dDMN) (15.2): Right posterior cerebellum; Left angular gyrus; Left middle temporal gyrus; Left pars triangularis; Left middle frontal gyrus; Left dorsomedial prefrontal cortex; Left precuneus.

Language Network/Dorsal Default Mode Network (dDMN) (15.3): Right pars triangularis; Left pars triangularis.

Figure 3.9 (cont'd):

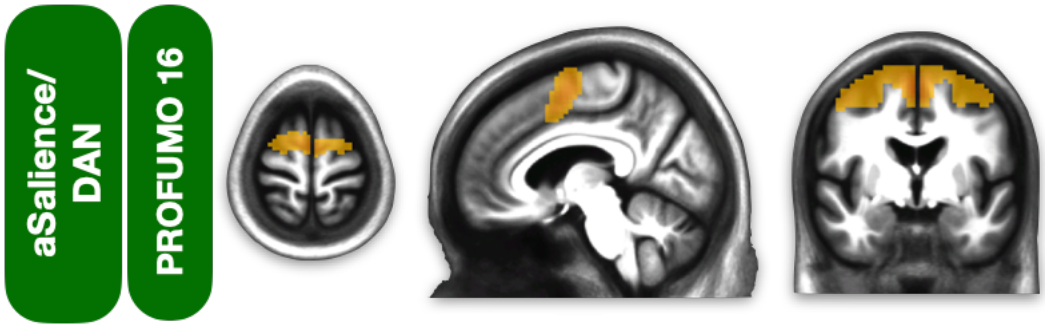

Anterior Salience Network (aSalience)/Dorsal Attention Network (DAN): Right superior precentral gyrus; Left superior precentral gyrus.

Language Network/Temporoparietal (TempParietal) Network: Right middle temporal gyrus; Left middle temporal gyrus.

Figure 3.9 (cont'd):

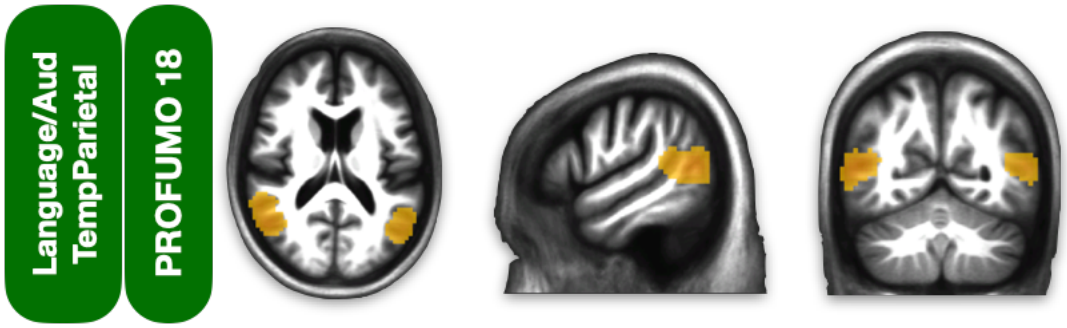

Language Network/Auditory (Aud) Network/Temporoparietal (TempParietal) Network: Right posterior middle temporal gyrus; Left posterior middle temporal gyrus.

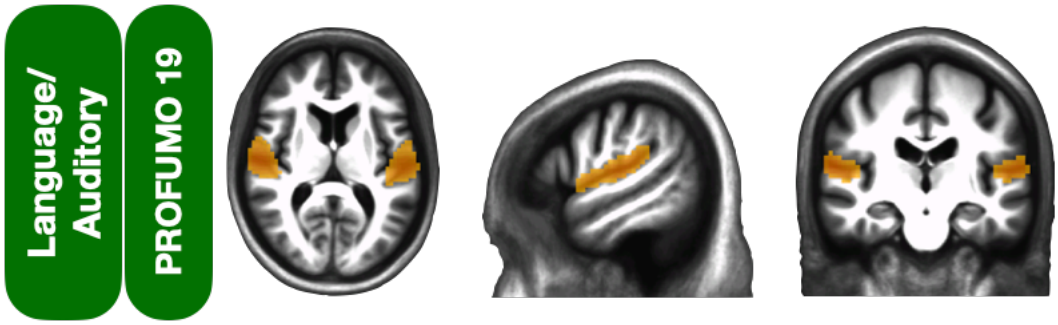

Language Network/Auditory Network: Right superior temporal gyrus; Left superior temporal gyrus.

TABLES

Table 3.1: Listing of each RSN from the 49-Component GICA Parcellation including the number of ROIs that comprise each RSN, and the names of each of those ROIs.

Network #	Network Label	# of ROIs	List of ROIs
1	Primary Visual Network	2	Right superior middle occipital gyrus (striate); Left superior middle occipital gyrus (striate cortex).
2	Sensorimotor Network	4	Right superior pre/postcentral gyrus (Sensorimotor cortex); Left superior pre/postcentral gyrus (Sensorimotor cortex); Right inferior precentral gyrus (Sensorimotor cortex); Left inferior precentral gyrus (Sensorimotor cortex).
3	Left Executive Control Network	6	Left inferior parietal lobe/angular gyrus; Left middle/inferior frontal gyrus; Left superior medial gyrus; Left posterior middle cingulate cortex; Left inferior/middle temporal gyrus; Right posterior cerebellum.
4	Precuneus Network	4	Right precuneus; Left precuneus; Right posterior/middle cingulate cortex; Left posterior/middle cingulate cortex.
5	Dorsal Attention/ Visuospatial Network	11	Right superior parietal cortex/precuneus; Left superior parietal cortex/precuneus; Right superior frontal cortex; Left superior frontal cortex; Right inferior frontal gyrus; Left inferior frontal gyrus; Right middle temporal gyrus; Left middle temporal gyrus; Right inferior temporal gyrus.
6	Ventral Default Mode Network	10	Right precuneus; Left precuneus; Right frontal eye field; Left frontal eye field; Right middle occipital gyrus; Left middle occipital gyrus; Right retrosplenial cortex; Left retrosplenial cortex; Right parahippocampal place area; Left parahippocampal place area.
7	High Visual Network	2	Right prestriate cortex; Left prestriate cortex.
8	Posterior Salience Network	10	Right supramarginal gyrus; Left supramarginal gyrus; Right precuneus/middle cingulate cortex; Left precuneus/middle cingulate cortex; Right thalamus; Left thalamus; Right insula; Left insula; Right superior cerebellum; Left superior cerebellum.
9	Anterior Salience Network	14	Right superior frontal gyrus; Left superior frontal gyrus; Right middle frontal gyrus; Left middle frontal gyrus; Right dorsal anterior cingulate cortex; Left dorsal anterior cingulate cortex; Right superior frontal gyrus/pre-supplemental motor area; Left superior frontal gyrus/pre-supplemental motor area; Right insula; Left insula; Right superior cerebellum; Left superior cerebellum; Right inferior cerebellum; Left inferior cerebellum.
10	Language Network	10	Right angular gyrus; Left angular gyrus; Right superior temporal gyrus; Left superior temporal gyrus; Right superior/middle temporal gyrus; Left superior/middle temporal gyrus; Right pars triangularis; Left pars triangularis; Right middle temporal gyrus; Left middle temporal gyrus.

Table 3.1 (cont'd):

11	Dorsal Default Mode Network	21	Right posterior cingulate cortex; Left posterior cingulate cortex; Right superior frontal gyrus; Left superior frontal/medial gyrus; Right angular gyrus; Left angular gyrus; Right superior medial gyrus; Right basal ganglia; Left basal ganglia; Right anterior cingulate cortex; Left anterior cingulate cortex; Right inferior frontal gyrus; Left inferior frontal gyrus; Right hippocampus; Left hippocampus; Right middle temporal gyrus; Left middle temporal gyrus; Right superior cerebellum; Left superior cerebellum; Right inferior cerebellum; Left inferior cerebellum.
12	Right Executive Control Network	8	Right inferior parietal lobe/angular gyrus; Right middle/inferior frontal gyrus; Right superior medial gyrus; Right posterior middle cingulate cortex; Right pars opercularis/inferior frontal gyrus; Right middle frontal gyrus; Right inferior/middle temporal gyrus; Left posterior cerebellum.
13	Auditory Network	2	Right superior temporal gyrus/operculum; Left superior temporal gyrus/operculum.
14	Basal Ganglia Network	2	Right basal ganglia; Left basal ganglia.
15	Limbic Network	4	Right temporal pole; Left temporal pole; Right pallidum; Left pallidum.

Table 3.2: Listing of each RSN from the 50-Mode PROFUMO parcellation including the number of modes that comprise each network, the number of ROIs within each mode, and the names of each of those ROIs.

Network #	Network Label	Subnetwork #	# of ROIs	List of ROIs
SINGLE NETWORKS				
1	Precuneus Network		6	Right precuneus; Left precuneus; Right posterior/middle cingulate cortex; Left posterior/middle cingulate cortex.
2	Primary Visual Network	2.1	2	Right superior middle occipital gyrus (striate); Left superior middle occipital gyrus (striate).
		2.2	2	Right inferior occipital gyrus; Left inferior occipital gyrus.
		2.3	4	Right superior occipital gyrus; Left superior occipital gyrus; Right middle occipital gyrus; Left middle occipital gyrus.
3	Left Executive Control Network		7	Left inferior parietal lobe/angular gyrus; Left medial/inferior frontal cortex; Left superior medial frontal cortex; Left inferior/medial temporal cortex; Left posterior middle cingulate cortex; Right inferior semilunar lobule of the cerebellum; Right posterior lobule of the cerebellum.
4	Sensorimotor Network	4.1	2	Right superior pre/postcentral gyrus; Left superior pre/postcentral gyrus.
		4.2	2	Right inferior precentral gyrus; Left

Table 3.2 (cont'd):

				inferior precentral gyrus.
		4.3	2	Right middle precentral gyrus; Left middle precentral gyrus.
		4.4	2	Right anterior cerebellum; Left anterior cerebellum.
		4.5	2	Right superior medial pre/postcentral gyrus; Left superior medial pre/postcentral gyrus.
5	High Visual Network	5.1	2	Right prestriate cortex; Left prestriate cortex
		5.2	2	Right inferior occipital gyrus; Left inferior occipital gyrus.
		5.3	2	Right superior occipital gyrus; Left superior occipital gyrus.
6	Right Executive Control Network		7	Right inferior parietal lobe/angular gyrus; Right medial/inferior frontal cortex; Right superior medial frontal cortex; Right inferior/medial temporal cortex; Right posterior middle cingulate cortex; Left inferior posterior cerebellum; Left posterior cerebellum.
7	Ventral Default Mode Network	7.1	10	Right precuneus; Left precuneus; Right frontal eye field; Left frontal eye field; Right middle occipital gyrus; Left middle occipital gyrus; Right retrosplenial cortex; Left retrosplenial cortex; Right parahippocampal place area; Left parahippocampal place area.
		7.2	2	Right precuneus; Left precuneus.

Table 3.2 (cont'd):

8	Dorsal Default Mode Network	8.1	10	Right posterior cingulate cortex; Left posterior cingulate cortex; Right angular gyrus; Left angular gyrus; Right superior frontal gyrus; Left superior frontal gyrus; Right medial prefrontal cortex; Left medial prefrontal cortex; Right middle temporal lobe; Left middle temporal lobe.
		8.2	2	Right posterior cerebellum; Left posterior cerebellum.
		8.3	2	Right prefrontal cortex; Left prefrontal cortex.
		8.4	4	Right anterior cingulate cortex; Left anterior cingulate cortex; Right 54cingulate cortex; Left middle cingulate cortex.
9	Posterior Salience Network	9.1	11	Right supramarginal gyrus; Left supramarginal gyrus; Right precuneus/middle cingulate cortex; Left precuneus/middle cingulate cortex; Right superior middle frontal gyrus; Left middle frontal gyrus; Right inferior frontal gyrus; Left inferior frontal gyrus; Right inferior middle frontal gyrus; Left inferior middle frontal gyrus; Right middle temporal gyrus.
		9.2	2	Right superior parietal lobule; Left superior parietal lobule.

Table 3.2 (cont'd):

10	Visuospatial Network	10.1	8	Right superior parietal cortex/precuneus; Left superior parietal cortex/precuneus; Right superior frontal cortex; Left superior frontal cortex; Right inferior frontal gyrus; Left inferior frontal gyrus; Right inferior temporal gyrus; Left inferior temporal gyrus.
		10.2	2	Right inferior parietal cortex and superior parietal cortex/precuneus; Left inferior parietal cortex and superior parietal cortex/precuneus.
		10.3	3	Right inferior parietal lobule; Right pars opercularis; Right middle frontal gyrus.
		10.4	2	Right inferior frontal gyrus; Left inferior frontal gyrus.
		10.5	2	Right intraparietal sulcus; Left intraparietal sulcus.
		10.6	2	Right superior parietal lobule; Left superior parietal lobule.
11	Anterior Salience Network	11.2	6	Right superior/middle frontal gyrus; Left middle frontal gyrus; Right dorsal anterior cingulate cortex; Left dorsal anterior cingulate cortex; Right insula; Left insula.
		11.2	2	Right middle frontal gyrus; Left middle frontal gyrus.

Table 3.2 (cont'd):

		11.3	2	Right secondary motor area (SMA); Left secondary motor area (SMA).
12	Limbic Network	12.1	2	Right orbitofrontal cortex; Left orbitofrontal cortex.
		12.2	2	Right temporal pole; Left temporal pole.
13	Basal Ganglia Network		2	Right basal ganglia; Left basal ganglia.
COMBINATORY NETWORKS				
14	Anterior Executive Control Network/Dorsal Default Mode Network		4	Right superior frontal sulcus; Left superior frontal sulcus; Right medial superior frontal gyrus; Left medial superior frontal gyrus.
15	Language Network/Dorsal Default Mode Network	15.1	8	Right angular gyrus; Left angular gyrus; Right middle temporal gyrus; Left posterior cerebellum; Right pars triangularis; Right middle frontal gyrus; Right dorsomedial prefrontal cortex; Right precuneus.
		15.2	7	Right posterior cerebellum; Left angular gyrus; Left middle temporal gyrus; Left pars triangularis; Left middle frontal gyrus; Left dorsomedial prefrontal cortex; Left precuneus.
		15.3	2	Right pars triangularis; Left pars triangularis.
16	Anterior Salience Network/Dorsal Attention Network		2	Right superior precentral gyrus; Left superior precentral gyrus.

Table 3.2 (cont'd):

17	Language Network/Temporoparietal Network		2	Right middle temporal gyrus; Left middle temporal gyrus.
18	Language Network/Auditory Network/Temporoparietal Network		2	Right posterior middle temporal gyrus; Left posterior middle temporal gyrus.
19	Language Network/Auditory Network		2	Right superior temporal gyrus; Left superior temporal gyrus.

CHAPTER 4: FUTURE DIRECTIONS AND GENERAL CONCLUSIONS

4.1 – Application of the rrAD240 functional atlas

The rrAD420 functional atlas defines the RSNs from baseline resting-state functional magnetic resonance imaging (rs-fMRI) scans of the rrAD cohort. Specifically, the rrAD trial seeks to investigate the effects of lowering blood pressure on cognition and brain functional connectivity in a cohort entirely comprised of hypertensive patients with an increased risk of developing Alzheimer's Disease (AD). The treatment groups that will be tested include standard treatment, intensive reduction of vascular risk factors (ISVR), exercise training, and ISVR in combination with exercise training.

The age-appropriate and cohort-specific RSNs presented in the rrAD420 functional atlas will be compared between rrAD treatment groups to gauge the effectiveness of each intervention in preserving brain functional connectivity. Correlation analyses of rs-fMRI time courses between nodes of each RSN will be performed using Analysis of Functional NeuroImages software (AFNI, NIH, USA) "3dfim+" (1). The mean correlation will be calculated for all node-pairs in each RSN. For group statistical analyses, correlation coefficients will be standardized through Fisher's Z-transformation. To compare RSN mean functional connectivity between treatment groups, we will calculate the average Z value for each RSN of interest for all subjects in each group. ANOVAs will be conducted on these Z value distributions across subjects, followed by Student's t-tests of RSNs between treatment groups. We will also explore the differences between specific connections via paired Student's t-tests within each RSN to investigate connections that could be driving overall changes in each RSN. Correlation coefficients will be obtained between each pair of nodes in each RSN to construct a correlation matrix for each RSN. We will then compare the connectivity of each RSN between both time points for each group to determine whether there was a chance in functional connectivity at the end of the study relative to baseline. The correlation matrix of each RSN will be then compared between groups

to locate the specific connections that show a group difference between treatment effects following Student's t-tests. The significance level will be set at $p \leq 0.05$ after Bonferroni correction in all statistical analyses.

To compare the effects of standard and intensive blood pressure reduction on AD-associated alterations in the default mode network (DMN), executive control network (ECN), and salience network as defined in the rrAD40 functional atlas. The DMN, ECN and salience network have been shown to be associated with each other and are collectively referred to as the triple network system (2). The DMN is responsible for inward thinking, while it the ECN is involved in external thinking involving an outward attention. There is evidence that suggests the salience network to be responsible for switching between these opposing states. Studies have shown this triple network system to be compromised along the AD continuum. Therefore, we can compare both mean within-network connectivity and between-network connectivity between the rrAD timepoints. If a difference is found, we can then compare between treatment groups to determine if there is an effect of the strategy used to reduce blood pressure. The triple network system has shown differences along the AD continuum, and this disrupted connectivity has exhibited predictive power in classifying AD progression (3–5). Here, we predict there will be no differences at baseline; however, we expect the ISVR group to prevent the disruption of RSNs relative to the standard treatment group after the two-year treatment.

Our findings on RSN functional connectivity can also be correlated to cognitive performance as inferred by established tests that were administered to all rrAD participants. The neuropsychological testing used in the rrAD study has been validated in prior studies and is widely used to effectively capture age-related cognitive decline, namely the Alzheimer's Disease Cooperative Study Preclinical Alzheimer's Cognitive Composite (ADCS-PACC) and NIH-Toolbox cognition battery (6,7).

Similarly, we will use the rrAD420 atlas determine the combined effects of physical exercise and hypertensive treatment on AD-associated disruptions in neural network connectivity and cognitive decline. We will investigate the effects of exercise training alone, and combined with intensive blood pressure reduction, on RSN functional connectivity and cognitive performance on the ADCS-PACC and NIH-Toolbox cognition battery. Once again, we will focus on the triple network system comprised of the DMN, ECN, and salience network as defined in the rrAD420 functional atlas.

Overall, we do not expect to see differences in RSN organization between groups at baseline. However, following treatment we expect the ISVR group to offer more benefit than standard treatment in protecting against cognitive decline and altered functional connectivity profiles of the DMN, ECN, and salience network. We further anticipate that exercise combined with ISVR confers more benefit on these measures than either exercise or ISVR alone. If successful, the rrAD trial would underscore the importance of an integrated blood pressure reduction approach in maintaining brain health and provide an intervention to control modifiable risk factors associated with cognitive decline and AD in hypertensive individuals with increased risk of AD development. While the rrAD420 functional atlas will clearly be instrumental in accomplishing the specific primary aims of the rrAD trial described here, we also believe that the age-related nuisances captured by our atlas could be extended to older adults in general.

We could validate the rrAD420 functional atlas with a direct comparison to legacy atlases, such as the Shirer functional atlas, using the rrAD dataset (8). This could allow us to determine if the rrAD420 functional atlas can capture functional connectivity differences between rrAD treatment groups potentially missed by existing alternatives. We could further test the predictive value of the rrAD420 atlas by comparing its performance to an existing functional atlas using data from an open-access database like the Alzheimer's Disease Neuroimaging Initiative (ADNI; http://adni.loni.usc.edu; (9). The ADNI study includes scans from subjects at each stage of the

AD continuum (healthy controls, subjective cognitive impairment, mild cognitive impairment, and AD). They also maintain longitudinal documentation on some groups within the dataset, which allows for the tracking of some characteristics of disease progression to better predict cases that will develop into a full AD diagnosis. From this dataset, RSNs like the DMN have been shown to have a gradual degradation pattern along the continuum (10,11). Therefore, we could test how this progression is captured by the rrAD420 functional atlas and compare our results to existing functional atlas options used in already published work (12).

4.2 – Translational Potential of RSNs in a novel rat model of Alzheimer's Disease with hypertension

The triple network system defined above is not unique to humans. In fact, it has been found in both rodents and nonhuman primates (13). This system has already shown a similar pattern of disruption in AD rats compared to controls (14,15). Through collaborative efforts with the labs of Dr. Anne Dorrance, Dr. Scott Counts, and Dr. Chunqi Qian, we have rs-fMRI data from a novel transgenic Frankenrat model designed to explore the combined effects of hypertension and AD (16). The Frankenrat model was created by crossbreeding TgF344-AD rats onto the SHRSP background. TgF344-AD rats offer a model that captures hallmarks of AD pathology including amyloid-beta plaque accumulation, neurofibrillary tangles, frank neuronal cell loss, cognitive impairment, and the expression of human amyloid precursor protein (APPswe) and presenilin 1 (PS1ΔE9) genes (17,18). Additionally, SHRSP rats provide an excellent model for hypertension that develops by 4 months of age (19). The cross between TgF344-AD and SHRSP rats yields a novel hypertensive model that also expresses familial AD risk genes, APPswe and PS1ΔE9. In addition, we will have comparable scans from age-matched control groups of normotensive AD, hypertensive rats with no AD, and normotensive rats with no AD available for comparison. Using the rs-fMRI scans from these animals we will determine

whether AD-associated disruptions of the triple network system are exacerbated by hypertension, and if hypertension alone can impact RSN functional connectivity.

In our preliminary analysis, we used a total of 9 Transgene-positive or Transgene-negative Frankentats rats (4 male, 5 females). Animals were first anesthetized with 5% isoflurane in a chamber and baby cream (Meijer) was injected into the ear to recover the signal loss and to avoid noise contamination as described in our recently published article (16). The animals then received an initial subcutaneous injection of dexmedetomidine (0.1 mg/kg). Following the injection, isoflurane was discontinued, and the animal was transferred to the scanner. While in the scanner, dexmedetomidine was delivered subcutaneously at a constant rate to maintain the anesthesia (0.1 mg/kg/h). The animal's body temperature, arterial oxygen saturation level, and respiration rates were monitored and maintained within normal ranges when the animal was inside the scanner. Spontaneous respiration rate ranged from 50 to 70 breaths per min during rs-fMRI image acquisition. All images were acquired with a 7 T/16 cm aperture bore small-animal scanner (Bruker BioSpin). Functional images were acquired with a 3D gradient-echo EPI (GE-EPI) sequence with the following parameters: time of echo (TE) = 20 ms, time of repetition (TR) = 1 s, field of view (FOV) = 2.6 cm × 2.6 cm × 1.6 cm, matrix size = 52 × 52 × 32, voxel size = 0.5 mm × 0.5 mm × 0.5 mm. Each rs-fMRI scan acquired 900 time points over 15 mins. All signal processing and analyses were implemented in MATLAB software (Mathworks, Natick, MA), FMRIB Software Library (FSL) and AFNI. The preprocessing procedures followed the commonly used AFNI protocol for rat rs-fMRI data, including motion correction, despike, spatial blurring with a kernel of 4-mm full width at half maximum, and bandpass filtering from 0.001-0.4 Hz (20,21). Then, we conducted ICA analysis with 60 components using MELODIC in FSL to identify and remove non-neural artefacts. We manually identified each component as real signal or noise based on their spatial, temporal, and spectral features. After denoising the components defined as noise, fMRI data from each rat were aligned to the averaged anatomical RARE

template. We then performed a see-based correlation analysis using the posterior cingulate cortex set as the seed region to create a rat DMN spatial map (Figure 4.1). Specifically, the rat DMN is comprised of the entorhinal cortex, prelimbic cingulate, rostral dorsal prelimbic cortex, retrosplenial granular and dysgranular cortex, globus pallidus, hypothalamus, and hippocampus (21,22). Next, we will identify the remaining two RSNs of the triple network system, the ECN and salience network, in order to assess functional connectivity differences between groups. However, DMN itself has shown decreased connectivity in healthy aging across species, including rodents (21–23). Furthermore, studies have found disruptions in TgF344-AD rat DMN functional connectivity relative to age-matched controls. Our initial DMN spatial map can already enable us to elaborate on whether hypertension exacerbates this deteriorative effect as the mean DMN functional connectivity can be compared between Frankenrats, and each control group.

Once our rs-fMRI analysis is complete, our results can be combined with behavioral assessments to investigate the effect of AD and hypertension interplay on functional connectivity of the triple network system and cognition. Specifically, age-matched SHRSPs and Frankenrats underwent behavioral testing including the open-field task, spontaneous alternation test in the Y-maze, and the novel object task prior to scanning in order to compare hippocampus-related memory function. To test short-term spatial reference memory function, we performed the spontaneous alternation test in the Y-maze. Rats were allowed to run the maze for a 5-minute period. We recorded sessions and implemented Ethovision XT 11.5 software from Nodulus to detect the sequence in which they visit each arm of the maze (Noldus, Nijmegen Area, The Netherlands). We then used Noldulus to quantify the number of correct triads and divide that number by the total entries to ascertain the percentage of spontaneous alternation. Rats have an innate desire to explore novel environments. As such, they tend to visit each arm of the maze in an alternating fashion by entering the arm which they have least

recently visited. However, if the rat does not remember the arms, they have already entered, then it will make more errors in its alternating behavior. We also tested hippocampus-dependent, nonspatial memory using the novel object task. Rats were placed in the arena and allowed to explore two identical “familiar” objects for 10 minutes. After initial exposure, rats were removed from the arena and placed into separate holding cages. After 90 minutes, one of the familiar objects was replaced with a novel object. The rat was placed back into the arena and, again, allowed to explore the arena for 5 minutes. We recorded sessions and implemented Ethovision XT 11.5 software to track the amount of time spent exploring each object. Videos were checked for quality to ensure tracking software was correct, and errors were manually corrected in the program’s track editor. Cumulative duration was calculated by dividing the time spent with one object by the combined time spent exploring both objects. Cognitively normal rats are more interested in the novel object and spend more time exploring it than the familiar object. However, cognitively impaired rats are expected to spend an equal amount of time exploring both objects, as they may not remember the familiar object. We also employed the open-field task to ensure that our findings in the Y-maze and novel object task are not influenced by differences in locomotor activity. Rats were placed into a Plexiglas box equipped with motion sensors and allowed to freely move around for 30 minutes while being recorded by Fusion Open Field Activity Monitoring System (Omnitech Electronics, Inc. Columbus Ohio, USA). After completion, time spent in each zone, total distance traveled, and average velocity will be calculated by the software. Student’s t-tests will be used to compare behavioral findings between SHRSP and Frankenrat groups. We anticipate no difference in locomotive behavior assessed by the open field task between groups. However, we do expect Frankenrats to display worse hippocampus-related spatial and nonspatial memory function as inferred by spontaneous alternating behavior and novel object task.

In addition, preclinical animal studies allow for the investigation of important factors that cannot be directly measured in humans. For instance, binding of BDNF to tropomyosin receptor kinase B (TrkB) mediates trophic coupling between neurons and cerebral endothelial cells and yields a neuroprotective effect (24). Studies have shown BDNF to be compromised in cases of both hypertension and AD (25,26). Similarly, a study by Raz and colleagues investigated the effects of both (1) hypertension and (2) genetic variants in several single nucleotide polymorphisms on age-related 7 cognitive performance (27). They found that processing speed and episodic (association) memory performance were negatively affected by the BDNF Val66Met polymorphism, and this effect was exacerbated by hypertension. This finding was consistent with extant literature that shows BDNF Methionine allele carriers Val66Met to be associated with a significant decrease in BDNF expression relative to Valine allele homozygotes (28). However, further investigation requires preclinical research that supplements findings of this nature in humans to uncover the location where BDNF expression is mostly reduced. While previous studies have noted hypertension-related differences in total BDNF, it is possible that decreased BDNF may be more specific to certain BDNF variants (29). As such, there may be a subsequent compensatory increase in other BDNF RNA isoforms which we would not detect in the quantification of total BDNF (30). Therefore, it is possible to use primers specific to exon-1 and exon-4 containing BDNF as an alternative to investigate region specific changes in BDNF expression between Frankenrats and SHRSPs, as these isoforms are expressed primarily in the hippocampus and cortex respectively. Indeed, animal studies have shown BDNF to be down regulated in hypertensive rats, specifically in the cortex and hippocampus (31), which can be rescued through antihypertensive pharmacological intervention (32,33). Another recent study indicates the BDNF system as a potential therapeutic target to rescue hippocampus-related cognitive deficiencies in an AD mouse model using a TrkB agonist, AS86 (34). This study shows promise particularly because previous treatments have not been able to rescue AD-associated cognitive decline (35). Together, these findings implicate BDNF in the relationship between

hypertension and AD-associated cognitive decline and brain changes. However, more evidence is needed on a model that captures both hypertension and AD pathology to validate this claim. After each scan, the animals were sacrificed, and the brains were extracted. They were subsequently micro-dissected and the bilateral samples of hippocampus, caudate, and cortex were collected. We intend to quantify the amount of BDNF expression in these regions to determine if reduced hippocampal and cortical BDNF expression is related to disruptions in triple network system functional connectivity.

4.3 – General Conclusions

In conclusion, this dissertation has examined methodologies of rs-fMRI in a variety of ways. Firstly, we show RSN behavior differentially changes throughout rest conditions. To do so, we completed a comprehensive examination of seventeen cortical RSNs presented in an existing functional atlas through four rest conditions with varying levels of cognitive load (36). We showed that each RSN responded differentially to changes in rest condition, with some networks being more resilient than others even with the relatively high stimulation of the movie condition. However, for the most part we showed that more external stimulation led to more overall changes in resting-state functional connectivity. We also show some RSNs are more susceptible to deviations in functional connectivity as subtle changes in rest condition are introduced. For example, DMN showed a difference in functional connectivity between eyes-open and eyes-closed conditions. Furthermore, we showed that internal cognitive processing was not observed to affect functional connectivity at any level for any RSN.

Next, we establish a functional atlas for older adults that will immediately benefit the recently concluded rrAD clinical trial, as well as future studies that are interested in network modeling approaches that assess RSN functional connectivity within a similar late-adulthood demographic. Our rrAD420 functional atlas provides multiple options for the study of RSN functional connectivity in older adults. Specifically, we include a high-resolution seed-based

spatial map of DMN, a complete parcellation of maximally independent RSNs derived through traditional group independent component analysis, and a complete parcellation of RSNs that allows for overlap between each RSN as derived from a probabilistic functional mode decomposition.

Finally, we assist in the validation of a novel hypertensive AD animal model by providing a RSN spatial map for the model derived from a seed-based correlation approach using the posterior cingulate cortex as the seed region. This spatial map contains regions of the previously reported DMN, which were captured using novel ICE ear bars. This novel preparation reduced susceptibility weighted artifacts and increased signal in relatively deeper regions of the brain, such as the entorhinal cortex. The enhanced signal allows for a reliable DMN of this model that can be compared healthy controls and other types of assays that are difficult to obtain in human studies, such as region-specific BDNF expression. With this well-matched translational model that is comparable to participants of the rrAD studies, we can further expand on the underlying mechanisms that contribute to observed differences in RSN connectivity following a reduction in systolic blood pressure.

REFERENCES

1. Cox J.S. RW; H. AFNI: Software for analysis and visualization of functional magnetic resonance neuroimages. Computers and Biomedical Research [Internet]. 1996;29(29):162–73. Available from: https://ac-els-cdn-com.ezp-prod1.hul.harvard.edu/S0010480996900142/1-s2.0-S0010480996900142-main.pdf?_tid=c22bae7a-b8f5-4a8b-9dac-91c1ed841d53&acdnat=1549393398_e37181b8933a2ac88c2d7dc0eab14413

2. Menon V. Large-scale brain networks and psychopathology: A unifying triple network model. Vol. 15, Trends in Cognitive Sciences. 2011. p. 483–506.

3. Zhu H, Zhou P, Alcauter S, Chen Y, Cao H, Tian M, et al. Changes of intranetwork and internetwork functional connectivity in Alzheimer's disease and mild cognitive impairment. J Neural Eng. 2016 Jun 1;13(4).

4. Meng X, Wu Y, Liang Y, Zhang D, Xu Z, Yang X, et al. A Triple-Network Dynamic Connection Study in Alzheimer's Disease. Front Psychiatry. 2022 Apr 4;13.

5. Wu X, Li Q, Yu X, Chen K, Fleisher AS, Guo X, et al. A triple network connectivity study of large-scale brain systems in cognitively normal APOE4 carriers. Front Aging Neurosci. 2016 Sep 28;8(SEP).

6. Weintraub S, Dikmen SS, Heaton RK, Tulsky DS, Zelazo PD, Slotkin J, et al. The cognition battery of the NIH toolbox for assessment of neurological and behavioral function: Validation in an adult sample. Journal of the International Neuropsychological Society. 2014;20(6):567–78.

7. Donohue MC, Sperling RA, Salmon DP, Rentz DM, Raman R, Thomas RG, et al. The preclinical Alzheimer cognitive composite: Measuring amyloid-related decline. JAMA Neurol. 2014;71(8):961–70.

8. Shirer WR, Ryali S, Rykhlevskaia E, Menon V, Greicius MD. Decoding subject-driven cognitive states with whole-brain connectivity patterns. Cerebral Cortex. 2012 Jan;22(1):158–65.

9. Petersen RC, Aisen PS, Beckett LA, Donohue MC, Gamst AC, Harvey DJ, et al. Alzheimer's Disease Neuroimaging Initiative (ADNI) Clinical characterization [Internet]. 2010. Available from: www.neurology.org

10. Kuang L, Jia J, Zhao D, Xiong F, Han X, Wang Y. Default Mode Network Analysis of APOE Genotype in Cognitively Unimpaired Subjects Based on Persistent Homology. Front Aging Neurosci. 2020 Jun 30;12.

11. Nakagawa T, Ishida M, Naito J, Nagai A, Yamaguchi S, Onoda K. Prediction of conversion to Alzheimer's disease using deep survival analysis of MRI images. Brain Commun. 2020;2(1).

12. Penalba-Sánchez L, Oliveira-Silva P, Sumich AL, Cifre I. Increased functional connectivity patterns in mild Alzheimer's disease: A rsfMRI study. Front Aging Neurosci. 2023 Jan 9;14.

13. Raichle ME. The Brain's Default Mode Network. Annu Rev Neurosci. 2015 Jul 8;38:433–47.

14. De Waegenaere S, van den Berg M, Keliris GA, Adhikari MH, Verhoye M. Early altered directionality of resting brain network state transitions in the TgF344-AD rat model of Alzheimer's disease. Front Hum Neurosci [Internet]. 2024 Apr 5;18. Available from: https://www.frontiersin.org/articles/10.3389/fnhum.2024.1379923/full

15. Tudela R, Muñoz-Moreno E, Sala-Llonch R, López-Gil X, Soria G. Resting state networks in the TGF344-AD rat model of Alzheimer's disease are altered from early stages. Front Aging Neurosci. 2019;10(JUL).

16. Chen Y, Fernandez Z, Scheel N, Gifani M, Zhu DC, Counts SE, et al. Novel inductively coupled ear-bars (ICEs) to enhance restored fMRI signal from susceptibility compensation in rats. Cerebral Cortex. 2023 Dec 13;

17. Cohen RM, Rezai-Zadeh K, Weitz TM, Rentsendorj A, Gate D, Spivak I, et al. A transgenic alzheimer rat with plaques, tau pathology, behavioral impairment, oligomeric Aβ, and frank neuronal loss. Journal of Neuroscience. 2013;33(15):6245–56.

18. Saré RM, Cooke SK, Krych L, Zerfas PM, Cohen RM, Smith CB. Behavioral Phenotype in the TgF344-AD Rat Model of Alzheimer's Disease. Front Neurosci. 2020;14(June):1–10.

19. OKAMOTO K, AOKI K. Development of a Strain of Spontaneously Hypertensive Rats. Jpn Circ J [Internet]. 1963;27(3):282–93. Available from: https://www.jstage.jst.go.jp/article/bpb1993/17/11/17_11_1460/_pdf/-char/ja

20. Liu Y, Perez PD, Ma Z, Ma Z, Dopfel D, Cramer S, et al. An open database of resting-state fMRI in awake rats. Neuroimage. 2020 Oct 15;220.

21. Hsu LM, Liang X, Gu H, Brynildsen JK, Stark JA, Ash JA, et al. Constituents and functional implications of the rat default mode network. Proc Natl Acad Sci U S A. 2016 Aug 2;113(31):E4541–7.

22. Egimendia A, Minassian A, Diedenhofen M, Wiedermann D, Ramos-Cabrer P, Hoehn M. Aging Reduces the Functional Brain Networks Strength—a Resting State fMRI Study of Healthy Mouse Brain. Front Aging Neurosci. 2019 Oct 11;11.

23. Albertson AJ, Landsness EC, Tang MJ, Yan P, Miao H, Rosenthal ZP, et al. Normal aging in mice is associated with a global reduction in cortical spectral power and network-specific declines in functional connectivity. Neuroimage. 2022 Aug 15;257.

24. Guo S, Kim WJ, Lok J, Lee SR, Besancon E, Luo BH, et al. Neuroprotection via matrix-trophic coupling between cerebral endothelial cells and neurons. Proc Natl Acad Sci U S A. 2008;105(21):7582–7.

25. Connor B, Young D, Yan Q, Faull RLM, Synek B, Dragunow M. Brain-derived neurotrophic factor is reduced in Alzheimer's disease. Molecular Brain Research. 1997;49(1–2):71–81.

26. Kadoya M, Koyama H, Kanzaki A, Kurajoh M, Hatayama M, Shiraishi J, et al. Plasma brain-derived neurotrophic factor and reverse dipping pattern of nocturnal blood pressure in patients with cardiovascular risk factors. PLoS One. 2014;9(8).

27. Raz N, Rodrigue KM, Kennedy KM, Land S. Genetic and Vascular Modifiers of Age-Sensitive Cognitive Skills: Effects of COMT, BDNF, ApoE, and Hypertension. Neuropsychology. 2009;23(1):105–16.

28. Egan MF, Kojima M, Callicott JH, Goldberg TE, Kolachana BS, Bertolino A, et al. The BDNF val66met polymorphism affects activity-dependent secretion of BDNF and human memory and hippocampal function. Cell. 2003;112(2):257–69.

29. Aid T, Kazantseva A, Piirsoo M, Palm K, Timmusk T. Mouse and ratBDNF gene structure and expression revisited. J Neurosci Res. 2007 Feb;85(3):525–35.

30. Perovic M, Tesic V, Mladenovic Djordjevic A, Smiljanic K, Loncarevic-Vasiljkovic N, Ruzdijic S, et al. BDNF transcripts, proBDNF and proNGF, in the cortex and hippocampus throughout the life span of the rat. Age (Omaha) [Internet]. 2013 Dec 21;35(6):2057–70. Available from: http://link.springer.com/10.1007/s11357-012-9495-6

31. Lee TH, Yang JT, Kato H, Wu JH. Hypertension downregulates the expression of brain-derived neurotrophic factor in the ischemia-vulnerable hippocampal CA1 and cortical areas after carotid artery occlusion. Brain Res. 2006;1116(1):31–8.

32. Hasegawa Y, Nakagawa T, Uekawa K, Ma M, Lin B, Kusaka H, et al. Therapy with the Combination of Amlodipine and Irbesartan Has Persistent Preventative Effects on Stroke Onset Associated with BDNF Preservation on Cerebral Vessels in Hypertensive Rats. Transl Stroke Res. 2016;7(1):79–87.

33. Kishi T, Hirooka Y, Sunagawa K. Telmisartan protects against cognitive decline via up-regulation of brain-derived neurotrophic factor/tropomyosin-related kinase B in hippocampus of hypertensive rats. J Cardiol [Internet]. 2012;60(6):489–94. Available from: http://dx.doi.org/10.1016/j.jjcc.2012.08.004

34. Wang S, Yao H, Xu Y, Hao R, Zhang W, Liu H, et al. Therapeutic potential of a TrkB agonistic antibody for Alzheimer's disease. Theranostics. 2020;10(15):6854–74.

35. Long JM, Holtzman DM. Alzheimer Disease: An Update on Pathobiology and Treatment Strategies. Cell [Internet]. 2019;179(2):312–39. Available from: https://doi.org/10.1016/j.cell.2019.09.001

36. Yeo BT, Krienen FM, Sepulcre J, Sabuncu MR, Lashkari D, Hollinshead M, et al. The organization of the human cerebral cortex estimated by intrinsic functional connectivity. J Neurophysiol. 2011 Sep;106(3):1125–65.

APPENDIX

FIGURES

Figure 4.1: Default-mode network (DMN) shown in color as constructed from PCC seed-based analysis of rs-fMRI data (n =5) overlaid on RARE structural images (adapted from Chen, 2023).